Tuneable RF Filter based on acoustically coupled Ferroelectric Resonators

by

Vangjush Komini

Submitted to the Department of Micro- and Nanotechnology
in partial fulfillment of the requirements for the degree of

Master in Smart System Integration

at the

Buskerud and Vestfold University College

July 2015

Author .....
Department of Micro- and Nanotechnology
July 24^{th},2015

Certified by .....
Ulrik Hanke
Professor
Thesis Supervisor

Accepted by .....
.
Chairman, Department Committee on Graduate Theses

Tuneable RF Filter based on acoustically coupled Ferroelectric Resonators

by

Vangjush Komini

Submitted to the Department of Micro- and Nanotechnology
on July 24^{th},2015, in partial fulfillment of the
requirements for the degree of
Master in Smart System Integration

Abstract

Tuneable filters are a great solution for wireless telecommunications. Micro-actuators resonators are being employed in different configuration in order to provide a much better selectivity. Ferroelectric materials are the main key materials which are being employed as the medium of the resonators and a bias voltage is superimposed with the input signal. The bias voltage varies the main properties of the ferroelectric materials and therefore the impedance profile of the resonator gets shifted into higher frequencies. The drawback associated with homogeneous structure is that resonance frequency has a lower tuneability rate compare to the antiresonance frequency. This is a critical feature since in real tuneable filter the bias voltage increases of the bandwidth rather than shifting the bandpass filter into higher frequencies. Another approach has been proposed in order to overcome this restriction. The new structure contains two distinct ferroelectric layers sandwiched by the electrode. The simulated data exhibits a enhanced tuneability for the resonance frequency. This is a competitive approach for implementation of tuneable filter.

Thesis Supervisor: Ulrik Hanke
Title: Professor

Acknowledgments

I would like to benefit from this chance and express my grateful feelings to my supervisor *Professor Ulrik Hanke* for his systematic help and feedback on this thesis. Moreover for sincere regards goes for *Professor Lars Hoff* and *Professor Agne Johannessen* for the co-supervision throughout the whole semester. My other gratitude foes for the RF group of students where the weekly meetings gave me a lot of inspiration for the accomplishment of this work. I am feel very happy to be part of the Smart System Integration master and this has been a very great even thanks to the coordination of *Dr Resh S. Dhariwal, Dr Knut E Aasmundtveit* and *Dr Ferenc Ender*. Norway in particular has been a great experience with all the activities and social events and am pleased to thank Merete for all her dedication. All the work load of this thesis went very smooth thanks to my girlfriend who was always with her support. *Me ne fund dua te falenderoj familjen time ne shqiper per dashurine e tyre pa kushte.*

Contents

List of Figures

List of Tables

Motivation

The rapid evolution of wireless technology has improved the exchange of information globally. Due to the extensive research worldwide this service became more affordable. Consequently the number of users up-scaled tremendously within two decades.

This market revolutionised with the first release of smart phone. An exponential growth of services is occurring into a limited range of frequencies and therefore crowding it significantly. However, high bandwidth is a very important requirement for the quality of specific operation. Communication channels needs to be displaced by some unused frequencies to ensure zero interference. In order to efficiently use the spectrum, high selective filters must be employed. Film bulk acoustic resonator FBAR system are commercial candidates which have been under research for several decades promising a much higher quality factor at GHz range in comparison to LC tanks [17]. Further more, low volume, low power, low cost, good coupling are the main key drivers for FBAR filters .

Since the majority of FBAR filters cannot be tuned, different hardware manufacturer are restricted to integrate big bank of filters into a single functional device. This is a vital functional requirements in order to ensure no interference among different channels. This existing solution requires high power and big space in the device in order to ensure a reliable functionality.

The goal of this work is addressing all these challenges into a tunable filter. Biasing operation frequency via a DC voltage will replace banks into a single highly tunable filter[24]. BST ferroelectric material is a very advantageous medium exhibiting physical properties consistently to the functional requirements with a temperature for non-polar phase transition close the ambient. Good tunability, significantly low dielectric loss and room temperature functionality, fast response, were the essential properties for this material choice [6].

Last but not least, coupling multiple FBAR is mostly performed electrically namely much energy leakage occurs when the power is conveyed from one resonator to another. This is therefore translated into high insertion in-band losses [41]. Bandwidth in electric coupling is also smaller due to pole-zero characteristic of the transfer function. In order to overcome this constrain, acoustic coupling resonators approach will deliver an enhanced functionality [34]. The main objective of this thesis is the improvement of the resonator tuneability.

This page is left blank intentionally

Chapter 1

Introduction

Bulk acoustic resonators performing a bandpass filter technology are integrated into mobile phones. Main advantages of this bandpass filters are good selectivity, small size and low power consumption. Frequency selectivity in RF system is carried out under the physical laws of acoustic waves. Filtering in electromagnetic domain requires the dimensions of the structures to be comparable to the wavelengths signal. However for $1GHz$ the wavelength of electromagnetic waves is in the 30 cm range which is much higher the dimensions of most mobile phones. In order to decrease the dimensions and enhance other filter parameters microactuator where the only candidates. Herein the range of frequencies is unchanged but the velocity of acoustic waves is at a range of $300 - 11000$ m/s. Since the velocity is reduced from $3 * 10^8$ to several 10^3 the wavelength is reduced with the also scale down by the fraction. In the GHz range this correspond to μm dimensions.

Surface acoustic waves (SAW) is another propagation mode utilized in RF filter. This technology is extensively commercialised and well applicable for wireless communication below 2 GHz[7]. Above this frequency they start to suffer critical size and very expensive to manufacture. Bulk acoustic waves (BAW) in comparison to SAW exhibit better properties, including lower frequency drift with temperature, able to handle higher power, good electrostatic discharge and easier IC compatibility technology [17].

BAW resonators have two main geometrical configuration film bulk acoustic resonator (FBAR) and solidly mounted resonator (SMR) [39]. Efforts in this case are addressed on increasing quality factors of the resonator.

The aim of these resonators is to increase Q-quality factor. Both these configurations trap a big amount of energy inside the piezoelectric bulk. In SMR topology different layers are smartly deposed with appropriate thickness and acoustic impedance in order to reflect back all the bulk waves. This is an adoption from optics where based Bragg law a multiple layer acoustic mirror is design with appropriate thickness. FBAR anchors the resonators into a bridge structure. The air/medium interface on both sides confines bulk waves inside the piezoelectric medium. Reflection

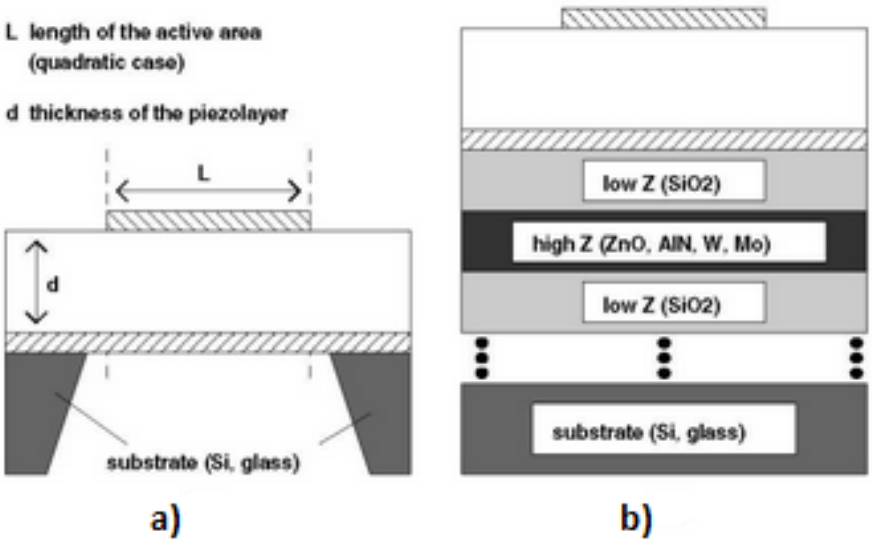

Figure 1-1: Two main BAW resonators where a) is the FBAR topology whereas b) is a outiline of SMR with multiple layers [28]

of waves is proportional to the difference of acoustic impedance of two mediums. Therefore a total internal reflection occurs due to extremely low acoustic impedance of air comparing to electrodes. FBAR design parameters usually requires only the optimisation of anchors whereas SMR needs critical selection of materials and thickness for each layer. Moreover adding layers underneath the resonator with degrade a bit the coupling factor and will add some additional loss mechanism in the total quality factor[39]. In this work FBAR will be the only configuration studied,

A solid understanding and interpretation of acoustic phenomenon is needed in order to develop and improve FBAR filter technologies. As hardware implementation, FBAR is packaged and integrated with other components of the mobile phone radio system creating a single board figure 1-2. The common implementation of FBAR's is to arrange these devices into a filter bank 1-3.

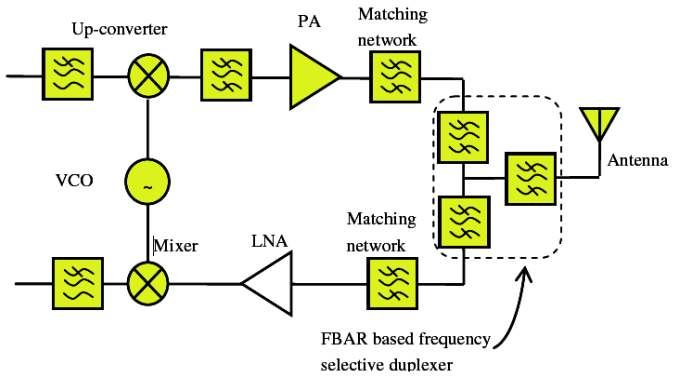

Figure 1-2: Mobile phone radio system[19]

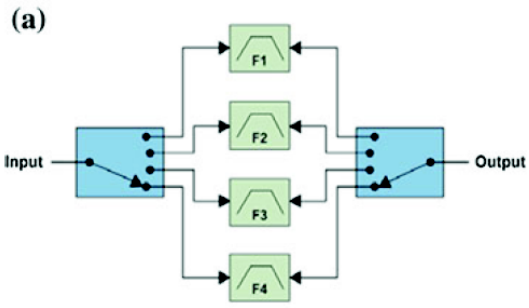

Figure 1-3: Filter bank[19]

Tuneable FBAR is a competitive candidate to replace this bank of filters with a single one. The choice of material and geometrical topology needs special attention. Resonator is biased via an external DC voltage, whereby materials properties and impedance curve will change. Shifting as

much as possible in frequency within the supported breakdown voltage of resonator medium is the focus of this work[19].

In order to provide a bandpass filter out of the impedance curve of the FBAR two or more resonators are coupled together. Resonating frequencies of the FBARs consist of both electric and acoustic domain giving the opportunity to couple these FBAR either acoustically or electrically. Topologies of electrical coupling are ladder and lattice topologies where resonators are acoustically isolated as in figure 2-25 and 2-26. Acoustic coupling isolate these resonators electrically and letting through only the acoustic waves via a non-conductive layer as in figure 2-31.

1.1 Structure of the report

The work flow of this thesis is divided into five chapters.

Chapter 2 introduces from the basis all properties of ferroelectric material accompanied with governing equations. Acoustic wave displacement inside the medium is also outlined in this section. Further more, FBAR investigation and all the physical consideration take place in this chapter.

Chapter 3 contains all the methodology and analytical models proposed for the improvement tuneability. In addition the quantity of electrical field inside the medium is also derived in this part. Analysis of acoustic coupling together with the impact of tuneability is described in the last part of this section.

Chapter 4 consist of simulation results acquired from different models. It starts with the simplest tuneable FBAR where its geometry has been extensively used today. In the next part are the results of the proposed structure and how is it beneficial for filter implementation. The impact of highly tuneable FBAR on acoustic coupling approach is simulated in this part.

Chapter 5 is the most important chapter where all the simulation data are discussed and analysed. This chapter is a very important since it contains the crucial point of this work together with all the challenges of the proposed structure. At the very end all the details are summed up shortly.

Chapter 2

Background

A coherent introduction of FBAR filter implementation is explained in this chapter.

2.1 Acoustic waves

Acoustic wave is a vibration of particles in a medium due to the variation in time of the applied stress. Differently from electromagnetic waves propagation into vacuum cannot be possible. Analytical analysis is simplified since this wave inherit classical mechanical properties (Newton's law, momentum etc) and wave phenomena (diffraction, interference). The quanta of acoustic wave is phonon[16]. Singular wavelengths with predefined levels of energy oscillate in this homogeneous medium. This assumption make this methodology easy to understand and analyse. Homogeneous material is a strict periodic repetition of atoms into a perfectly oriented geometric structure.

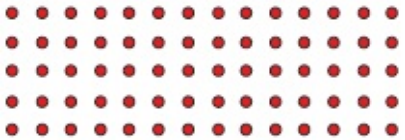

Figure 2-1: Homogeneous structure presentation[31]

Wherein displacement of an atom is rather predictable and governed accurately by a set of equations. Mechanical boundary conditions rely on the continuity of the stress and velocity at the interface for every dissimilar composition of a vibrating structure [37][10]. Acoustic particle itself is a small volume with dimension bigger than interacting space and smaller than the operation range of wavelength [16]. There numerous mode of wave propagation outlined into four basic subset.

- Longitudinal waves are driven by a compression and rarefaction in the same direction as the propagation.
- Shear (transverse) waves associate an angle between the direction of propagation and the acoustic particle displacement

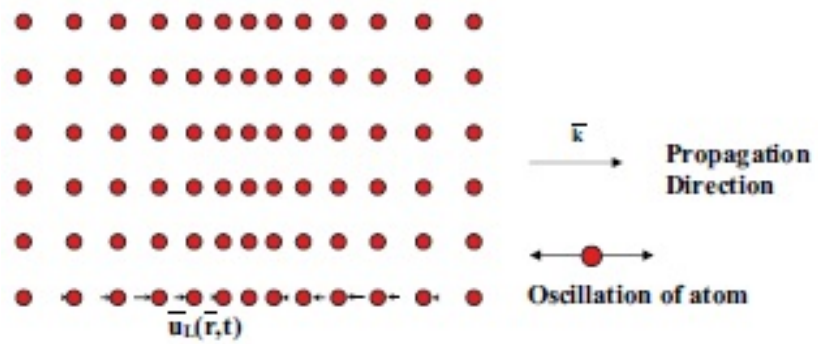

Figure 2-2: Longitudinal wave [31]

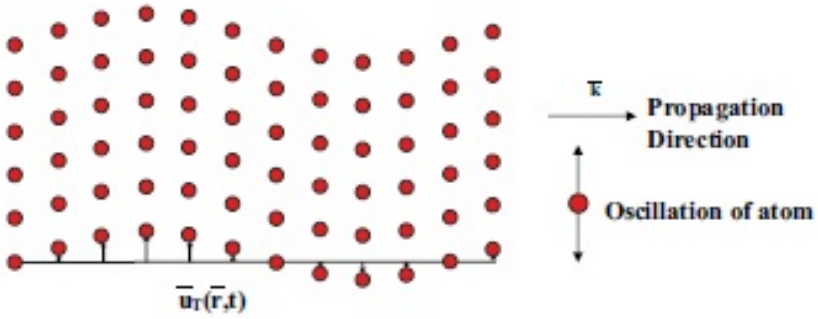

Figure 2-3: Shear (transverse) waves[31]

Solids can support both modes of propagation whereas liquids can handle only longitudinal propagation. Analogues to electromagnetic waves, the displacement is equationed as below respectively to the wave types:

$$\overrightarrow{U}_L(r,t) = Re\{\overrightarrow{U}_{LO}e^{i(\overrightarrow{k}_L\overrightarrow{r}-wt)} \quad (2.1)$$

$$\overrightarrow{U}_T(r,t) = Re\{\overrightarrow{U}_{TO}e^{i(\overrightarrow{k}_T\overrightarrow{r}-wt)} \quad (2.2)$$

$$\nabla^2\overrightarrow{U}_L = \frac{1}{c_L^2}\frac{\delta^2\overrightarrow{U}_L}{\delta t^2} \quad (2.3)$$

$$\nabla^2\overrightarrow{U}_T = \frac{1}{c_T^2}\frac{\delta^2\overrightarrow{U}_T}{\delta t^2} \quad (2.4)$$

$$k_T = |\overrightarrow{k}_T| = \frac{\omega}{c_T} \quad (2.5)$$

$$k_L = |\overrightarrow{k}_L| = \frac{\omega}{c_L} \quad (2.6)$$

Where $\overrightarrow{U}_L(r,t)$ and $\overrightarrow{U}_T(r,t)$ are displacement vector of longitudinal and shear mode, c_L and c_T are the velocity of each particle motion respectively to each mode, this is property of material and $\overrightarrow{k}_T$ and $\overrightarrow{k}_L$ are the wave vectors transverse and longitudinal mode respectively. This are the fundamental equations which will be the road map for analytical description of each wave. SAW and BAW are the predominant types of waves into a medium, whereby the two main microactuator technologies SAW filter and FBAR are based on. Practically these technologies employ two different types of waves therefore different behaviour was confirmed from each technology respectively to the operational frequencies [7].

- SAW occurs only at the interface of different materials[10].
- BAW where propagation occurs throughout all the mediums[10].

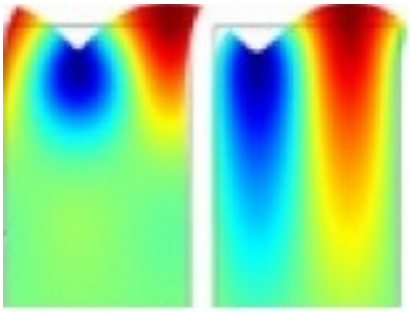

Figure 2-4: SAW mode[46]

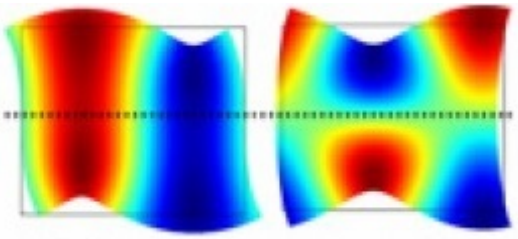

Figure 2-5: BAW propagation [46]

2.1.1 Governing equations

In order to uniquely identify an acoustic particle we need to take into consideration certain parameters. Particle velocity $v(r,t)$ from an applied pressure $p(r,t)$ into a density variation $\rho(r,t)$ can be spatially characterise at any time instance. In order to do this, motion equation, continuity equation together with the equation of state are the main set of equations which mathematically driving these physical properties[16].

Equation of motion

Applied force over a surface depends on the pressure distribution. Expressing change of velocity of moving particle due to applied force using Newton's second $F = mx$" law will lead to equation of motion. Having that $\frac{\delta v}{\delta t}$ describes the change of velocity of moving particle due to distribution of applied ∇p of material density ρ[16]. Hereby the Euler equation of motion is

$$\rho[\frac{\delta v}{\delta t} + (v\nabla)v] = -\nabla p \tag{2.7}$$

Continuity equation

Conservation of mass is related to velocity $v(r:t)$ density of the medium $\rho(r:t)$ over a volume V_0. The continuity equation for small shape describes the mass increase over a time δt inside the volume V_0 due to pressure P where $D = \nabla + \delta t$[16].

$$\frac{DP}{Dt} + \rho div(v) = 0 \tag{2.8}$$

Equation of state

This is an establishment of thermodynamic variables such as pressure p, velocity v into an adiabatic process. Given by Euler equation the variation of pressure and density are linked into equation [16]:

$$\frac{\delta \rho}{\delta t} + vgrad(\rho) = \kappa \rho_o[\frac{\delta p}{\delta t} + vgrad(p)] \tag{2.9}$$

where κ is the compressibility give by: $\kappa = \frac{1}{\rho_o}\frac{\delta\rho}{\delta p}$. These equations together with fundamental wave equation will be employed later in the design of acoustic coupling layers between two resonators.

2.2 Material properties

Physical characteristics define the operation of the resonator respective to the stiffness, piezoelectricity, dielectric constant, temperature and electrical field. Properties of different materials enable a variety of commercial applications. Electrostriction is a fundamental property of all dielectric material . When an external electric field is applied on the crystal lattice, a displacement of ions occurs. Positively charged ions will move along the direction of field whereas negatively charged ions will move opposite to the field direction. Collecting all this displacement throughout the bulk will result into a strain. This strain is proportional to the polarization driven by the formula in equation 2.10 and 2.11

$$u = QP^2 \qquad (2.10) \qquad\qquad P = P_s + \chi E \qquad (2.11)$$

In this case **u** is strain, **Q** is electrostriction coefficient [40][15]. Regarding polarisation P, it is the sum of spontaneous polarization P_s with the polarization due to an external electrical field E and χ is the susceptibility . Inserting equation 2.11 into equation 2.10 will lead to the full term of electrostriction equation [40]

$$u = QP_s^2 + 2QP_s\chi E + Q\chi^2 E^2 \qquad (2.12)$$

The first term represent the spontaneous strain, second term is the piezoelectric strain and the third term is the electrostrictive strain [15]

2.2.1 Piezoelectricity

Piezoelectricity is the most important features, enabling the electro-acoustic conversion through practical configuration. This is an invertible process composed by direct and inverse conversion of stress to charge. From the figures 2-6, 2-7, 2-8 a piezoelectric crystal under an applied stress displaces centrally located atoms, consequently imposing a net polarization within the unit volume. In order to avoid total cancellation individual instances within the crystal configuration, **must** contain only antisymmetric allocations of the molecules[33]. Polarization itself is a conceptual definition of total dipole moment over a unit volume $\overrightarrow{P} = \frac{\sum \overrightarrow{\mu}}{V}$. Whereas the electric dipole $\overrightarrow{\mu} = \overrightarrow{r}q$ from figure 2-6 is a vectorial representations of the opposing force within contrary charges.

Polarization is computed as sum of total charge over surface area, $P = \frac{Q}{A}$. This could be directly proportioned to stress via $P = d\sigma$. Whereas coupling electrical field into displacement known

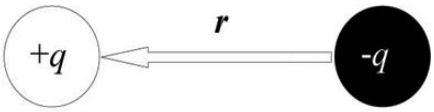

Figure 2-6: Dipole momentum within opposing charges [2]

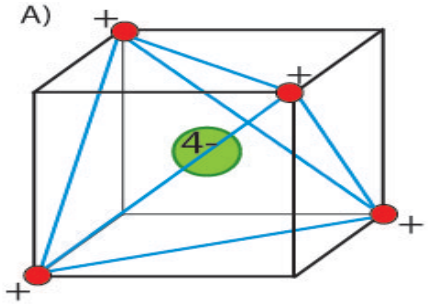

Figure 2-7: First positioning of the center [2]

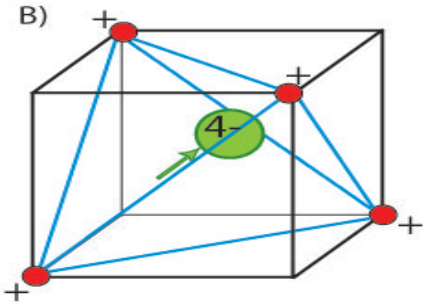

Figure 2-8: Displacement r imposing a momentum $\mu = rq$[2]

as inverse piezoelectric effect is $\epsilon = dE$. P is the total polarization and d in both cases is the piezoelectric coefficient of the material as a solid physical property, ϵ is the acquired strain and σ is the applied stress.

This conversion happens combined with both mechanical and electric effects take place during this conversion meaning an impact of both mechanical and electrical parameters simultaneously. An external inducers could be either force or electrical field. Electrical field E will impose an electrical charge density displacement in addition to strain, $D = \epsilon E$ and $S = \sigma E$. Likewise under an applied stress a piezoelectric crystal will remove and electrical displacement $D = \sigma T$ in addition to a strain respectively to Hook's law $S = sT$. Due to the linear behavior these effects are superimposed together at any instance of time and interpreted through these linear equation:

$$D_i = d_{ikl}T_{kl} + \epsilon^T_{ik}E_k \qquad (2.13)$$

$$S_{ij} = s^E_{ijkl}T_{kl} + d_{kij}E_k \qquad (2.14)$$

Components of these equations are tensors of different ranks. In table 2.1 and 2.2 are listed this items together with its mean.

	Quantity	Rank
d	Piezoelectric coefficient	3-rd
ϵ	Permittivity	3-rd
s	Compliance	4-th

Table 2.1: Physical parameters and tensor rank

	Quantity	Rank
D	Electric displacement	1-st
E	Electrical field	1-st
T	Stress	2-nd
S	Strain	2-nd

Table 2.2: Physical outcome and tensor rank

2.2.2 Pyroelectricity

Temperature is another important external inducer imposing relatively drift of the total net polarization. Named **pyroelectricity** this is a feature only for a subset of the piezoelectric group of materials[33]. Under heat transfer into the crystal structure, additional alignment of the dipoles occurs, deducing the total charge of individual unit cells. Increase of temperature above the **Curie**

point place all the atoms into a perfect central symmetry and therefore cancelling out piezoelectric effect down to zero.

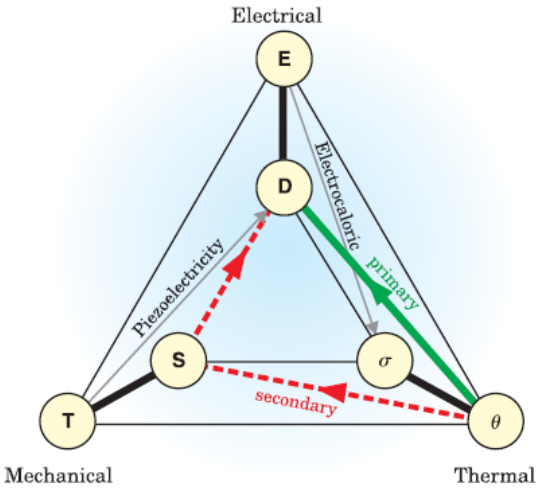

Figure 2-9: Heckman diagram [26]

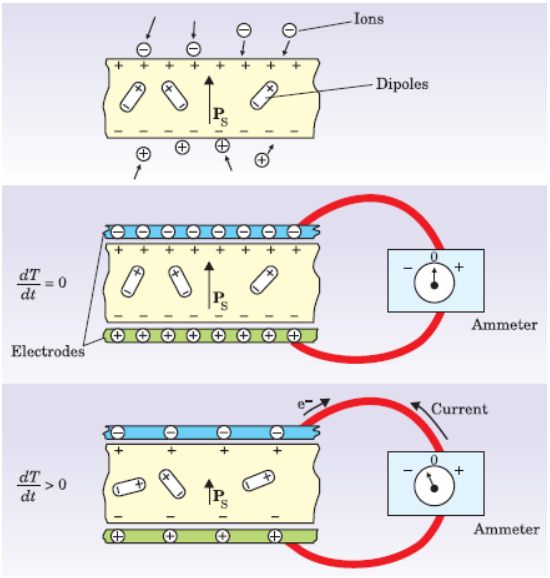

Figure 2-10: Pyroelectricity from heat transfer [26]

Pyroelectric material differ spontaneous polarization **P** proportional to change of temperature where ΔT as in equation 2.15

$$\Delta P = \mathbf{p}\Delta T \tag{2.15}$$

Consequence of the heat transfer into the crystal lattice is observed from the figure 2-9 as the primary impact is the electrical displacement together with a direct strain. A driven current is observed under a positive gradient of temperature in figure 2-10.

2.2.3 Ferroelectricity

Further observation outcomed another important categorisation among pyroelectric materials. Ferroelectric material which are the mainstream of this work towards the highly tunable FBAR filters.

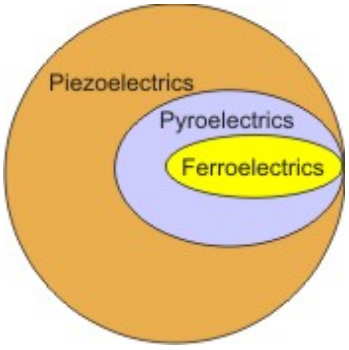

Figure 2-11: Hierarchical properties [1]

Sustaining all the previously discussed properties a Vernier diagram and an outline of the hierarchical behaviour is figure 2-11 were ferroelectricity is an intersection of all three sets. Opposing the direction of the spontaneous polarization via an external electrical field is the ability possessed only by ferroelectric materials. Remanent polarization is another important feature of this process relating electrical field E and polarization P into a hysteresis relation curve occurring below the Curie temperature in the figure 2-12.

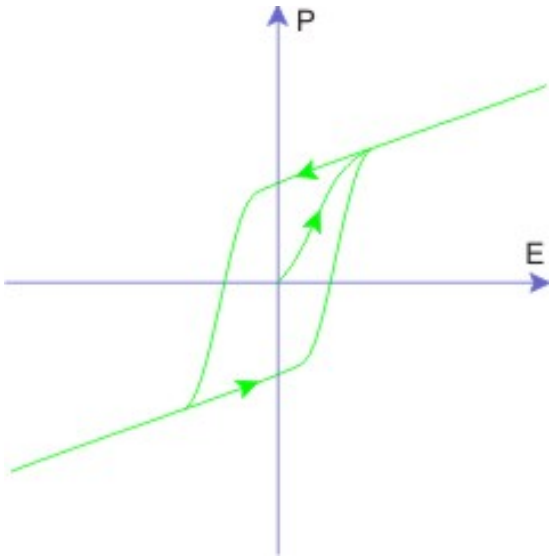

Figure 2-12: P-E hysteresis relation [1]

$$D_i = d_{ikl}T_{kl} + \epsilon^T_{ih}E_k + P^r_i \tag{2.16}$$

$$S_{ij} = s^E_{ijkl}T_{kl} + d_{kij}E_k + S^r_{ij} \tag{2.17}$$

Extension of piezoelectric equations[35]

Electrical field at the onset will polarise the crystal by aligning dipoles, afterwards this field gradually is decreased to zero whereby remanent polarization is observed in figure 2-12. Adding this remanent polarization together with stress equations 2.13,2.14 will give the extension of ferroelectric constitutive equation 2.16,2.17 . Decreasing negatively the electrical field will inverse the direction of the polarization. Dielectric permittivity has a quadratic dependence from the applied electrical field as a result making this materials practically tunable [6]. Through the remanent polarization this can be used to memorise logical 1 and 0 bits in digital circuit. This is applied only below the Curie temperature.

In the equation 2.18 $\epsilon_0 = 8.85 * 10^{-12} F/m$ is the permittivity of free space, β is a coefficient from the free energy expansion of the Landua theory [8]. In addition C us the Curie-Weiss constant and T_C is the phase transition (Curie) temperature [6]. The tuneability is defined in equation 2.20. Above the Curie temperature this material can be utilized as tunable microwave device [6]. In principal, ability of being tuned is defined as permittivity at zero electrical field over specific permittivity at applied electrical field equation 2.20. Slightly below the Curie point dielectric constant behaves very much dispersive thus the system is undesirably sensitive to the temperature. Overcoming this drawback, material is approached just above Curie temperature. Tuning this material into this temperature range is much more practical.

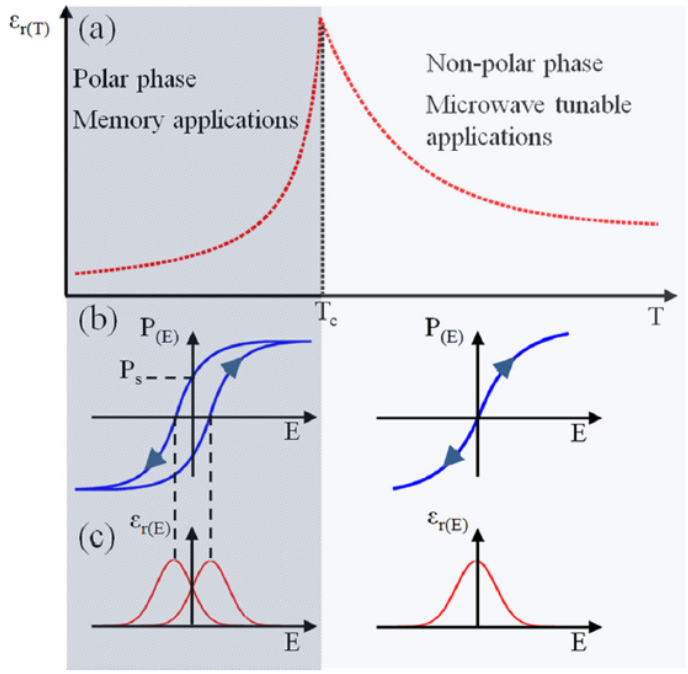

Figure 2-13: P-E hysteresis relation [6]

$$\epsilon_r(E,T) = \frac{\epsilon_r(0,T)}{1 + 3\beta\epsilon_o^3\epsilon_r^3(0,T)E^2} \tag{2.18}$$

$$\epsilon_r(0,T) = \frac{C}{T - T_C} \tag{2.19}$$

$$n = \frac{\epsilon(0)}{\epsilon(|E| \neq 0)} \tag{2.20}$$

2.3 Resonator

Adapting many terminologies from optics, acoustic resonators are promising approaches for highly selective filters. Basis of this technology starts with the four main principal requirements[24]:

- Low insertion losses
- Q factor
- Sufficient coupling coefficient
- Free spurious resonances

Consider a bulk medium locked by two electrodes on both sides. It will resonate on thickness extension mode via an AC applied voltage which has an impedance curve as in figure 2-15.

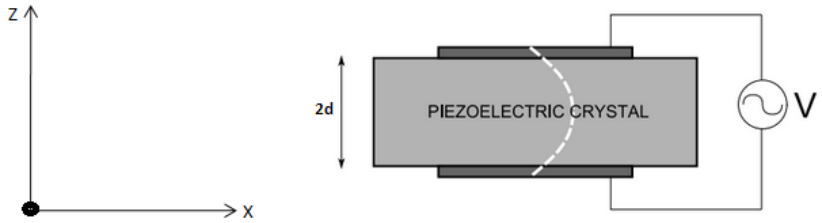

Figure 2-14: Acoustic particle profile displacement [48]

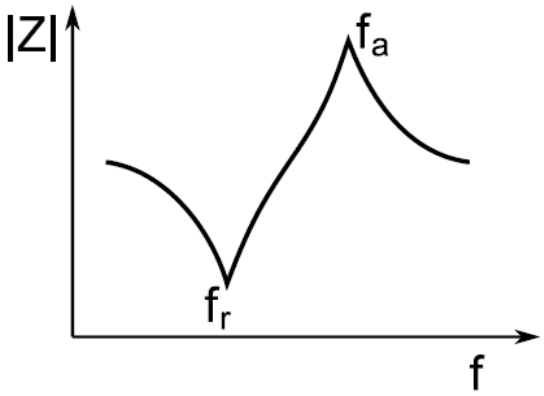

Figure 2-15: Impedance curve[48]

Mechanical resonating is a coherent action of displacement arising from applied stress, where both displacement and stress are conditioned at the boundaries of the resonator[37].

The distribution of stress is goes from zero at the edges of the resonator to the maximum value in the center of the medium. Both sides of the resonator under the applied electric field will displace

$$T(z) = \frac{eD}{\epsilon^s}\left\{\frac{cos(kz)}{cos(kd)} - 1\right\} \quad (2.21) \qquad U(z) = \frac{eD}{c^D\epsilon^S k}\frac{cos(kz)}{cos(kd)} \quad (2.22)$$

the ions to the center, therefore the contribution of each will result in the maximum stress when they reach the center. The reason that we have zero stress at the edges is that ions sitting at the edge are the first which are being pushed therefore there is no mechanical stress at this point. Regarding the displacement follow the a similar pattern to stress with nonzero values at the edges of the resonator. However the displacement is still minimum at the edges. Material capability of conveying mechanical energy to electrical is defined from the piezoelectric constitutive equations 2.24 and 2.25 as the capability of electro-acoustic conversion 2.23,

$$K_t = \frac{e^2}{c^E\epsilon^s} \quad (2.23)$$

$$T = c^E S - eE \quad (2.24)$$

$$D = eS + \epsilon^s E \quad (2.25)$$

FBAR is capable of simulating a capacitor where impedance profile over the frequency spectrum behaves in correspondance to the physical properties of dielectric medium. Again from the equation 2.24 and 2.25 electrical field is acquired as a function of stress **T** and electric displacement **D** as in the equation 2.26. Further voltage imposed within the plates is proportioned to the geometry and physical properties of the FBAR equation 2.27 and [21]:

$$E(z) = -\frac{e}{c^D\epsilon^s}T(z) + \left\{\frac{1}{\epsilon} - \frac{e^2}{c^D\epsilon^{s2}}\right\}D \quad (2.26) \qquad V = \int_{-d}^{+d} E(z)d(z) = \frac{2dD}{\epsilon^s}\left\{1 - \frac{e^2}{c^D\epsilon^s}\frac{tan(kd)}{(kd)}\right\} \quad (2.27)$$

Correlation of resistance profile with frequency domain draws the transfer function of the FBAR and the analytical expression is in equation 2.29. It measures the oppose of current $I = jwAD$ flowing through medium over different operational frequencies. In this case A is the cross-section surface of the FBAR.

$$Z = \frac{V}{I} = \frac{2dD}{\epsilon_0 jwAD}\left\{1 - K_t^2\frac{tan(kd)}{kd}\right\} \quad (2.28)$$

$$Z = \frac{V}{I} = \frac{1}{jwC_0}\left\{1 - K_t^2\frac{tan(kd)}{kd}\right\} \quad (2.29)$$

$$K_t^2 = \frac{e^2}{c^D\epsilon^s} \quad (2.30)$$

$$C = \frac{\epsilon_0 2d}{A} \quad (2.31)$$

$$kd = \frac{\pi}{2}\frac{\omega_r}{\omega_{a,0}} \quad (2.32)$$

In this expression $2d$ is the thickness of the resonator, k is a propagation constant, ω_r is the resonance frequency and $\omega_{a,0} = (n+1)\frac{\pi}{2}\frac{v}{d}$ is the antiresonance frequency. Resonance frequency (series) 2.38 and anti-resonance (parallel) 2.33 frequencies are the two main properties of the resonator corresponding at the minimum and maximum impedance respectively.

BVD model is a electrical RLC circuit representing the impedance. It facilitate the analysis through existing methodologies of electric circuit analysis. In figure 2-17 is a simple circuit model

$$|Z| = 0 \tag{2.33}$$

$$tan(\frac{\pi}{2}\frac{w_r}{w_{a,0}})(\frac{\pi}{2}\frac{w_r}{w_{a,0}})^{-1} = \frac{1}{K_t^2} \tag{2.34}$$

$$K_t^2 = cot(\frac{\pi}{2}\frac{w_r}{w_{a,0}})(\frac{\pi}{2}\frac{w_r}{w_{a,0}}) \tag{2.35}$$

$$K_t^2 \approx \frac{\pi}{4}^2 \frac{f_a^2 - f_r^2}{f_a^2} \tag{2.36}$$

$$f_r = \frac{2}{\pi} f_a \sqrt{(\frac{\pi^2}{4} - K_t^2)} \tag{2.37}$$

$$|Z| = \infty \tag{2.38}$$

$$kd = (2n+1)\frac{\pi}{2} \tag{2.39}$$

$$\frac{w_a}{v}d = (2n+1)\frac{\pi}{2} \tag{2.40}$$

$$2\pi f_a = (2n+1)\frac{\pi}{2}\frac{v}{d} \tag{2.41}$$

$$f_a = \frac{v}{2 * d} \tag{2.42}$$

$$f_a = \frac{\sqrt{c}^D}{2 * d\sqrt{\rho}} \tag{2.43}$$

Figure 2-16: Resonance and antiresonance frequency derivation

utilized to simulate FBAR loss free impedance behavior.

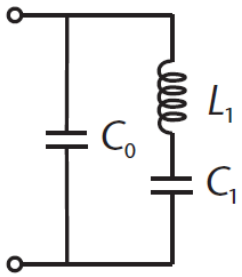

Figure 2-17: BVD model[45]

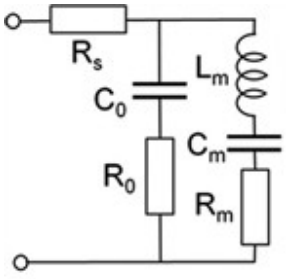

Figure 2-18: mBVD model[45]

$$Z_{mBVD}(w) = R_s + \left\{ \frac{1}{R_0 + \frac{1}{jwC_o}} + \frac{1}{R_m + j(wL_m - \frac{1}{wC_m})} \right\}^{-1} \tag{2.44}$$

$$Z_{BVD}(w) = \frac{j(wL_1 - \frac{1}{wC1})}{1 - w^2 C_0 L_1 + \frac{C_0}{C_1}} \tag{2.45}$$

BVD model has a theoretical zero damping factor which is an ideal implementation, consequently a modified BVD circuit in figure 2-18 is introduced with an overall nonzero damping. The quality factor of in resonance and antiresonance frequency is respectively in equation 2.46 and equation 2.47 [45]:

In here an important correlation is the proportionality of gradient of the impedance phase ϕ. This is an important derived parameter for the selectivity of different filter topologies [25]. The higher the quality factor the better the selectivity of the filter. Quality factor has an interpretation as the ratio of energy lost over the energy conveyed throughout a period.

2.3.1 Electro acoustic conversion

Conversion efficiency is driven under two main coefficients:

Conservation of energy is represented as a decomposition of three main forms [13],

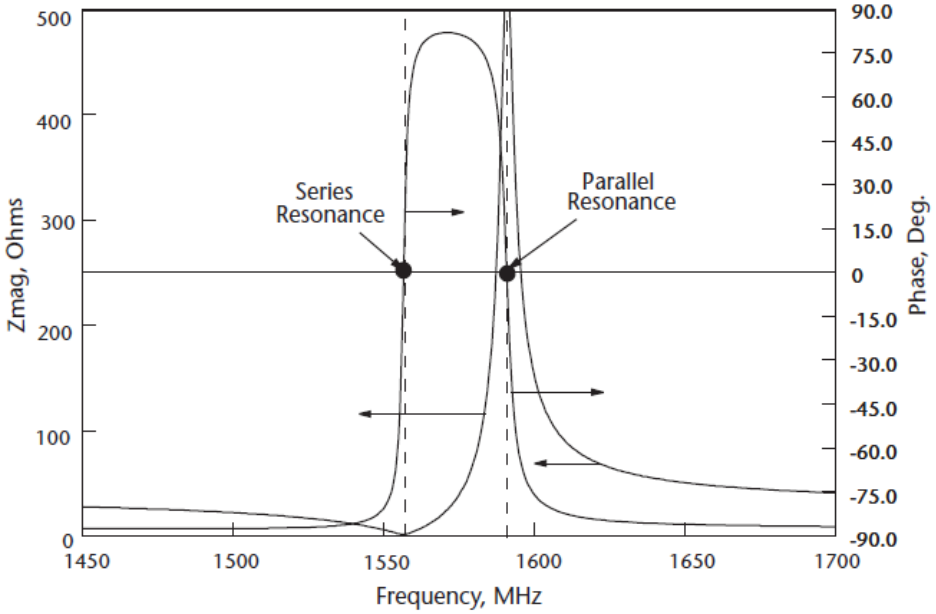

Figure 2-19: Phase and impedance profile of a FBAR[21]

$$Q_r = -\frac{1}{2}\omega_r \frac{\delta\phi_r}{\delta\omega} \qquad (2.46)$$

$$Q_a = -\frac{1}{2}\omega_a \frac{\delta\phi_a}{\delta\omega} \qquad (2.47)$$

Material-coupling coefficient: $K^2 = \frac{e^2}{c^E \epsilon^s}$. Effective coupling:$K^2_{eff} = \frac{\pi}{2}\frac{f_s}{f_p} cot \frac{\pi}{2}\frac{f_s}{f_p} = \frac{U_m^2}{U_e U_d}$.

- Mechanical vibration:$U_m = \frac{1}{2}\int_V TS^E TDV$
- Electrical oscillation:$U_e = \frac{1}{e}\int_{V_{bulk}} E\epsilon^T EdV$ Effective coupling: $K^2_{eff} = \frac{U_m^2}{U_e U_d}$.
- Mutual energy: $U_M = \frac{1}{2}\int_{V_{bulk}} (TdE + EdT)dV$

Figure 2-20: Coupling coefficient

V_{bulk} is the piezoelectric volume, V is the whole FBAR volume of electrode together with bulk. All the derivation so far were acquired under the assumption of infinitely small thickness of the electrodes. Taking into account a finite thickness lead to a modified derivation of the essential parameters such as coupling coefficient and resonance frequency [21]

$$k^2_{eff,n} = \frac{e^2}{\epsilon^s c^E}\frac{8}{\pi^2}\frac{cos^2\{(2n+1)^2\frac{\pi}{2}\frac{t}{d+t}\}}{(2n+1)^2(1-\frac{t}{d+t})} \qquad (2.48)$$

$$\omega_{a,n} = (2n+1)\frac{2\pi}{2}\frac{v}{d+t} \qquad (2.49)$$

Equation 2.49 is derived under the assumption of the same stiffness coefficient of electrodes and piezoelectric medium.

Since FBAR operation has the main goal trapping the resonating energy as much center as possible, many leakages arise including here:

- Electrical power dissipation due to finite Ohmic resistance of the electrodes conductors
- Acoustical attenuation from the material inelastic absorption or heat conversion.

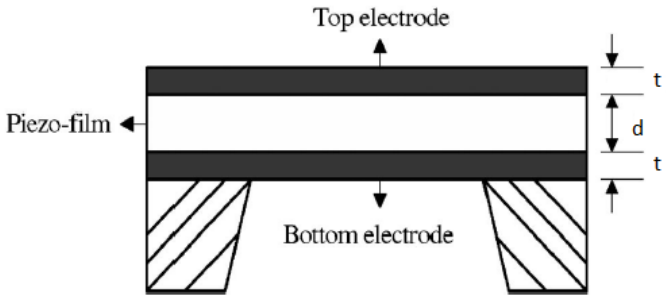

Figure 2-21: Finite thickness electrodes [47]

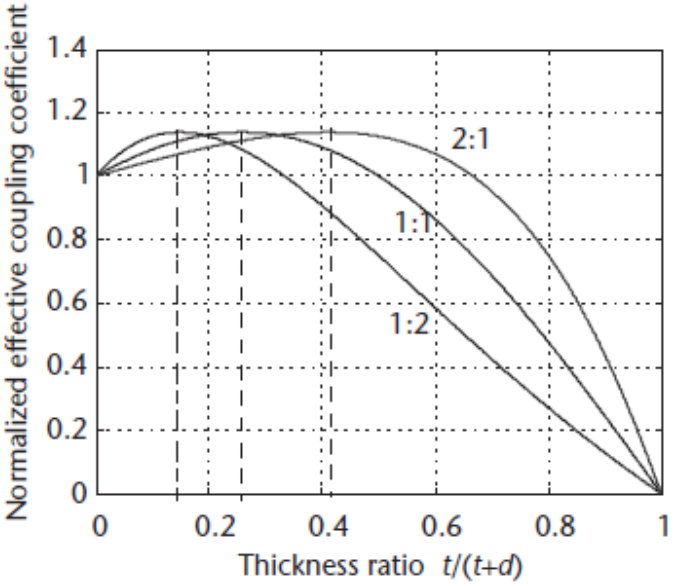

Figure 2-22: Impact of electrode thickness on electro acoustic coupling[21]

- Leaking waves are a combination of finite impedance mismatch of interfaces, shear wave generation or waves escaping on the lateral boundaries.

These phenomena superimpose together and acting as a combined loss mechanism [42]. A more consistent derivation of quality factor is equation 2.50 where E_i is the loss of respectively mechanism. Whereas Q_i is the quality factor in correspondence to individual loss mechanism [20]. A figure of merit is conducted here through equation 2.51.

$$\frac{1}{Q_{tot}} = \frac{1}{E_{tot}} \sum_i \frac{E_1}{Q_i} \tag{2.50}$$

$$FOM = k_{eff} Q_{tot} \tag{2.51}$$

Spurious mode are important phenomena taken into account when designing high efficient resonator. The main source of this phenomena is the finite dimension of the resonator where reflection of unwanted waves occurs on the interface of the bulk with the outer part. This are just another resonance conditioning into an undesirable frequency. This unwanted resonating condition steal some of the energy that was meant for the main mode lower down the quality factor[43]. This arise mainly from the standing Lamb waves in the active area of the resonator[23] and from the finite boundaries of the device [18]. These appear as narrow-band ripples effects in the impedance and phase diagram relatively close to the resonance frequencies. Suppression of these modes is mainly achieved by tuning the dispersion diagram [18][37]. Many geometrical design are being proposed for this [20],[29] however this is an ongoing research area.

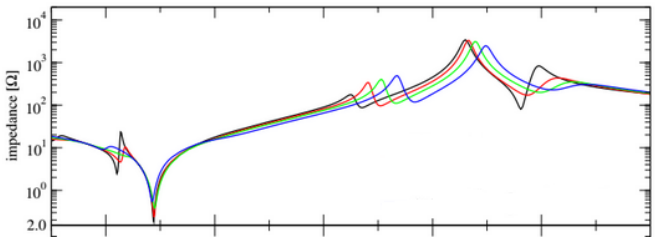

Figure 2-23: Impedance with spurious[43]

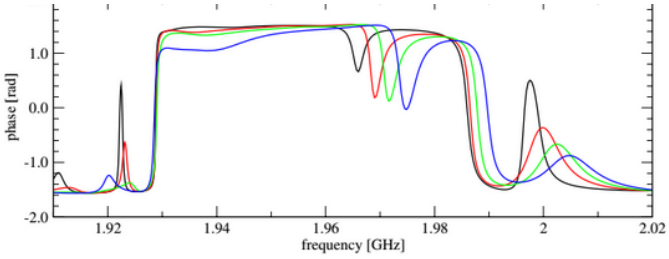

Figure 2-24: Phase with spurious [43]

2.3.2 Filter topologies and tuning

FBAR are IC-compatible technologies with a very promising properties in RF filter implementation. Two main topologies ladder figure 2-25 and lattice figure 2-26 aim a bandpass transfer function filter. Their operation is consistent to the impedance frequency characteristic.

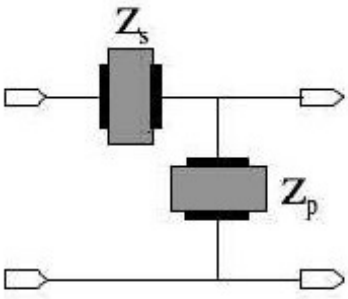

Constrains:

- Point 1 $Z_p \approx 0$
- Point 2 $Z_p \approx \infty$
- Point 2 $Z_s \approx 0$
- Point 3 $Z_s \approx \infty$

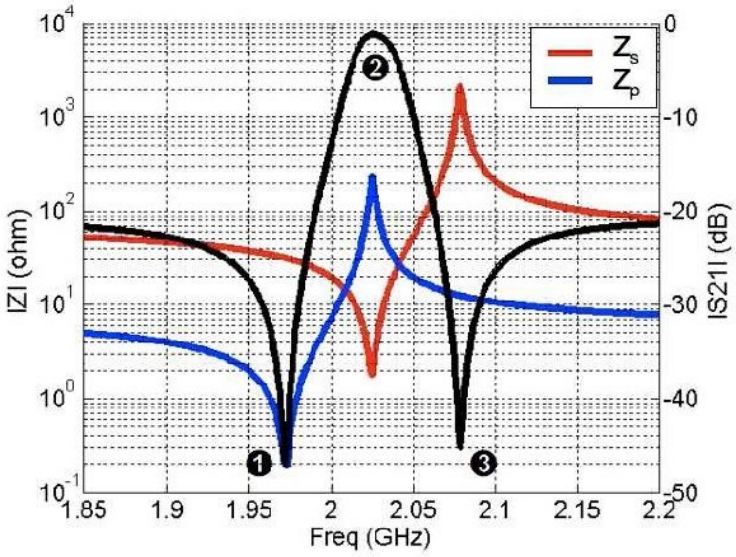

Figure 2-25: Ladder topology[14]

For a signal with frequency lower than the resonance frequency of the series FBAR it sees a very high impedance towards the ground. It is very similiar behavior when the frequency risies above the resonance frequency for the series FBAR to the anti-resonance frequency of the shunt FBAR. In this range the signal feels a very low impedance towards the ground. This is the region of our interest and as one of the main task this needs to be adjustable rather than static through an external our interest which will be let through. When the signal has a frequency higher than the antiresonance of the shunt FBAR it faces again a very high impedance towards the ground [24],[21]. In order to get a higher out of band rejection many stages could be placed in series. Employing ferroelectric material as medium onto FBAR makes it practically tunable [12] via a DC bias external voltage figure 2-27. Extensive research has been done on the physical properties of barium strontium titanate (BST) [5],[6], fabrication technologies [30] characterisation techniques for composition, structural properties and other relevant features to the application [11],[44]. Structural gradient strategies [4],[32] or

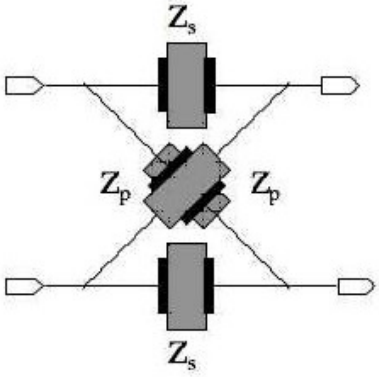

Constrains:

- Point 1 $Z_s = Z_p$
- Point 2 $Z_p Z_s = Z_o^2$
- Point 3 $Z_p Z_s = Z_o^2$
- Point 4 $Z_s = Z_p$

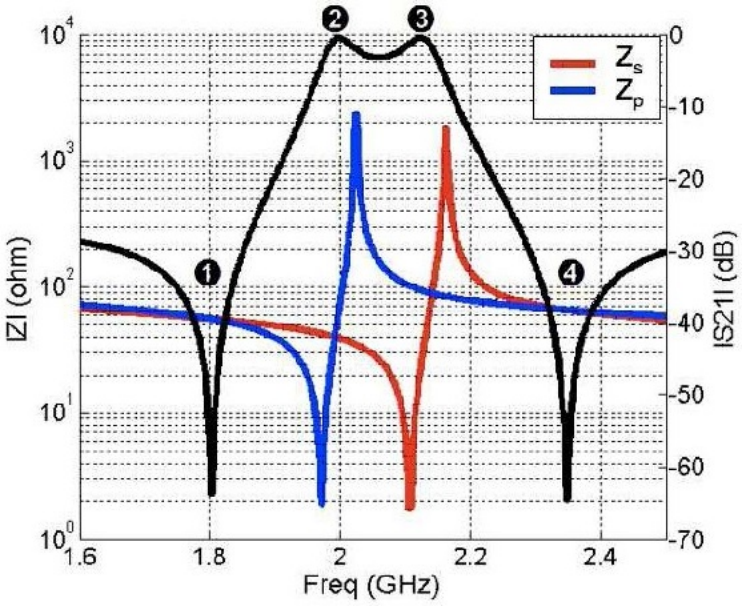

Figure 2-26: Lattice topology[14]

different doping concentration [27],[8] in enhancing tunability.

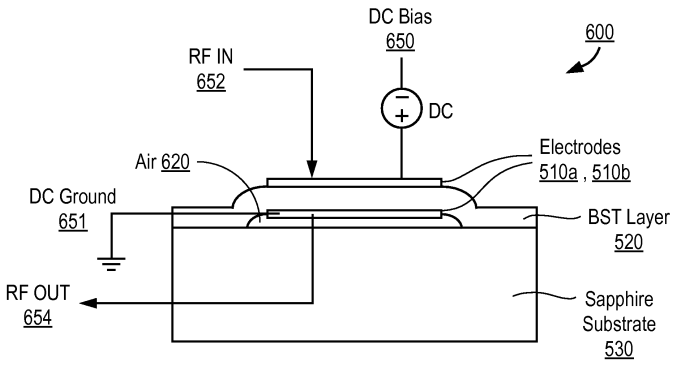

Figure 2-27: Tunable resonator[12]

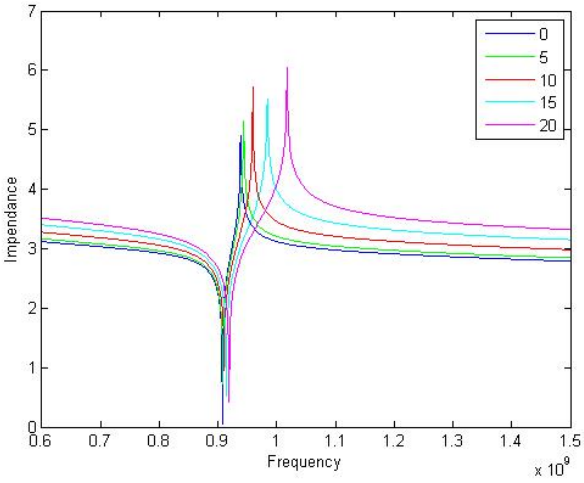

Figure 2-28: Tuneability of impedance profile

A strong electrical field perpendicular to the medium is used to tune dielectric constant[6],

$$\epsilon_r(E,T) = \frac{\epsilon_3(0,T)}{1 + 3\beta\epsilon_o^3\epsilon_r^r(0,T)E_{DC}^2} \tag{2.52}$$

electrostriction coefficient[9],

$$e(E) = e_{E=0}(1 + \mu E) \tag{2.53}$$

and elastic constant[21]

$$c^D(E) = c^E + \frac{e(E)}{\epsilon(E)} \tag{2.54}$$

These three parameters change differently the impedance profile for different operational frequency.

$$Z(E) = \frac{1}{jwC_0}\left\{1 - \frac{e^2(E)}{c^D(E)\epsilon_r(E)}\frac{tan(kd)}{kd}\right\} \tag{2.55}$$

Different material parameter ϵ, e, c^D have different contribution on the tuneability of the impedance. The two main restriction in tuning FBAR are the breakdown voltage of the ferroelectric material and the maximum operational voltage of circuit board.

2.3.3 Acoustic coupling

Coupling different FBAR in order to bring up a filter topology is another crucial point. It is possible to be done either electrically such as ladder and lattice schematic or acoustically. Coupling acoustically FBAR means conveying the energy from one resonator to the other via mechanical waves. Since FBAR operates mainly on thickness extension mode,[36] coupling among resonators is be done via thickness extension as well as in figure 2-29.

Figure 2-29: Stack resonator filter[36]

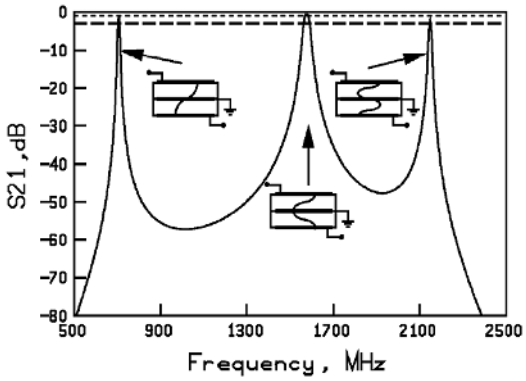

Figure 2-30: Response of filter [36]

Stack resonator filter SRF is the first topology proposed at [38] where its proximity will actuate non evanescent acoustic waves to the proximity of other resonator. Response of this structure gives a maximum transmission for half wavelength of the whole structure corresponding to the first point. Half wavelength of each resonator gives the second point and three half wavelength across the whole structure for the last peak in figure 2-30. In order to make these two resonators electrically isolated a non-conductive acoustic coupling layer separate these resonators as in figure 2-31. This topology called coupled resonator filter CRF acts as a two port filter with an equivalent circuit figure 2-32.

Coupling layer in the figure 2-31 is considered as an perfect matching layer where it transmission efficiency is described by the equation 2.56 [16]. Herein the Z_{01},Z_{02} are the acoustic impedance of the upper and lower part of the coupler layer whereas Z_{03} is the acoustic impedance of the coupler layer itself. In order to define the acoustic impedance of an multiple layer structure a delay line approach will be employed. Using equation 2.57 where γ_i is the propagation constant first layer Z_i

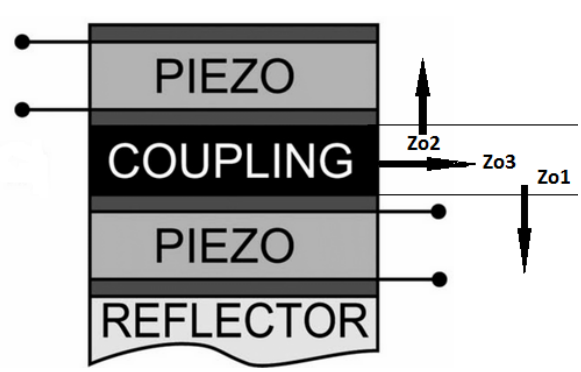

Figure 2-31: Couple resonator filter[38]

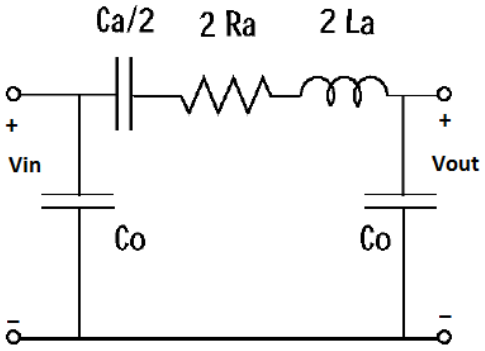

Figure 2-32: BVD model [38]

is acoustic impedance of the first layer and Z_l is the acoustic impedance of the layer attached and t_i is the thickness of the layer. A more detailed recursive method for equivalent acoustic impedance will be treated on the next chapter.

$$T = \frac{4Z_{03}Z_{01}}{(Z_{01}+Z_{03})^2 cos(\theta)^2 + (Z_{02} + \frac{Z_{01}Z_{03}}{Z_{02}})^2 sin(\theta)^2} \quad (2.56) \qquad Z_{in} = Z_i \frac{Z_i + Z_L tan(\frac{2*\pi}{\lambda} t_i)}{Z_L + Z_i tan(\frac{2*\pi}{\lambda} t_i)} \quad (2.57)$$

A resonator respond consistently to the frequencies of the signal that excite the input electrode. The outcome signal depends on its frequency and the resonance and antiresonance frequency of the resonator. The energy accumulated on the second electrode is composed of electrical and mechanical oscillation. In order to convey this further to second resonator there are choices of doing it, which are electrically and acoustically. Further more this signal will pass through another resonator where frequency components of the signal face another impedance profile. Those frequencies who will not survive both resonators will be filtered out and the remaining will form the band pass filter as in figure 1-2. Making possible for this signal to go throughout two resonators via acoustic wave will offer big advantages. Owing good energy transfer, acoustically coupling will be used to overcome generalised pole-zero nature of electrical coupled filters [24]. Moreover there is no constrain applied in this case regarding the resonance and anti-resonance frequency of each resonator as in ladder and lattice topology figure 2-25 and figure 2.3.2. This approach however has a drawback which stands for the coupling layer. This medium has distinct properties such as thickness, acoustic impedance, elastic constant. All these parameters combined together will driver from one resonator to another only certain frequencies therefore the bandwidth of the filter will be bounded to the range of frequencies which could be coupled. This was not present on the electrical coupling since the electric wire can guide much wider range of frequencies compare to acoustic medium. A methodology will be developed on the next chapter in order to optimise the coupling via multiple distinct piezoelectric layers.

Chapter 3

Methods and Implementation

This chapter contains the method developed to improve the tuneability of the tuneable FBAR.The model is a simple multilayer medium and it is brought up into a analytical description. In addition, the interaction of the electrical field is investigated since it is the key driver for the the tuning process. In addition to this acoustic coupling is discussed together with the variation that comes from the tuneability. This is a very promising topology where tuneability will impact its performance significantly.

3.1 Tuneability of FBAR

Tuning a FBAR via a DC external voltage is an outcome of interaction between electrical field and atoms of the medium. This will result in a displacement in the same direction of the resonance and antiresonance frequency figure 2-28. Tunable FBAR aim to replace bank of filters with a single tuneable filter. The first challenge of this goal is the different rate of tunability for resonance and antiresonance frequency. This could be pointed out even from the figure 2-28. The key drivers of ferroelectric material are dielectric permittivity , stiffness constant c_D and piezoelectric coefficient e. There are several proposal in enhancing piezoelectricity [32] which will lead to better tuneability. These are mostly constrained on the fabrication technology and deposition process.

$$\frac{df_a}{dE} = \frac{d}{dE}\left\{\frac{\sqrt{c}^D(E)}{2 * d\sqrt{\rho}}\right\} \tag{3.1}$$

$$\frac{df_r}{dE} = \frac{d}{dE}\left\{\frac{2}{\pi} f_a(E)\sqrt{\frac{\pi^2}{4} - K_t^2(E)}\right\} \tag{3.2}$$

Tuneability rate is defined from the derivative of f_a f_r with respect to electrical field as in the equation 3.2 and equation 3.1. These are plotted for a range of values in figure 3-1 and figure 3-2 and the simulation model is in A.1. An increase of piezoelectric coefficient and decrease of dielectric permittivity lead to a high rate of tuneability for both resonance and antiresonance rate. BST is a very sensitive material depending drastically on the stoichiometry, temperature and technology of

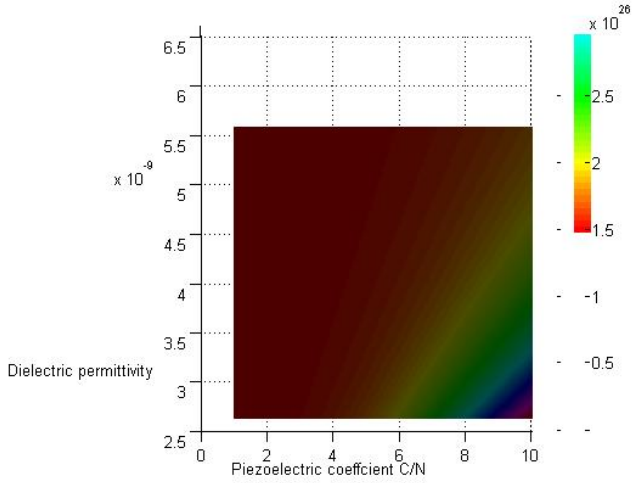

Figure 3-1: Resonance rate

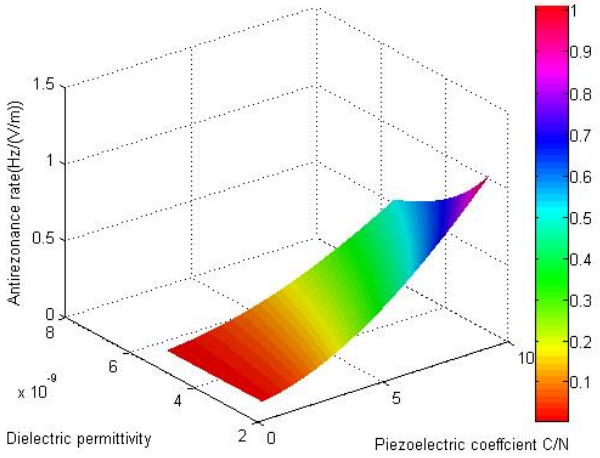

Figure 3-2: Antiresonance rate

deposition [44]. However there is still a lot of space of performance improvement via geometrical optimisation. Most of the tuneable FBAR studies are based on homogeneous ferroelectric medium. A double layer of two different ferroelectric material is studied. The homogeneous structure has already been analysed in the previous chapter. At the very end the impedance profile equation is:

$$Z = \frac{V}{I} = \frac{1}{jwC_0}\left\{1 - K_t^2 \frac{tan(kd)}{kd}\right\} \tag{3.3}$$

Composite structure

In composite structure the situation is very similar to homogeneous since the electrical and mechanical boundary conditions are similar. This is a simple 1D model thereby we will consider the boundary condition only in one dimension. In addition the electrodes need to be considered infinitely thin in order to simplify the analysis of the model. Notation of each materials properties are in table 3.1.

Properties	First	Second
Dielectric permittivity	ϵ_1	ϵ_2
Piezoelectric coeff	e_1	e_2
Stiffness coeff	c_1^D	c_2^D
Wave vector	$k_1 = \frac{w}{v_1}$	$k_2 = \frac{w}{v_2}$

Table 3.1: Properties of each medium

Further more mechanical properties are listed in table 3.2 and electrical properties are listed in table 3.3 .

Moving on the mechanical boundary condition at each junction of the composite FBAR located at the z axis, $z = 0$, $z = d_1$, $z = d_2$. At $z = 0$ we have the continuity of stress and displacement whereas the side attached to the electrodes are stress free.

When there is an applied voltage over the electrodes, there is no accumulation of charges through-

Properties	First	Second
Displacement	$u_1(z)$	$u_2(z)$
Stress	$S_1(z)$	$S_2(z)$
Strain	$T_1(z)$	$T_2(z)$

Table 3.2: Properties of each medium

Properties	First	Second
Electric displacement	$D_1(z)$	$D_2(z)$
Electrical field	$E_1(z)$	$E_2(z)$
Voltage	$V_1(z)$	$V_2(z)$

Table 3.3: Electric properties

$$u_1(0^+) = u_2(0^-) \quad (3.4) \qquad T_1(0^+) = T_2(0^-) \quad (3.5) \qquad T_2(-d_2) = T_2(d_1) = 0 \quad (3.6)$$

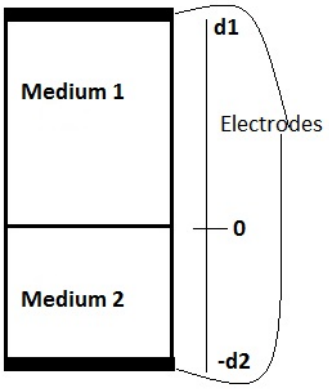

Figure 3-3: Composite ferroelectric medium

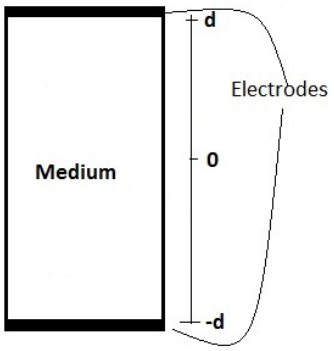

Figure 3-4: Homogeneous medium

out the inner part of the medium. Moreover over the Gaussian law takes place throughout the whole structure $\bigtriangledown D_1 = 0$ $\bigtriangledown D_2 = 0$. The currebt going through the series of resonators will also be the same $j\omega A D_1 = j\omega A D_2$ this is translated into this equality $D_1 = D_2$. Displacement is a simple wave equation different in respective medium as in equation 2.56. For further simplicity time dependent part is omitted and the result is the equation 3.8.

$$u_{1,2}(z,t) = \{a_{1,2}sin(k_{1,2}z) + b_{1,2}sin(k_{1,2}z)\}e^{-jwt} \quad (3.7)$$

$$u_{1,2}(z) = a_{1,2}sin(k_{1,2}z) + b_{1,2}sin(k_{1,2}z) \quad (3.8)$$

From the piezoelectric constitutive equations stress is in equation and strain is a derivate of displacement. Stress distribution over the z direction will therefore be:

$$T_{1,2}(z,t) = c_{1,2}S_{1,2} - \frac{e_{1,2}}{\epsilon_{1,2}}D \quad (3.9) \qquad S_{1,2}(z) = \frac{d\{u_{1,2}(z)\}}{dz} \quad (3.10)$$

$$T_{1,2}(z,t) = c_{1,2}k_{1,2}\{a_{1,2}cos(k_{1,2}z) - b_{1,2}sin(k_{1,2}z)\} - \frac{e_{1,2}}{\epsilon_{1,2}}D \quad (3.11)$$

There are four coefficient a_1 a_2 b_1 b_2 from the equation 3.7 that needs to be defined. This will be solved by employing fours mechanical boundary condition at equations 3.4, 3.5, 3.6. The system of equations with four equation of boundary conditions will give:

The final boundary condition are:

$$c_1k_1\{a_1cos(k_1z) - b_1sin(k_1z)\} - \tfrac{e_1}{\epsilon_1}D = c_2k_2\{a_2cos(k_2z) - b_2sin(k_2z)\} - \tfrac{e_2}{\epsilon_2}D \qquad z = 0$$

$$a_1sin(k_1z) + b_1cos(k_1z) = a_2sin(k_2z) + b_2cos(k_2z) \qquad z = 0$$

$$c_1k_1\{a_1cos(k_1z) - b_1sin(k_1z)\} - \tfrac{e_1}{\epsilon_1}D = 0 \qquad z = d_1$$

$$c_2k_2\{a_2cos(k_2z) - b_2sin(k_2z)\} - \tfrac{e_2}{\epsilon_2}D = 0 \qquad z = -d_2$$

$$c_1k_1\{a_1\} - c_2k_2\{a_2\} = \frac{e_1}{\epsilon_1}D - \frac{e_2}{\epsilon_2}D \tag{3.12}$$

$$b_1 = b_2 \tag{3.13}$$

$$c_1k_1\{a_1cos(k_1d_1) - b_1sin(k_1d_1)\} = \frac{e_1}{\epsilon_1}D \tag{3.14}$$

$$c_2k_2\{a_2cos(k_2(-d_2)) - b_2sin(k_2(-d_2))\} = \frac{e_2}{\epsilon_2}D \tag{3.15}$$

Solving the system of equations 3.13, 3.12, 3.14, 3.15 will yield the coefficient a_1 a_2 b_1 b_2 as:

$$b = b_1 = b_2 = \frac{D}{c_1k_1tan(k_1d_1) + c_1k_1tan(k_2d_2))}\left[\frac{e_2}{\epsilon_2}\left\{\frac{1 - cos(k_2d_2)}{cos(k_2d_2)}\right\} - \frac{e_1}{\epsilon_1}\left\{\frac{1 - cos(k_1d_1)}{cos(k_1d_1)}\right\}\right] \tag{3.16}$$

$$a_1 = b * tan(k_1d_1)\frac{e_1}{c_1\epsilon_1k_1}\left\{\frac{D}{cos(k_1d_1)}\right\} \tag{3.17}$$

$$a_2 = b * tan(k_2d_2))\frac{e_2}{c_2\epsilon_2k_2}\left\{\frac{D}{cos(k_2d_2)}\right\} \tag{3.18}$$

Moving on the electrical field equation of each medium derived from the piezoelectric constitutive equation

$$E_1 = -\frac{e_1}{c_1\epsilon_1}T_1 + (\frac{1}{\epsilon_1} + \frac{e_1^2}{c_1\epsilon_1^2})D \tag{3.19}$$

$$E_2 = -\frac{e_2}{c_2\epsilon_2}T_2 + (\frac{1}{\epsilon_2} + \frac{e_2^2}{c_2\epsilon_2^2})D \tag{3.20}$$

Voltage in respective medium is acquired as an integration of electrical field throughout the thickness of each material:

$$V_1 = \int_0^{d_1} E_1(z)dz \tag{3.21}$$

$$V_2 = \int_{-d_2}^{0} E_2(z)dz \tag{3.22}$$

$$V_t = V_1 + V_2 \tag{3.23}$$

Plugging equation 3.11 into equations 3.19, 3.20 will give a full description of the electric field in

each medium.

$$E_{1,2} = -\frac{e_{1,2}}{c_{1,2}\epsilon_{1,2}}\left\{c_{1,2}k_{1,2}\{a_{1,2}cos(k_{1,2}z) - b_{1,2}sin(k_{1,2}z)\} - \frac{e_{1,2}}{\epsilon_{1,2}}D\right\} + (\frac{1}{\epsilon_{1,2}} + \frac{e_1^2}{c_1\epsilon_1^2})D \tag{3.24}$$

Afterwards replacing all the constant a_1 a_2 b_1 b_2 with their equivalent in equations 3.16, 3.17, 3.18 will result in the full equation of the electrical field. The next step is performing the integral in equation 3.21 and 3.22. After a many steps of calculus steps we get the final equation for the total voltage in this structure 3.25.

$$\begin{aligned} V = {} & \frac{AD}{C_1}\left\{1 - \frac{e_1^2}{c_1^D\epsilon_1}\frac{tan(k_1d_1)}{k_1d_1}\right\} + \frac{AD}{C_2}\left\{1 - \frac{e_2^2}{c_2^D\epsilon_2}\frac{tan(k_2d_2)}{k_2d_2}\right\} \\ & + \left\{\frac{D}{c_1k_1tan(k_1d_1) + c_1k_1tan(k_2d_2))}\right\}\left[\left\{\frac{e_1}{\epsilon_1}\frac{1 - cos(k_1d_1)}{cos(k_1d_1)}\right\}^2 - \left\{\frac{e_2}{\epsilon_2}\frac{1 - cos(k_2d_2)}{cos(k_2d_2)}\right\}^2\right] \end{aligned} \tag{3.25}$$

The current travelling through the structure is $I = j\omega AD$ and remains the same in both structures. Impedance is a ratio of voltage over current wich is the equation needed to describe the behaviour.

$$\begin{aligned} Z = \frac{V}{jwAD} = {} & \frac{1}{jwC_1}\left\{1 - \frac{e_1^2}{c_1^D\epsilon_1}\frac{tan(k_1d_1)}{k_1d_1}\right\} + \frac{1}{jwC_2}\left\{1 - \frac{e_2^2}{c_2^D\epsilon_2}\frac{tan(k_2d_2)}{k_2d_2}\right\} \\ & + \frac{D}{jwA}\left\{\frac{1}{c_1k_1tan(k_1d_1) + c_1k_1tan(k_2d_2))}\right\}\left[\left\{\frac{e_1}{\epsilon_1}\frac{1 - cos(k_1d_1)}{cos(k_1d_1)}\right\}^2 - \left\{\frac{e_2}{\epsilon_2}\frac{1 - cos(k_2d_2)}{cos(k_2d_2)}\right\}^2\right] \end{aligned} \tag{3.26}$$

The new impedance behaviour is composed from three parts. The first two are the independent terms of each which contribute to the total impedance. This will also define the antiresonance frequency which is a very important quantity in designing a filter. The last parameter is a common quantity coming from the interaction between the two different mediums.

$$K_1 = \frac{1}{jwC_1}\left\{1 - \frac{e_1^2}{c_1^D\epsilon_1}\frac{tan(k_1d_1)}{k_1d_1}\right\} \tag{3.27}$$

$$K_2 = \frac{1}{jwC_2}\left\{1 - \frac{e_2^2}{c_2^D\epsilon_2}\frac{tan(k_2d_2)}{k_2d_2}\right\} \tag{3.28}$$

$$K_3 = \frac{D}{jwA}\left\{\frac{1}{c_1k_1tan(k_1d_1) + c_1k_1tan(k_2d_2))}\right\}\left[\left\{\frac{e_1}{\epsilon_1}\frac{1 - cos(k_1d_1)}{cos(k_1d_1)}\right\}^2 - \left\{\frac{e_2}{\epsilon_2}\frac{1 - cos(k_2d_2)}{cos(k_2d_2)}\right\}^2\right] \tag{3.29}$$

This composite resonator consist of two different resonance conditioning as in the figure 3-5 bellow where $Z = K_1 + K_2 + K_3$ simulation code is at A.2. In case of an 1D analysis of the of two different FBAR with respective medium properties and dimensions as the first and second layer of

the composite FBAR. The impedance behaviour will be precisely as in equation 3.27 and 3.28 with different individual resonance and antiresonance frequencies.

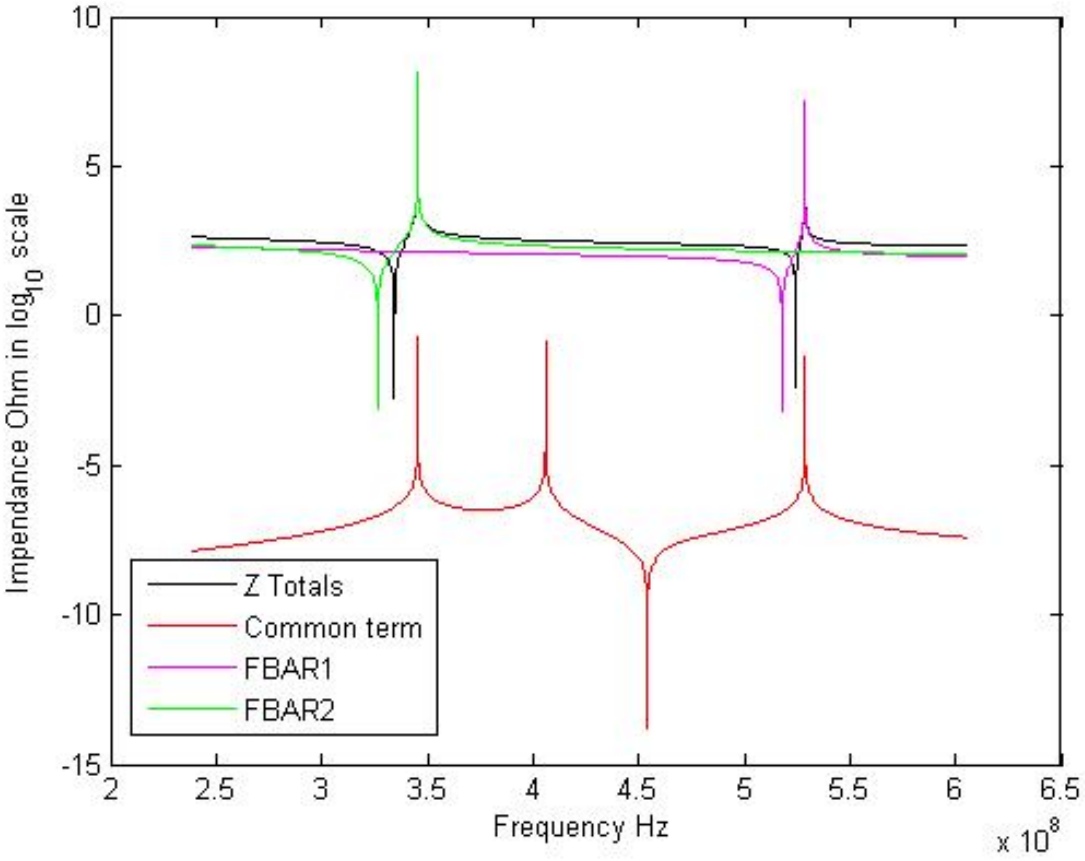

Figure 3-5: Composite impedance

This impedance is produces using a BST ferroelectric material with the dimensions in the table 3.4. The only assumption is infinitely thin electrodes where all the other properties of the electrodes are disregarded.

Properties	First layer	Second layer	Unit
Thickness	3	4.5	μm
Active surface	$1.7 * 10^{-3}$	$1.7 * 10^{-3}$	$\frac{kg}{(\mu m)^3}$

Table 3.4: Composite FBAR dimensions

BST material is a simply acquire from doped Barium Titanate (BTO) with strontium (Sr) thereby the microwave properties of both these materials are approximated the same. Regarding the piezoelectric coefficient it is enhance a bit from the ion dopands [32]. Stiffness coefficient remains insensitive to the concentration of Sr therefore the values are adopted from BTO[19] .

This FBAR has a total of two main antiresonance frequencies corresponding to $|Z| = \infty$. K_1 and K_3 goes to infinite for $(k_1 d_1) = (2n+1)\frac{\pi}{2}$, similarly K_2 ands K_3 goes to infinite for $(k_2 d_2) = (2n+1)\frac{\pi}{2}$. Two main antiresonance composing this FBAR are derived similarly as in figure 2-16:

Regarding the derivation of resonance frequency, a numerical computation is much easier than

Properties	Initial	First layer	Second layer	Unit	Unit
Density	ρ	$5.5 * 10^3$	$5 * 10^3$	kg/m^3	[19]
Piezoelectric coeff	e	11.9	10.9	C/m^2	[32]
Elastic constant	c^D	$1.214 * 10^{11}$	$2.214 * 10^{11}$	Pa	[19]
Dielectric permittivity	ϵ	1034	1134	$unit$	[19]

Table 3.5: BST material parameters

$$f_{a_1} = \frac{v_1}{2 * d_1} \tag{3.30}$$

$$f_{a_2} = \frac{v_2}{2 * d_2} \tag{3.31}$$

analytical model. Solving $|Z| = 0$ equation is a very difficult task. In figure 3-5 is an perfect overlap of the resonance frequency of composite with their equivalent resonance frequencies of K_1 and K_2. Antiresonance frequency of composite structure is shifted towards a higher frequency compare to its equivalence of K_1. This last characteristic will be the scope of this thesis.

3.1.1 Electrical field

The electrical field of the compositional material will differ from homogeneous FBAR. The method below is used to derive the electrical field of the homogeneous medium and the same method will be employed for the heterogeneous case.

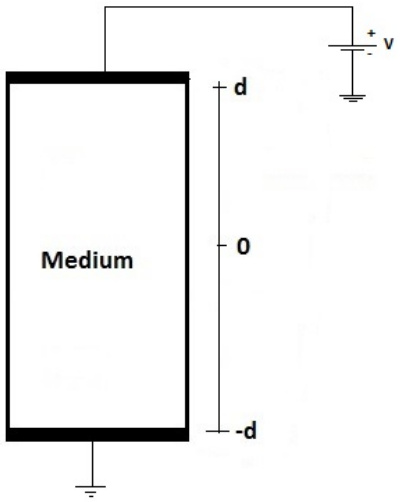

Figure 3-6: Tuned resonator

The voltage at DC level could be acquire from the equations 2.27

$$V = \frac{2dD}{\epsilon}\{1 - \frac{e^2}{c^D\epsilon}\} \tag{3.32}$$

Whereas the electric displacement from this voltage is simply:

$$D = \frac{V}{\frac{2d}{\epsilon}\{1 - \frac{e^2}{c^D\epsilon}\}} \tag{3.33}$$

Finally the electric field from this voltage accross the structure will be:

$$E = \frac{D}{\epsilon}\{1 - \frac{e^2}{c^D\epsilon}\} = \frac{V}{\frac{2d}{\epsilon}\{1 - \frac{e^2}{c^D\epsilon}\}}\frac{1}{\epsilon}\{1 - \frac{e^2}{c^D\epsilon}\} \tag{3.34}$$

$$E = \frac{V}{2d} \tag{3.35}$$

In case of the heterogeneous geometry the problem turns out to be a bit more complicated. Electrical field distribution in respective part of the medium is derived from the respective constitutive equations of piezoelectricity. In the equation 3.19 3.20 constant a_1, a_2, b_1, b_2 are replaced and the following equation express the electrical field:

$$E_{1,2}(z) = \frac{D}{\epsilon_{1,2}}\left\{1 - \frac{e_{1,2}^2}{c_{1,2}\epsilon_{1,2}}\frac{cos(k_1 z)}{cos(k_{1,2}d_{1,2})}\right\} - \frac{e_{1,2}k_{1,2}}{\epsilon_{1,2}}b\{tan(k_{1,2}d_{1,2})cos(k_{1,2}d_{1,2}) - sin(k_{1,2}d_{1,2})\} \tag{3.36}$$

Integration of electrical field as in equation 3.21 and 3.22 and the outcome is the following equation.

$$V_{1,2}(z) = \frac{Dd_{1,2}}{\epsilon_{1,2}}\left\{1 - \frac{e_{1,2}^2}{c_{1,2}\epsilon_{1,2}}\frac{tan(k_{1,2}d_{1,2})}{k_{1,2}d_{1,2}}\right\} - b\frac{e_{1,2}}{\epsilon_{1,2}}\left\{\frac{1 - cos(k_{1,2}d_{1,2})}{cos(k_{1,2}d_{1,2})}\right\} \tag{3.37}$$

The goal is to describe at DC level the electrical field in each component, therefore the constant component of electrical field and voltage are respectively in equation 3.38 and 3.39

$$E_{1,2} = \frac{D}{\epsilon_{1,2}}\left\{1 - \frac{e_{1,2}^2}{c_{1,2}\epsilon_{1,2}}\right\} \tag{3.38}$$

$$V_{1,2} = \frac{Dd_{1,2}}{\epsilon_{1,2}}\left\{1 - \frac{e_{1,2}^2}{c_{1,2}\epsilon_{1,2}}\right\} \tag{3.39}$$

Dielectric displacement is still unknown quantity and it is induced proportionally to the total voltage as in equation 3.41.

$$V = V_1 + V_2 = D\left\{\frac{d_1}{\epsilon_1}\left\{1 - \frac{e_1^2}{c_1\epsilon_1}\right\} + \frac{d_2}{\epsilon_2}\left\{1 - \frac{e_2^2}{c_2\epsilon_2}\right\}\right\} \tag{3.40}$$

$$D = \frac{V}{\frac{d_1}{\epsilon_1}\left\{1 - \frac{e_1^2}{c_1\epsilon_1}\right\} + \frac{d_2}{\epsilon_2}\left\{1 - \frac{e_2^2}{c_2\epsilon_2}\right\}} \tag{3.41}$$

Electrical field acquired in each medium as a result of applied DC voltage is as in equation 3.42.

$$E_{1,2} = \frac{V}{\frac{d_1}{\epsilon_1}\left\{1 - \frac{e_1^2}{c_1\epsilon_1}\right\} + \frac{d_2}{\epsilon_2}\left\{1 - \frac{e_2^2}{c_2\epsilon_2}\right\}}\frac{1}{\epsilon_{1,2}}\left\{1 - \frac{e_{1,2}^2}{c_{1,2}\epsilon_{1,2}}\right\} \tag{3.42}$$

The materials properties $e(E)$, $\epsilon(E)$, $c(E)$ depend on the applied electrical field significantly and they cannot sustain their value unchanged throughout the analysis. This is overcomed in the analysis

by making the formula as a recursive function for each electrical field as in equation 3.43 and equation 3.44

$$E_{1_k} = \frac{V}{d_1\left[1 + \frac{d_2\epsilon_1(E_{1_{k-1}})}{d_1\epsilon_2(E_{2_{k-1}})}\frac{\left\{1-\frac{e_2^2(E_{2_{k-1}})}{c_2(E_{2_{k-1}})\epsilon_2(E_{2_{k-1}})}\right\}}{\left\{1-\frac{e_1^2(E_{1_{k-1}})}{c_1(E_{1_{k-1}})\epsilon_1(E_{1_{k-1}})}\right\}}\right]} \tag{3.43}$$

$$E_{2_k} = \frac{V}{d_2\left[1 + \frac{d_1\epsilon_2(E_{2_{k-1}})}{d_2\epsilon_1(E_{1_{k-1}})}\frac{\left\{1-\frac{e_1^2(E_{1_{k-1}})}{c_1(E_{1_{k-1}})\epsilon_1(E_{1_{k-1}})}\right\}}{\left\{1-\frac{e_2^2(E_{2_{k-1}})}{c_2(E_{2_{k-1}})\epsilon_1(E_{2_{k-1}})}\right\}}\right]} \tag{3.44}$$

Due the complexity of these formula two main parts are subtracted as in equation 3.45 and 3.46.

$$B_1 = \frac{1-\frac{e_2^2}{c_2\epsilon_2}}{1-\frac{e_1^2}{c_1\epsilon_1}} \tag{3.45}$$

$$B_2 = \frac{1-\frac{e_1^2}{c_1\epsilon_1}}{1-\frac{e_2^2}{c_2\epsilon_2}} \tag{3.46}$$

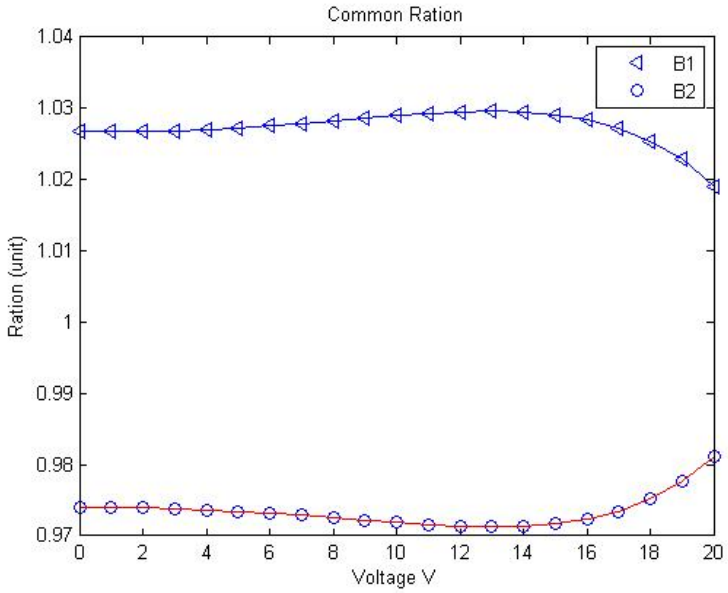

Figure 3-7: Rations of common terms

The parameters of the heterogeneous FBAR are from the table 3.4 and table 3.5 this data are utilised for the electrical field in figure 3-8. Parts of these electrical filed B_1,B_2 in respective electrical field will impact differently based on material parameters up to 20V DC. These values are plotted in figure 3-7 where a small variation from unit quantity is observed within this range of DC voltage. The following approximations of each electrical field in equations 3.47 and 3.48 are observed over a range of applied voltage.

These values are quite close to the real values acquired from equations 3.43 and 3.44. Since the values differ in small quantities for applied voltage close to the 20V electrical field will be used only

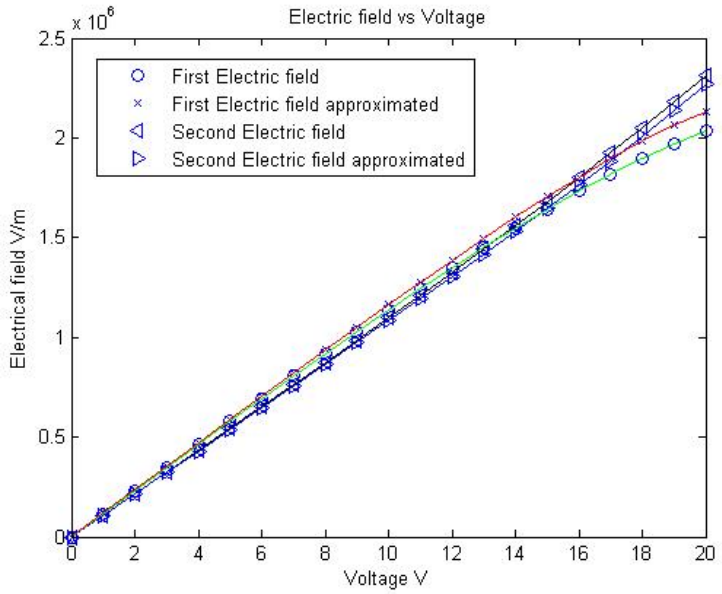

Figure 3-8: Electrical field in each medium together

as approximated over the analysis in the **Comsol** model. This is a very important property of the composite structure utilized for a enhancement of tuneability in latter analysis.

$$E_{1_k} \approx \frac{V_{k-1}}{d_1\left\{1+\frac{d_{2_{k-1}}\epsilon_{1_{k-1}}}{d_{1_{k-1}}\epsilon_{2_{k-1}}}\right\}} \qquad (3.47) \qquad E_{2_k} \approx \frac{V_{k-1}}{d_2\left\{1+\frac{d_{1_{k-1}}\epsilon_{2_{k-1}}}{d_{2_{k-1}}\epsilon_{1_{k-1}}}\right\}} \qquad (3.48)$$

Simulation model for this section can be found in listed in A.5. Last but not least in order to confirm the legitimacy of the formulas 3.43,3.44 in case of homogeneous material. This goes of $d = d_1 = d_2$ and all the other parameters are the same. After same simplification the formulas of total electrical field will be exactly as in equation 3.35. Formulas for the electrical field in all the above equations are the a real equality because the material parameters depend drastically on the previous conditions from the tuneability. Under a given voltage materials parameters needs to be tuned up to the consistent quantities whereby the electrical field will strictly depend on these quantities. Consequently an recursive method is needed to estimated every desired value up to needed value.

3.2 Acoustically coupling

FBAR will be smartly bounded together into a bandpass filter configuration. Acoustically coupling is a very promising approach where two distinct FBAR will transfer energy into one direction. The coupling layer could be either a single or multiple layer. Transmission line method has been employed to determine the input acoustic impedance of the FBAR. The DC bias voltage will tune the materials parameters significantly whereby weakening efficiency of the coupling. In this section a simple tuneable FBAR has been studied.

$$T(\omega) = \frac{4Z_{03}Z_{01}}{(Z_{01}+Z_{03})^2 cos^2(\theta) + (Z_{02} + \frac{Z_{01}Z_{03}}{Z_{02}})^2 sin^2(\theta)} \quad (3.49) \qquad Z_{in} = Z_i \frac{Z_i + Z_L tan(\frac{2*\pi}{\lambda} t_i)}{Z_L + Z_i tan(\frac{2*\pi}{\lambda} t_i)} \quad (3.50)$$

In order to have maximum transfer from one FBAR to another transfer function is approximately $T = 1$. This is achieved using $\theta = \frac{2*\pi}{\lambda} t = \frac{\pi}{2}$ and $Z_{02} = \sqrt{Z_{01} * Z_{03}}$. The thickness and the impedance of the coupling layer for the optimal coupling will thereby be:

$$Z_{02} = \sqrt{Z_{01} * Z_{03}} \qquad (3.51) \qquad t_i = \frac{\lambda}{4} \qquad (3.52)$$

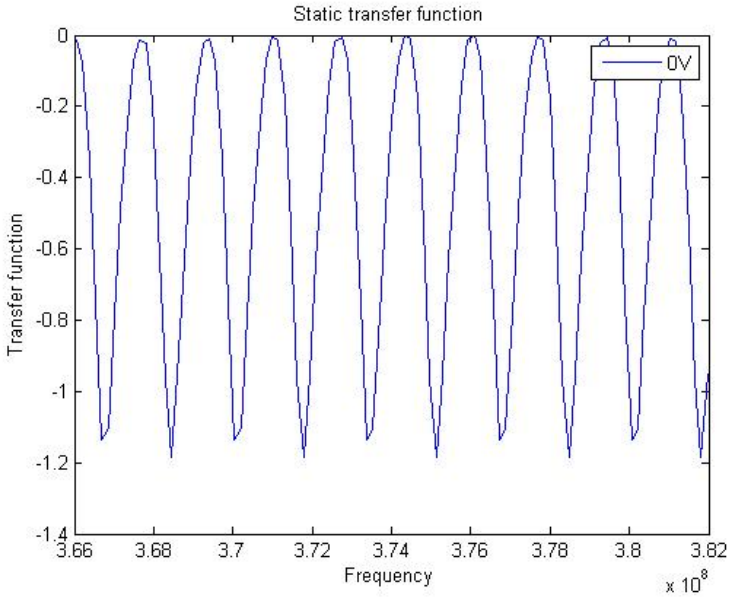

Figure 3-9: Transmission transfer function over a range of frequencies

In this case Z_{03} and Z_{01} are the input acoustic impedance of the FBAR seen from the interface coupling medium. This quantities are going to be subject of the change due to the DC bias voltage. The input impedance is modeled as a recursive computation of at least three layer structure. This is a simple schematic of an resonator where the red parts represent an aluminium electrodes whereas the green parts correspond to the ferroelectric medium.

Figure 3-10: Input acoustic impedance of the FBAR

In the figure 3-10 is a simple schematic of a ferroelectric medium sandwiched by two electrodes. The input impedance of this structure seen from the the electrode towards the structure is competed

as bellow:

$$Z_{in1} = Z_a \frac{Z_a + Z_{air} tan(\frac{2*\pi}{\lambda} d)}{Z_{air} + Z_a tan(\frac{2*\pi}{\lambda} d)} \qquad Z_{in2} = Z_{in1} \frac{Z_{in1} + Z_{a1} tan(\frac{2*\pi}{\lambda} D)}{Z_{a1} + Z_{in1} tan(\frac{2*\pi}{\lambda} D)} \qquad Z_{in} = Z_{in2} \frac{Z_{in2} + Z_a tan(\frac{2*\pi}{\lambda} d)}{Z_a + Z_{in2} tan(\frac{2*\pi}{\lambda} d)}$$

Acoustic impedance of the ferroelectric medium $Z(E) = c^D(E)\rho$ strictly depend on the applied electrical field coming from the DC bias voltage. The same method goes for the other FBAR paired with the coupling medium in a filter configuration. The situation turns out to be complicated since the desired acoustic impedance of the coupling layer will be $Z_{02}(E) = \sqrt{Z_{01}(E) Z_{03}(E)}$. In additional to this the desired thickness of the coupling layer will depend on the resonance frequency as in equation 3.53

$$t_i(E) = \frac{\omega(E)}{4V_{acoustic}} \qquad (3.53) \qquad t_i(E) = \frac{2 * \pi * f(E)}{4V_{acoustic}} \qquad (3.54)$$

Input acoustic impedance of the FBAR under the applied voltage will change accordingly to a quasi periodic pattern as in figure 3-12. This is as a result mainly from the variation of elastic constant of the ferroelectric medium. In addition to this, resonance frequency will increase significantly due to the tuneability. A compensation to this could be found by increasing the acoustic path of the coupling layer and the desired ration is plotted in figure 3-11.

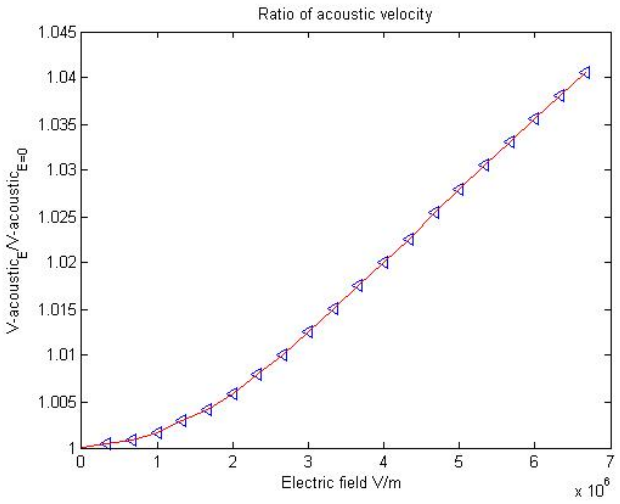

Figure 3-11: Variation of the acoustic field

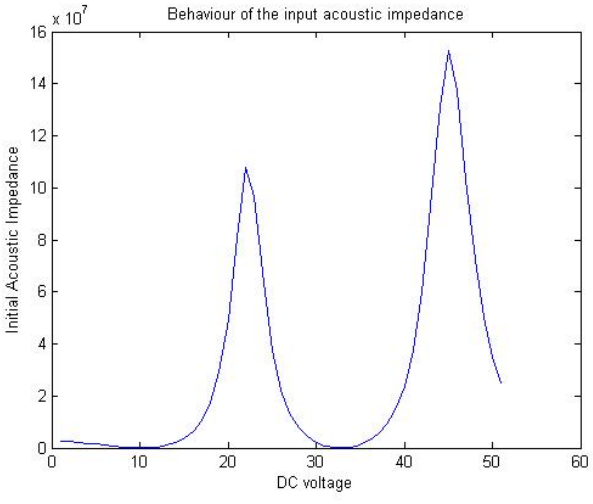

Figure 3-12: Input acoustic impedance

In the figure 2-31 is the an existing configuration where a single layer acts as an coupling layer. Using the same configuration in scenario of tuneable FBAR will require adjustment of the coupling layer parameters. An additional DC bias voltage to the coupling layer will interfere to the other resonators and will therefore change the filter response. Another topology has been proposed in the figure 3-13 .The very middle structure is a ferroelectric material sandwiched by two electrodes. The thickness of the electrodes needs to be as small as possible and they will be used to tune the elastic constant. Elastic constant needs to be adjusted in a way to fulfill the requirements of the optimised

acoustic coupling as in equation 3.52 and equation 3.51. This topology will couple the two FBAR using a dielectric layer (blue material) and the green material is the ferroelectric medium figure 3-13. Electrodes are represented very thin colored by red. Resonator is biased under a DC bias voltage where its effect will be electrically isolated by the dielectric layer. Input acoustic impedance seen on both sides of the coupling resonator will be plugged into the equation 3.49. These quantities will be estimated using the recursive transmission line method it was performed for the structure in figure 3-10.

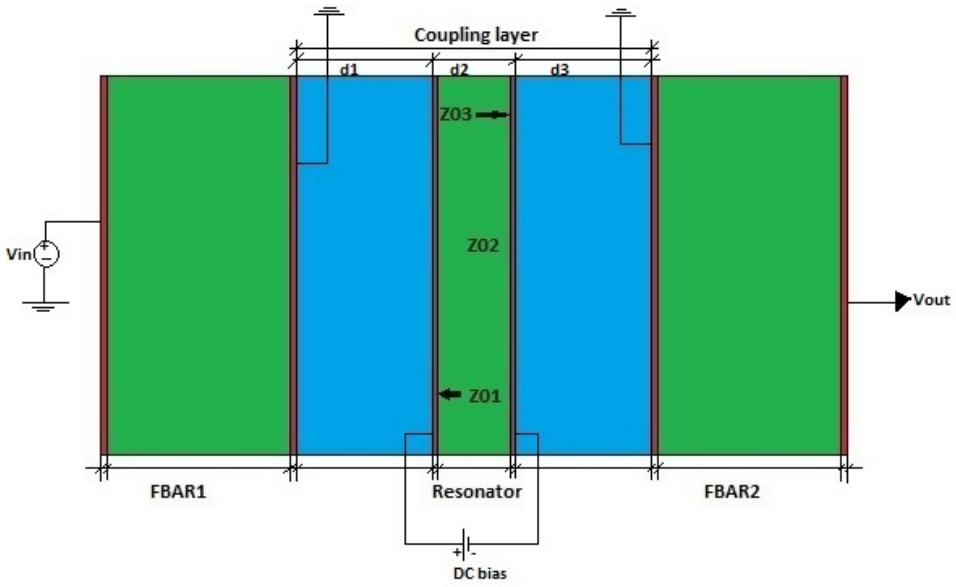

Figure 3-13: Tuneable coupling layer design

In case of a multiple layer structure, the thickness of each layer has been assigned to $d1 = d2 = d3 = \lambda/4$ [24]. In this case λ is the wavelength corresponding to the initial resonance frequency. Sandwiched resonator will therefore be considered a tuneable coupling layer biased by the DC voltage. Dielectric coupler in our case has been chosen Silicon Low k dielectric resin SiLK and carbon-doped oxide CDO [22].

Chapter 4

Simulations and Results

In this chapter are all the results are represented, which are acquired from different models. The start is dedicated to the simplest tuneable FBAR model and how the material properties behave. In the second part is the proposed structure geometry. The last part consist on the results from a acoustic coupled filter. The focus is mostly on how tuneability will impact coupling among FBAR.

4.1 Tuneability

FBAR is a simple bridge structure as in figure 4-1 where the BST piezoelectric material is sandwiched between two aluminium electrodes. Due to high mechanical resistance silicon has been chosen as substrate to handle the FBAR. Throughout all the simulations BST material will be utilized as ferroelectric material where its materials properties are listed in table 4.2

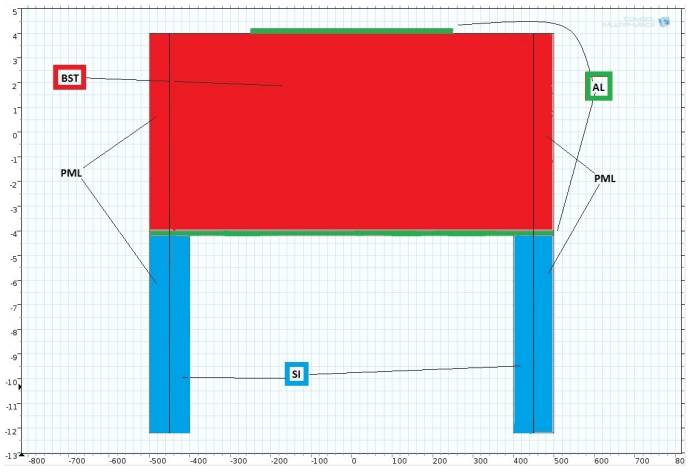

Figure 4-1: FBAR design

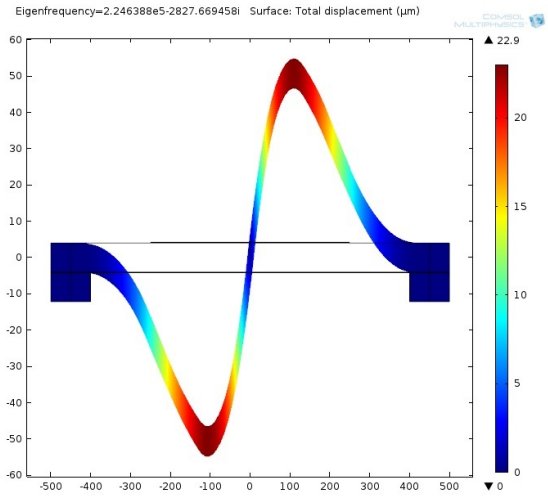

Figure 4-2: Eignemode outcome of the model

In figure 4-2 is an eigenmode displacement of the FBAR showing how a pure piston mode operation. The active area is far more affected from the electrical field compare to the rest of the medium. Anchors on the other hand sustain a very good stability of the structure during piston mode vibra-

tion. Air provides an acoustically isolation of the inner part of the medium. The dimension of the comsol model are listed in the table 4.1.

	Value	Unit
Active area	$1.7 * 10^{-9}$	m^2
Thickness	$3 * 10^{-6}$	m
Electrode thickness	$2 * 10^{-7}$	m
Anchor heights	$8 * 10^{-6}$	m

Table 4.1: Geometrical design parameters[19]

Properties	Initial	Value	Unit	ref
Density	ρ	$5.5 * 10^3$	kg/m^3	[19]
Piezoelectric coeff	e	9.9	C/m^2	[32]
Elastic constant	c^D	$1.014 * 10^{11}$	Pa	[19]
Dielectric permittivity	ϵ	1034	$unit$	[19]

Table 4.2: BST material parameters

Where dielectric permittivity of free space ϵ_0 is $8.8 * 10^{-12} F/m$. Admittance response over a range of frequencies is a very important property of the FBAR with regards to the filter implementation. In the figure 4-4 is the admittance response of this resonator acquired from **Comsol** model. The resonance frequency and antiresonance frequency sit around **350 MHz** and **375 MHz**. Admittance of this model is plotted into logarithmic scale over a predefined range of frequencies. Apart from **Comsol** model this resonator is constructed into a simple 1D analytical model via the analysis in section 2.3 where the resonance and antiresonance frequency are calculated using equations 2.38 and 4-10. Th electrode thickness is disregarded in the analytical model. Thus a shift at higher values of fundamental frequencies is observed at **360 MHz** and **375 MHz** respectively.

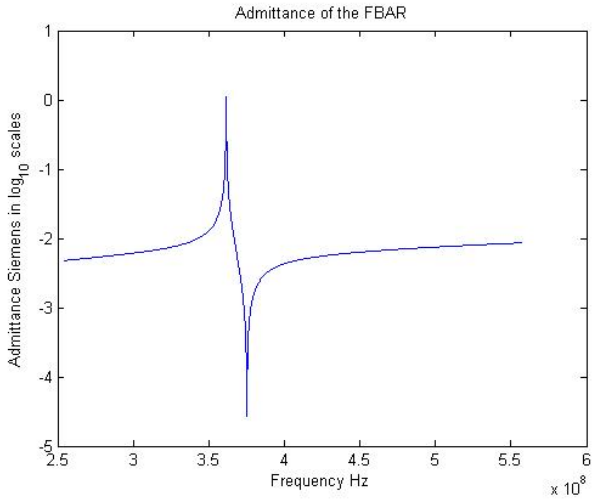

Figure 4-3: Analytical model

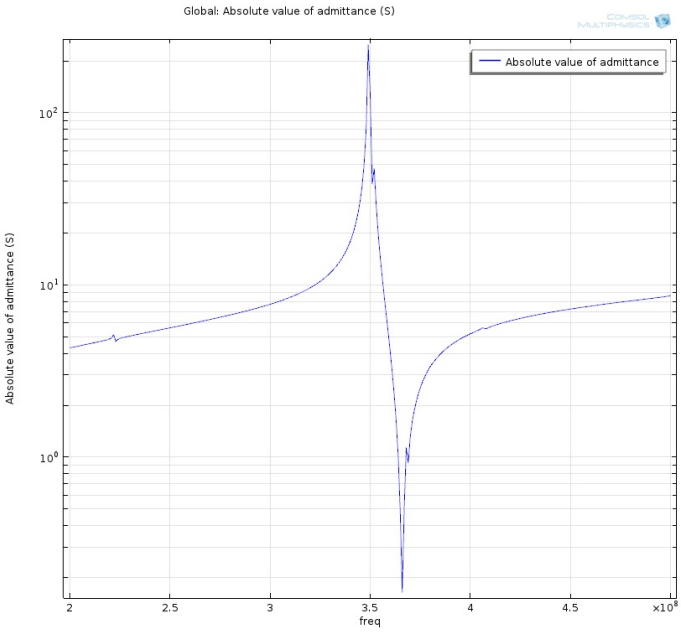

Figure 4-4: Comsol model

Comsol model shows a perfect behaviour impedance when the input signal of the resonator covers the spectrum of your interest. The matlab numerical model is listed in A.3.

In additional to the materials parameters, e, c_D, ϵ, there are two other important coefficient contributing to the tuneability. The first one μ is related to piezoelectricity as in equation 2.53 and β will vary the permittivity as in equation 2.52. These values are listed in table 4-5 and they depend drastically on the type of the material. The the value of β for BST material is acquired by curve fitting the plot in **fig 4** from Ahmed et al 2015 [6]. Using equation 2.52 and after few steps β could be write as equation 4.1.

	Value	Unit	Ref
μ	$463 * 10^{-12}$	$\frac{m}{V}$	[19]
β	$7 * 10^{10}$	$\frac{m^5}{C^3}$	[6]

Figure 4-5: BST tuneability parameters

$$\beta = \frac{1}{3\epsilon_o^3 \epsilon_r^3(E=0)E_{DC}^2}\left\{\frac{\epsilon_r(E=0)-\epsilon_r(E\neq 0)}{\epsilon_r(E\neq 0)}\right\} \tag{4.1}$$

In the equation 4.1 ϵ_0 is the dielectric permittivity of the free space. This model has been modified into a tuneable FBAR in order to study the changes of the impedance characteristic over a predefined range of frequencies. Employing this resonator into a ladder and lattice filter configuration describes the behaviour of a real tuneable filter. The simulation model for the resonator together with filter could be found in A.3. In the impedance profile there are two extrema corresponding to the resonance and antiresonance frequencies in the **x** axis figure 4-6. When a DC voltage will superimpose over this structure it will tune this FBAR consequently both extrema will shift at higher frequencies. In this figure is confirmed that antiresonance frequency is increasing much more compare to the resonance .

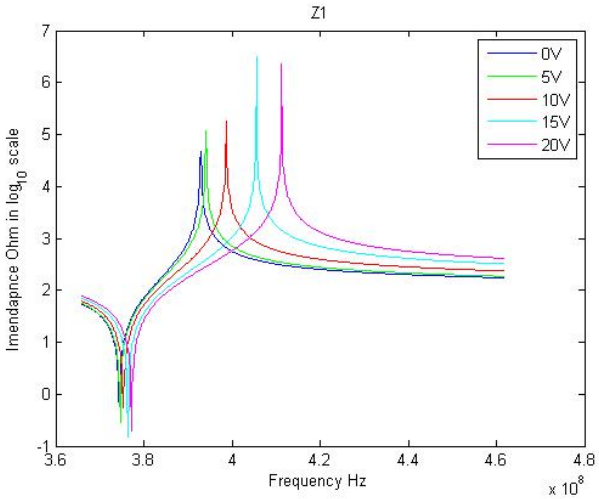

Figure 4-6: Simple tuneable FBAR

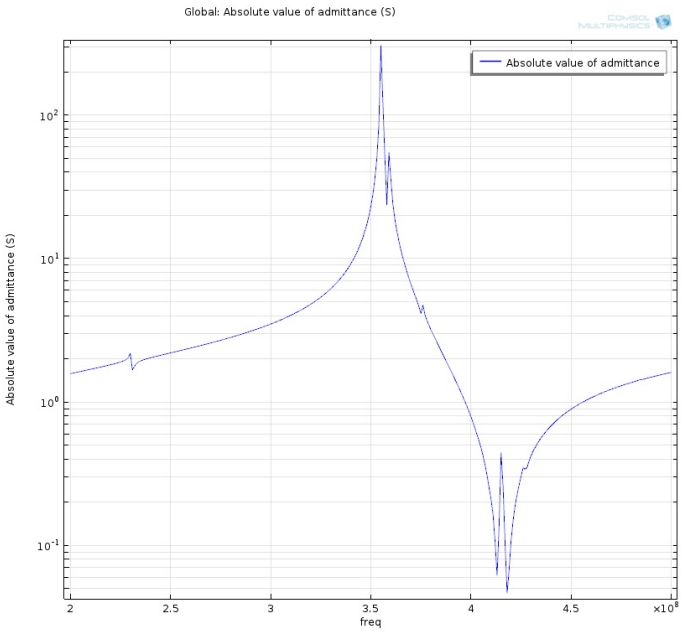

Figure 4-7: Comsol outcome of tuneable FBAR at DC bias voltage of 15V

The same analytical model was simulated in **Comsol** and the same shift of frequency is observed

in both resonance and antiresonance frequency compared to the unbiased model in figure 4-4. The issue with this approach is that rate is different for the resonance and antiresonance frequencies. This will shape the filter response into an undesirable pattern.

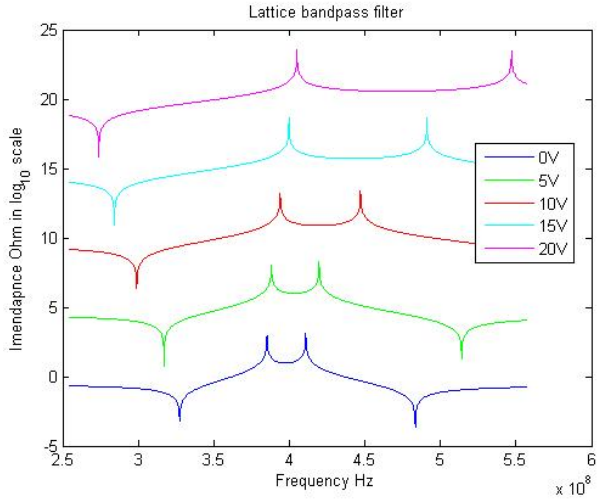

Figure 4-8: Lattice configuration

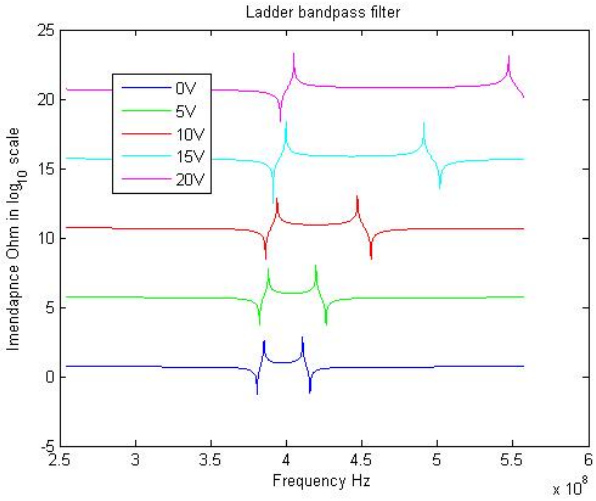

Figure 4-9: Ladder configuration

When bandpass filter gets tuned what happen the most is the increase of bandwidth rather than displacement of bandpass filter as a whole shape. This goes for both lattice and ladder topologies. The configuration of these model is described in figure 2-25 and 2-26.

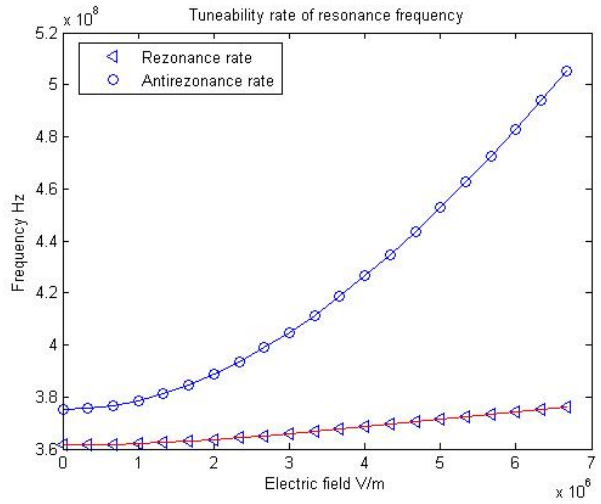

Figure 4-10: Tuneability of resonance and antiresonance frequency

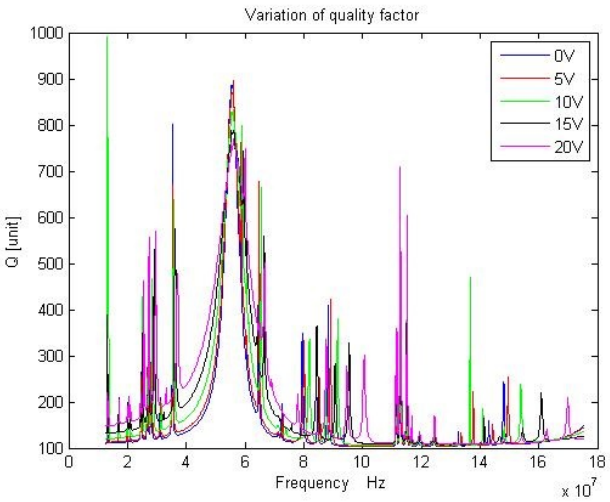

Figure 4-11: Quality factor tuned with 5V

In the figure 4-10 is a rate showing the increment rate of each frequency. The rate has a quadratic rate to voltage relation consequently high voltages yield much higher rate. Apart from the impedance, quality factor is inevitably part of this change as well. In the figure below there are two plots representing the quality factor Q at 0V up to 20V DC bias. The quality factor tends to slightly decrease and the shift of frequency is prevalent here as well . This results are acquired from the **FBAR2.mph** model and plotted with the code at A.4.

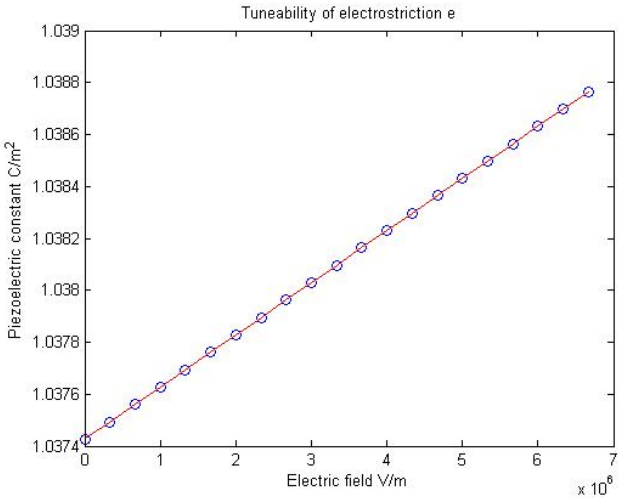

Figure 4-12: Elastic coefficient variation

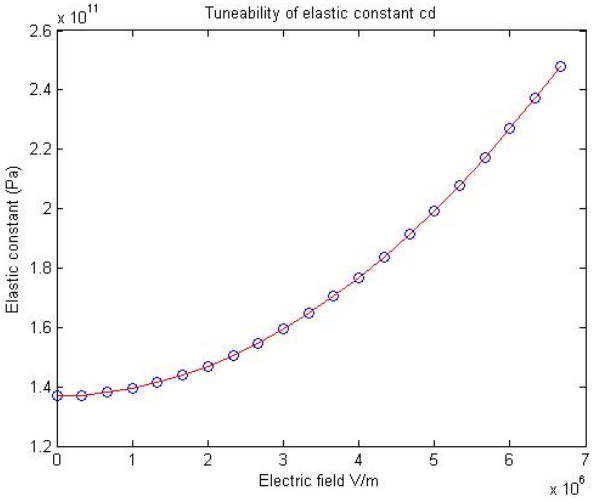

Figure 4-13: Piezoelectric coefficient variation

Coupling coefficient is also part of this changing event. It tends to increase with a quadratic scale as expected from the increase of filter bandwidth. The analytical formulation of coupling coefficient is approximated as in equation 2.30. Overall this phenomena happens due to the variation of the fundamental properties including here dielectric permittivity ϵ, elastic constant c_D and piezoelectric coefficient e. These are the main properties with the biggest contribution of the tuneability. Dielectric permittivity decreases significantly with the applied voltage as in figure 4-15. There is a totally different behaviour of the elastic and piezoelectric coefficient. In this last case the trend is increment as the electrical fields becomes bigger in figure 4-12 and 4-13.

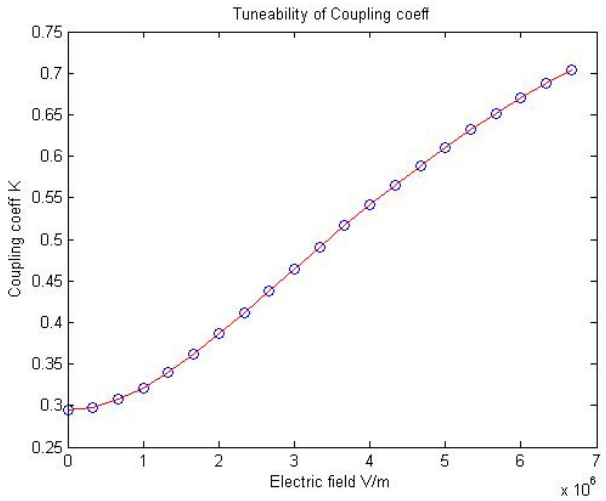

Figure 4-14: Variation of coupling coefficient

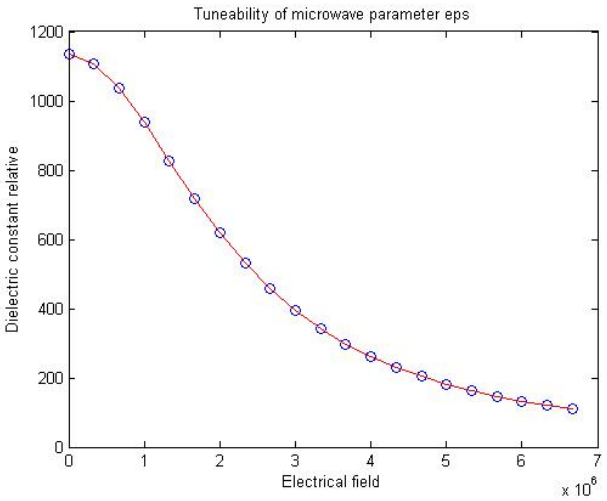

Figure 4-15: Dielectric permittivity

4.2 Composite structure

The need of a single tuneable filter requires the same rate of tuneability for both resonance and antiresonance frequency. In order to get as close as possible to this functional requirements a promising approach has been proposed in here. Analysed in the section 3.1 composite structure is a simple evolution of the homogeneous medium into two different medium attached together with different thicknesses as in figure 4-16.

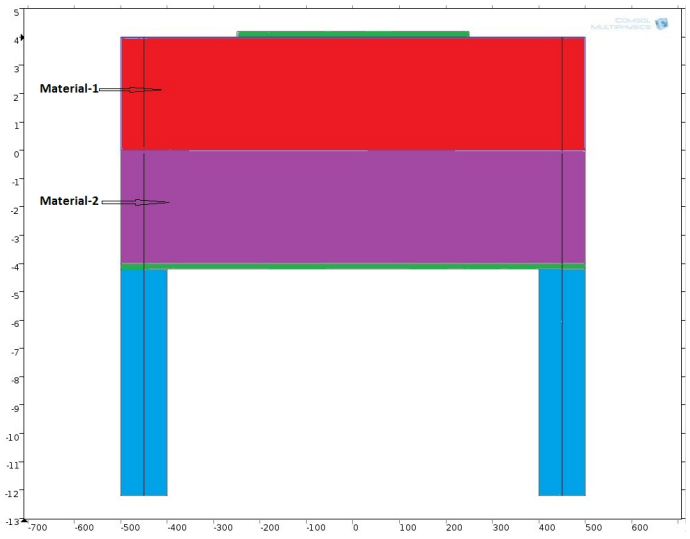

Figure 4-16: Composite FBAR

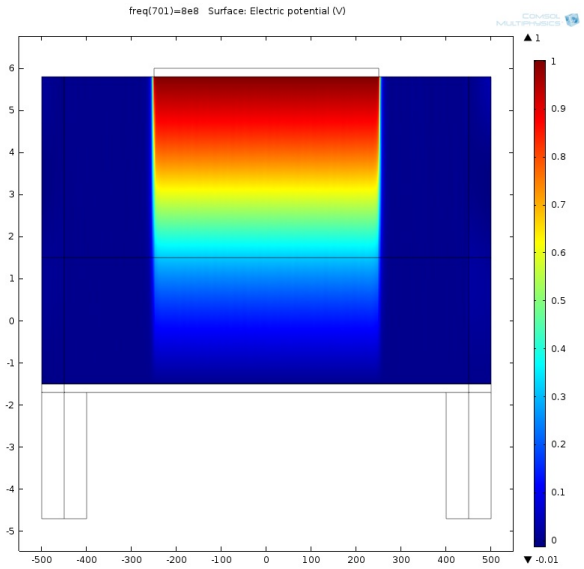

Figure 4-17: Active area

This is modeled in Comsol and found under the name **FBAR3.mph**. The equivalent analytical model is also programmed in matlab model A.5 and these results are refereed in the discussion part.

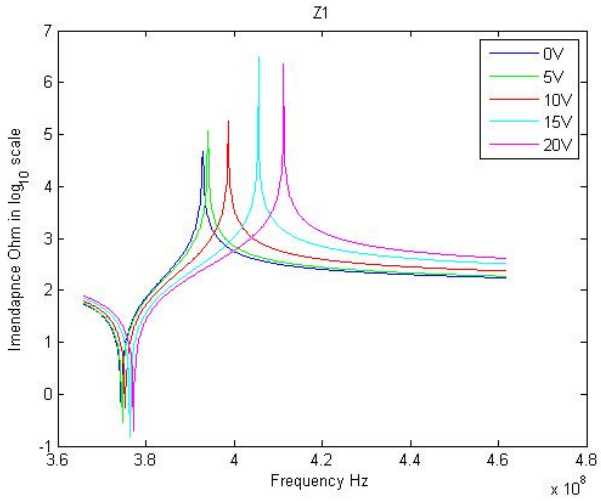

Figure 4-18: Homogeneous structure

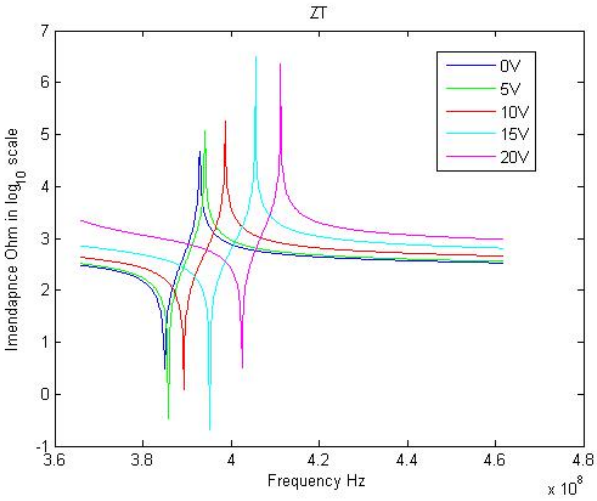

Figure 4-19: Heterogeneous structure

At first glance to the figure 4-19 there is a notable change of the tuneability. The rate of the resonance frequency is significantly higher. Both compositional and homogeneous model operate in the same antiresonance frequencies. This is estimate as the starting point because it is defined easily via the thickness of the medium. resonance frequencies of both models are approximated to be close

to each other. However a perfect match is very difficult due to the lack of analytical formulation in case of the heterogeneous structure. Antiresonance rate in both structure has absolutely no changes. resonance rate for the heterogeneous structure has an improvement emphasized on higher values of electrical field. In figure 4-20 the tuned impedance are plotted at the same scale in order to point out the improvement from the heterogeneous design.

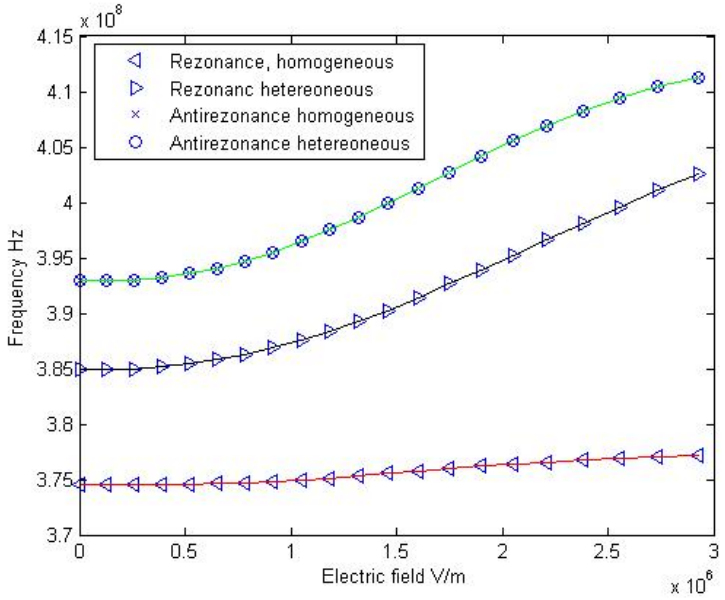

Figure 4-20: Resonance and antiresonance tuneability rate

Utilizing a heterogeneous structure for the lattice and ladder filter will yield a notable shift of the bandpass filter as a whole shape instead of just increasing the bandwidth of the structure. Since the heterogeneous structure is not fully analytically analysed, coupling coefficient doesn't have an accurate expression. Using the classical approximation in equation 2.36 was possible to compare the numerical capability of electro-mechanical coupling. In the table 4.3 and 4.4 are listed the materials parameters of each medium. For the first analysis the properties don't differ significantly.

Init	Value	Unit
Dielectric permittivity ϵ_r	1134	unit
Piezoelectric constant	11.9	C/N
Elastic constant	$1.114 * 10^{11}$	m/N
Densityρ	$5 * 10^3$	kg/m^3
μ	$463 * 10^{-12}$	$\frac{m}{V}$
β	$7 * 10^{10}$	$\frac{m^5}{C^3}$

Table 4.3: First medium BST[19]

Init	Value	Unit
Dielectric permittivity ϵ_r	1034	unit
Piezoelectric constant	10.9	C/N
Elastic constant	$1.014 * 10^{11}$	m/N
Densityρ	$5.5 * 10^3$	kg/m^3
μ	$463 * 10^{-12}$	$\frac{m}{V}$
β	$7 * 10^{10}$	$\frac{m^5}{C^3}$

Table 4.4: Second medium BST[19]

Dielectric permittivity of free space is $\epsilon_0 = 8.8{*}10^{-12} F/m$. The matlab model in A.5 is constructed with the assumption of infinitely thin electrodes. Regarding the other dimensions as active areas and medium thickness this are listed in table 4.5 and 4.6 for each medium.

Materials properties however differ much differently compare to the homogeneous structure. The

Init	Value	Unit
Active area	$1.7 * 10^{-9}$	m^2
Thickness	$3 * 10^{-6}$	m

Table 4.5: First medium dimension

Init	Value	Unit
Active area	$1.7 * 10^{-9}$	m^2
Thickness	$4.3 * 10^{-6}$	m

Table 4.6: Second medium dimension

first medium acquires a much higher electrical field compared to the second medium even though they both share the same voltage. These are plotted distinctly in figure 4-21. Biased voltage has a different impact on the materials properties of each medium.

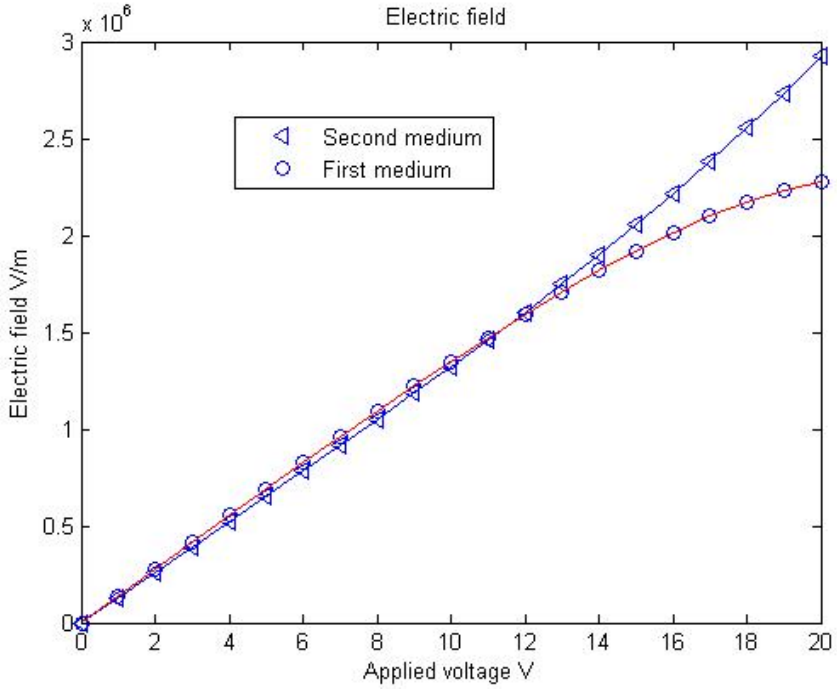

Figure 4-21: Electrical field in each medium due to DC bias voltage

Elastic constant will be enhanced in both mediums but the rate is different.

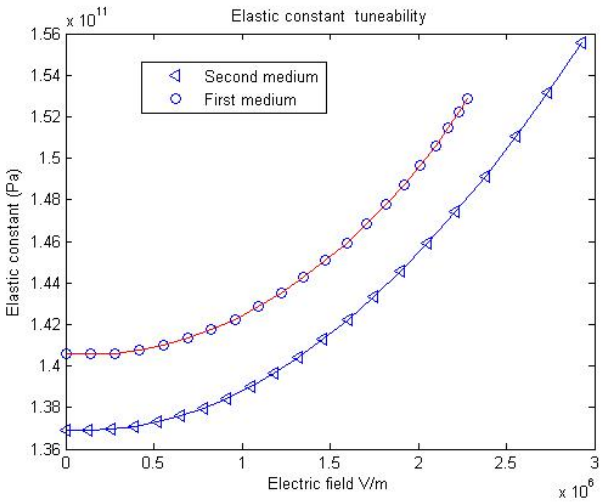

Figure 4-22: Elastic constant vs electric field

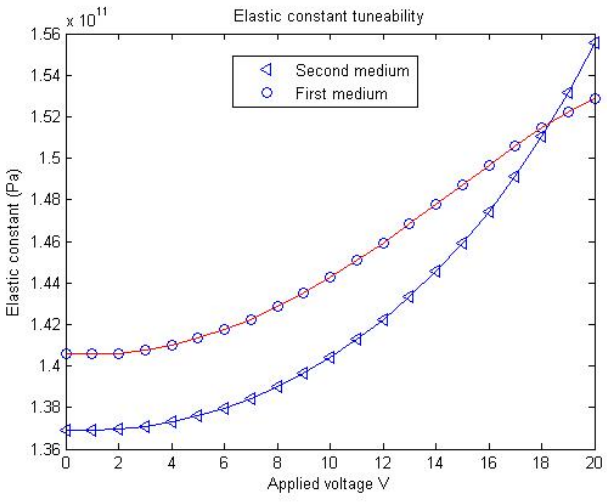

Figure 4-23: Elastic constant vs voltage

In figure 4-22 the picture reveals a different electrical interaction in the first medium causing a much higher enhancement compared to the second medium. Figure 4.2 shows the shared voltage

enhancing elastic constant in each medium. In these plots is notable a fact that second medium absorbs lower electrical field compared to the first. The same behaviour takes place when tuning the dielectric permittivity. Dielectric permittivity in the second medium decreases much more compare to the first medium. Different rate comes as result of different electrical field interaction in each medium. This distribution of electric field is a result of a set parameters parameters of each medium. Equation 3.43 and 3.44 describe a recursive relation of electrical field. The set of parameters driving the electrical field, are predecessor electrical field, piezoelectricity, elastic constant and dielectric permittivity of both mediums.

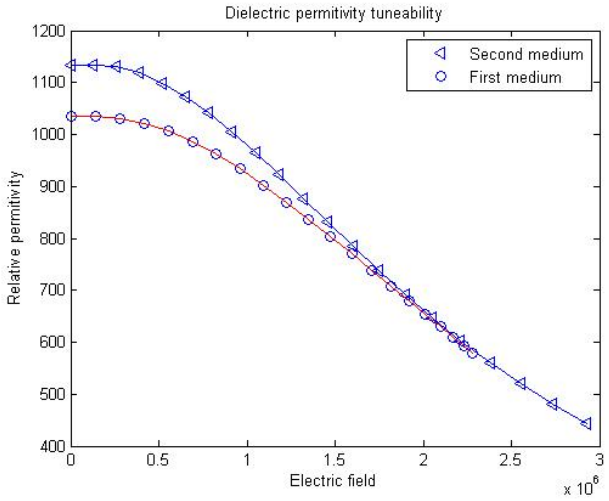

Figure 4-24: Dielectric constant vs voltage

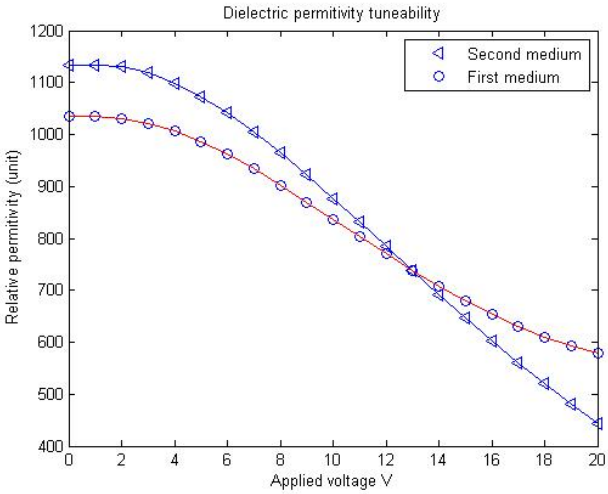

Figure 4-25: Dielectric constant vs voltage

Last but not least piezoelectric coefficient is a very important property of each BST material. It will vary with a least rate compare to dielectric permittivity and the electrical field acquired from each material will be different as well.

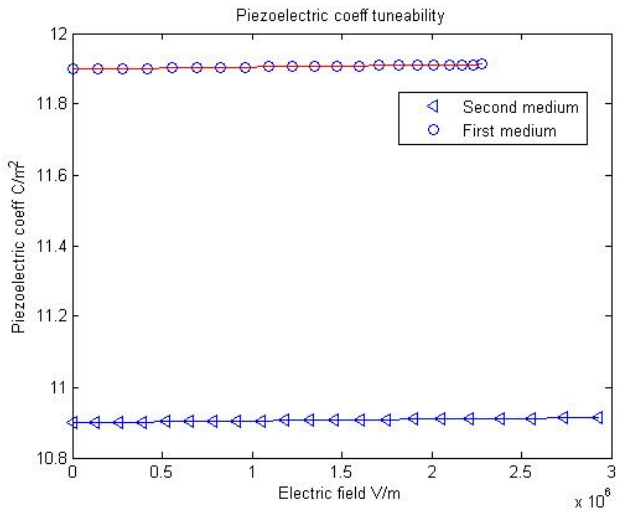

Figure 4-26: Piezoelectric coefficient vs voltage

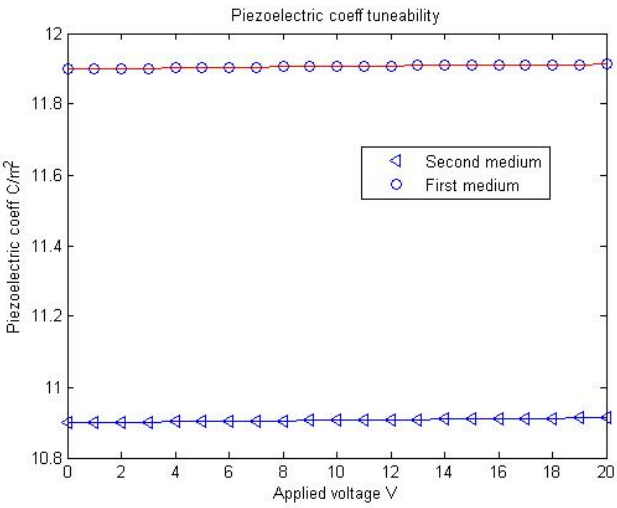

Figure 4-27: Piezoelectric coefficient vs voltage

In figure 4-26 clearly indicate voltage dependent of the piezoelectric coefficient. In figure 4-27 is the equivalent variance electric field dependent of the same range of electric field in respective mediums.

Coupling coefficient is another quantity which will be affected from the compositional structure. Due to the lack of an analytical description in the compositional structure, the approximated equation 2.36 will be employed for this analysis in both structures. In the figure 4-28 is plotted the coupling coefficient and compared among both structures. Since the resonance and antiresonance rate of composite structure is are brought close to each other significantly, coupling coefficient will increase slower compare to the homogeneous structure. Further coupling coefficient has a much lower initial value in the heterogeneous case.

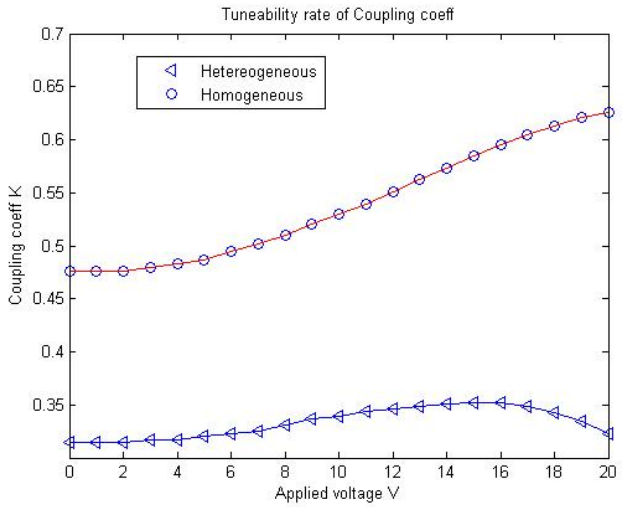

Figure 4-28: Coupling coefficient

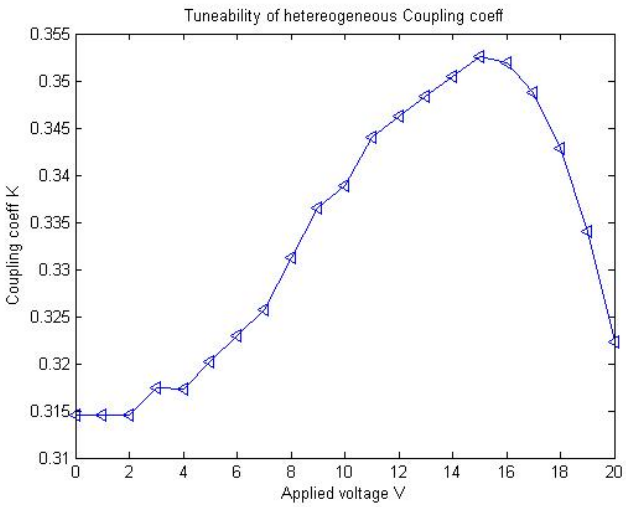

Figure 4-29: Heterogeneous coupling coefficient

Electrical field is a very important key driver in this process. It is responsible for tuning different material properties proportionally to its value. The ration of thicknesses among two mediums has the main contribution to the distribution of electric field. The increase is quite similar for low voltage. Whereas for high voltages the rate is quite high in the second medium.

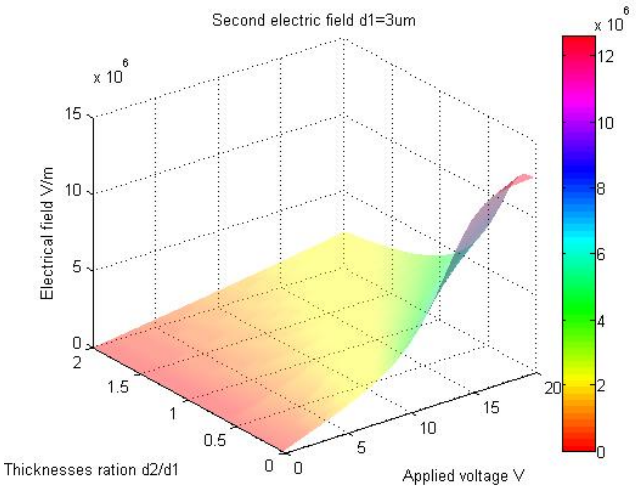

Figure 4-30: Electric field in the first medium

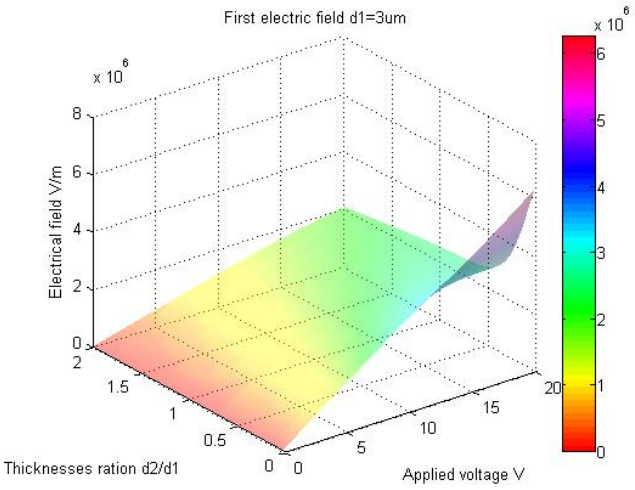

Figure 4-31: Electric field in the second medium

In a real electrical coupled (ladder and lattice) filter implementation the effect of the composite structure implementation will be emphasized on displacing the bandwidth as a whole structure

instead of just widening the bandwidth as in homogeneous case.

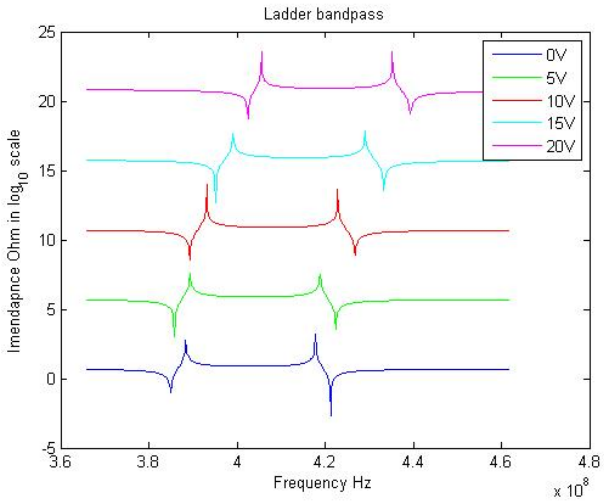

Figure 4-32: Ladder bandpass filter

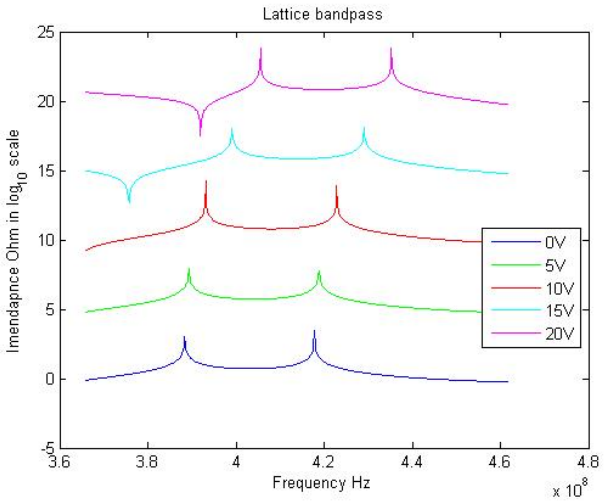

Figure 4-33: Lattice bandpass filter

In figure 4-32 it is easily seen that bandpass filter will be shifted entirely instead of just the shift the higher cutoff frequency figure 4-9. The same phenomena happens in the lattice topology. Analytical model for this design structure can be found under the matlab code in A.5. In order to confirm the legitimacy of this analytical formulation, the same structure has been modeled in **Comsol** which could be found under the name **FAB3.mph**.

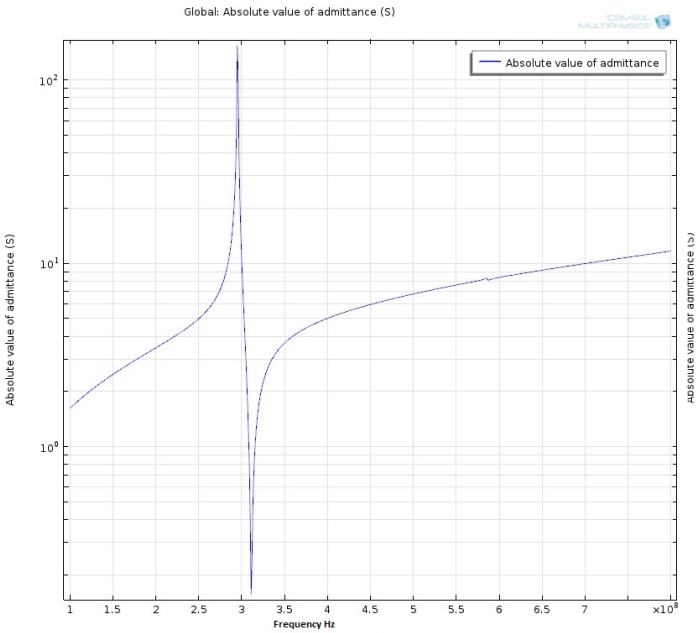

Figure 4-34: Untuned impedance

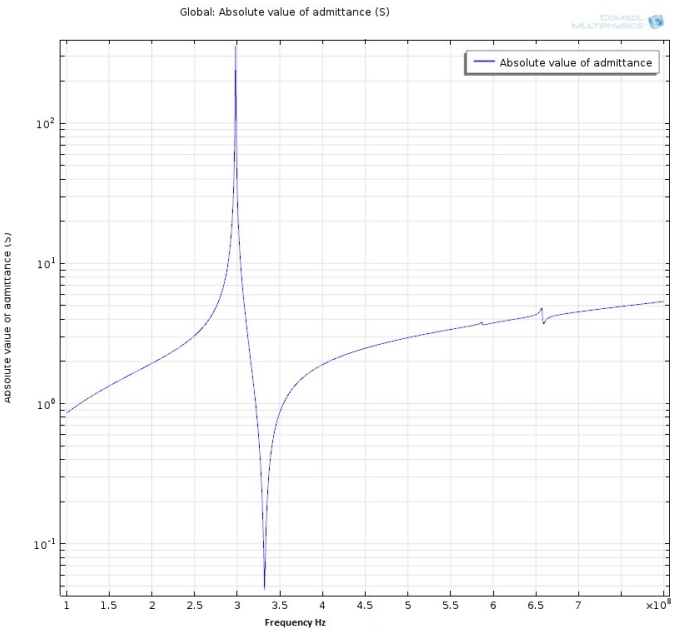

Figure 4-35: Tuned transfer function

This FBAR has the geometry outline as in figure 4-16. This is a 1D model and the dimensions of each layer in this structure are listed in the table 4.7. The outcome admittance from this model at zero DC bias has been plotted in figure 4-34. The same model has been simulated under a DC bias of 5V. A significant shift of frequencies of both resonance and antiresonance occurs with almost the same rate.

Layer	Material	Thikness(A)
Electroced	Alumimium	200
Ferroelectric	BST1	3000
Ferroelectric	BST2	4300
Anchor	Si	8000

Table 4.7: FBAR dimensions

4.3 Acoustically coupled

In order to see the efficiency of an acoustic coupled filter, coupling efficiency has been studied over a range of frequencies. Bandwidth of the filter is very restricted from the ability of the coupling layer. In the figure 4-36 is a simple structure consisting of two FBAR coupled by a single CDO layer. The range of frequencies where this structure is analysed varies starts at 360 MHz up to 380 MHz. Moreover each FBAR is being tuned by a DC bias voltage from 0 up to 35 V. In order to simplify the simulation this structure has been considered symmetric with regards to the coupling layer.

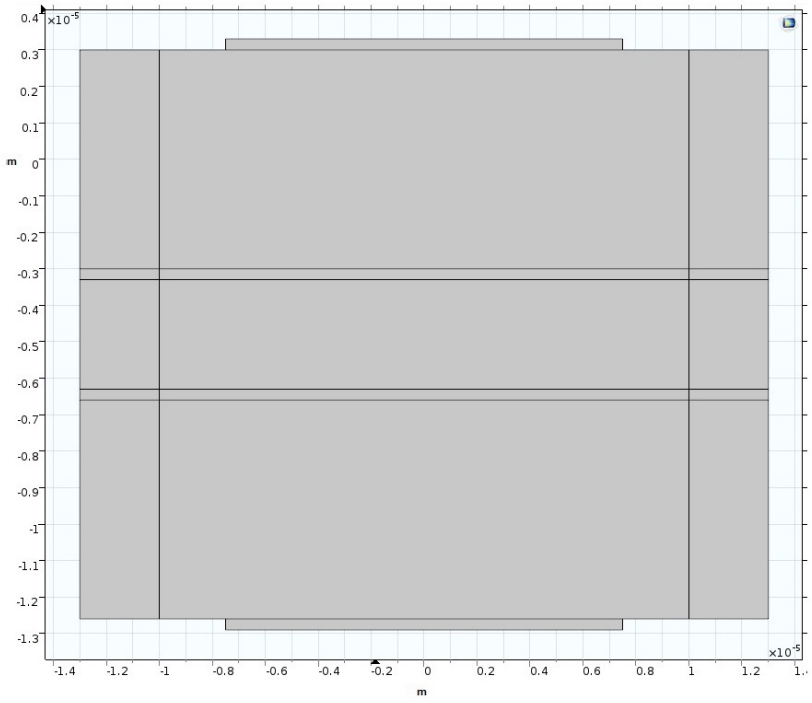

Figure 4-36: Tuned transfer function

The design parameters are listed in the table 4.8 including here acoustic impedance and velocity together with its respective thickness.

	Thikness(A)	Velocity(m/s)	Impedance(MRayls)	Ref
BST	6000	11040	20	[19]
Al	200	10520	40.6	[3]
CDO	530	3400	4.8	[22]

Table 4.8: Material design parameters

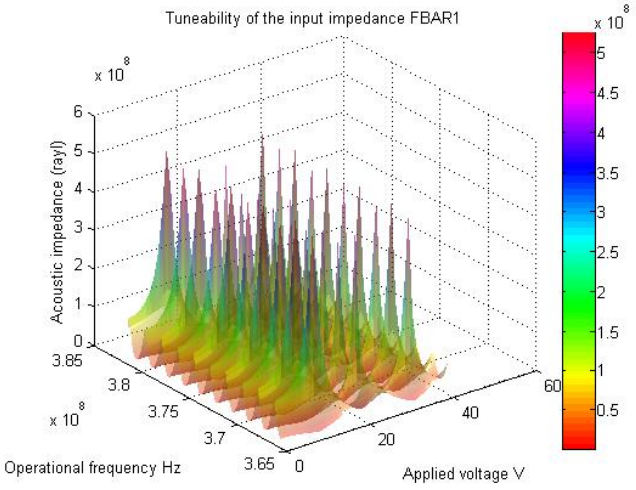

Figure 4-37: Acoustic impedance of FBAR1

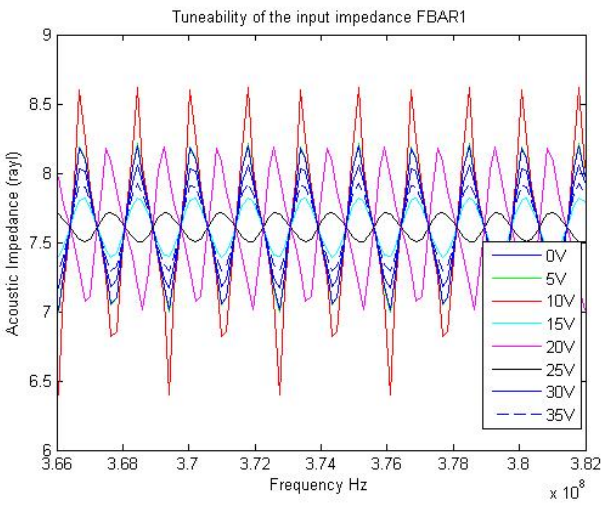

Figure 4-38: Acoustic impedance of FBAR1

Transmission line method described in 3.2 has been utilized to calculate the input acoustic impedance of stack layer. This is a quantity depending strictly on the operational frequency into a periodic pattern. Moreover due to the bias voltage input acoustic impedance will vary significantly as in figure 4-38. Acoustic impedance depending on the frequency is plotted in the figure 4-37. Input acoustic impedance sustain a periodicity in both frequency and voltage axis.

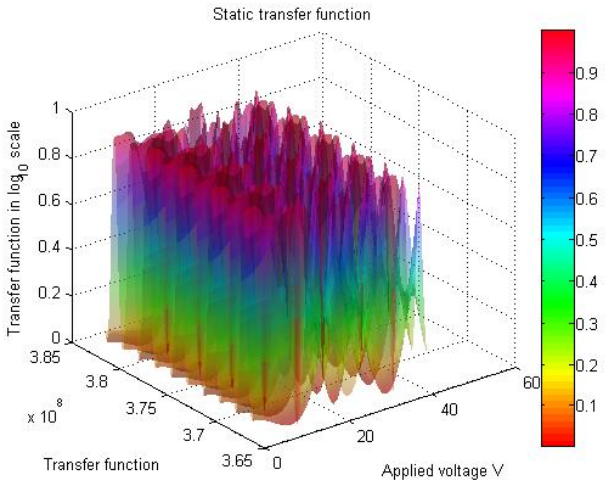

Figure 4-39: Static transfer function

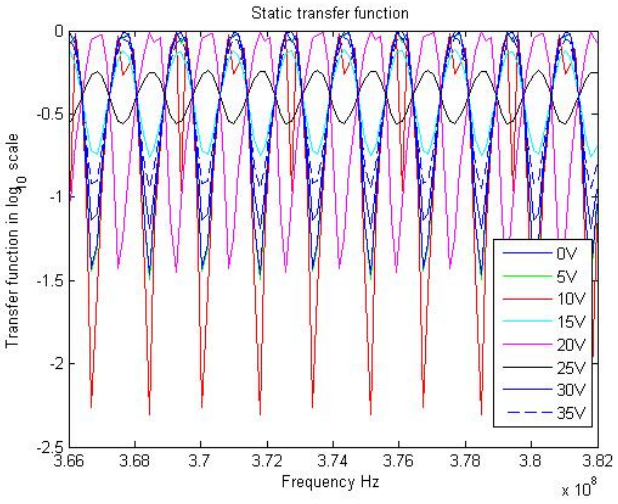

Figure 4-40: Static transfer function

Utilizing the CDO as a coupling layer does not provide a tuneable acoustic resistance. It performs a good coupling when there is no DC bias voltage because it fulfill the condition for perfect coupling as in equation 3.52 and 3.51. Similar to the input acoustic impedance this structure transmission has a 2D periodicity both in frequency and voltage as plotted in figure 4-39. The bias voltage will affect transfer capability significantly and in figure 4-40 is plotted the variation of the transmission coefficient.

In order to sustain the coupling layer requires a variations of the acoustic impedance consistently to the variation of the FBAR input acoustic impedance. The desired behaviour of the coupling layer acoustic impedance is plotted in figure 4-44. This quantity sustain a static value over the range of

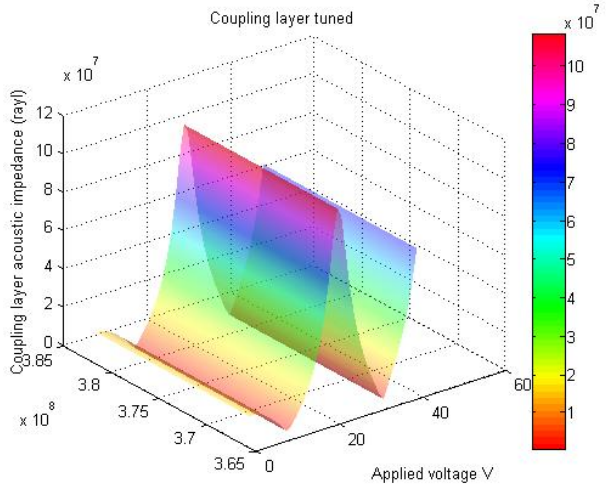

Figure 4-41: Desired behavior of coupling layer

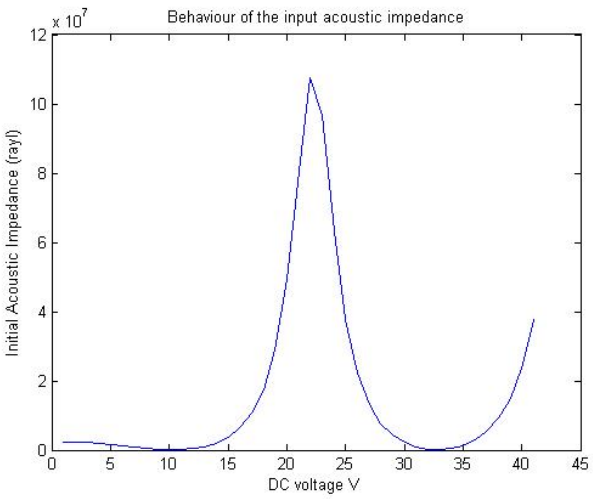

Figure 4-42: Acoustic impedance

frequencies as in figure 4-43. There are almost no functional material which could be change its acoustic properties with a flexible flow.

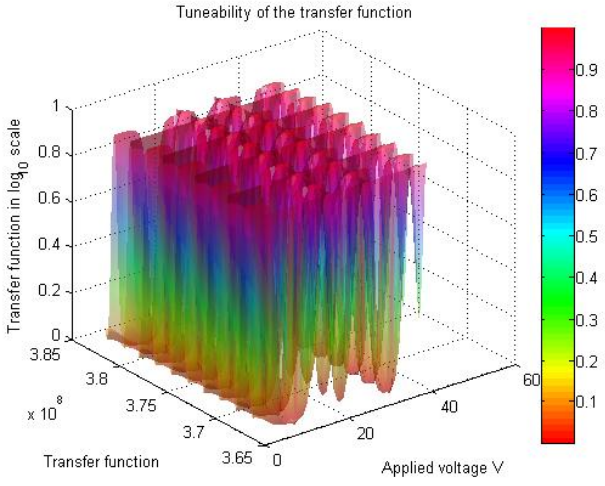

Figure 4-43: Tuneability transfer function

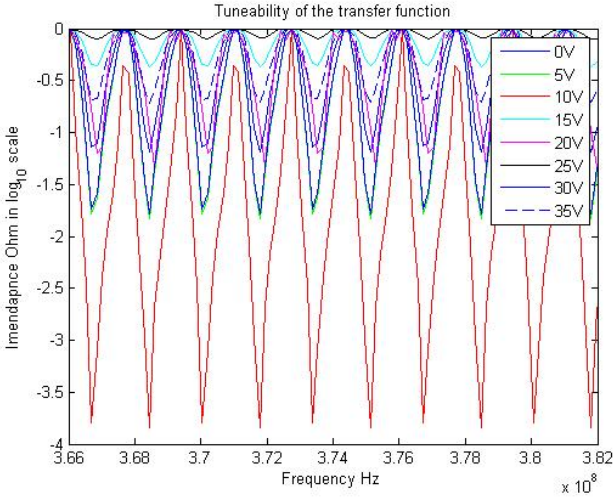

Figure 4-44: Tuneability transfer function

The outcome from the acoustic coupling gives three communication channel respective at 0.7 MHz 1.1 MHz and 1.4 MHz 4-45. The as already described this are the three bandpass channel which makes this a perfect tool for multi-direction channel.

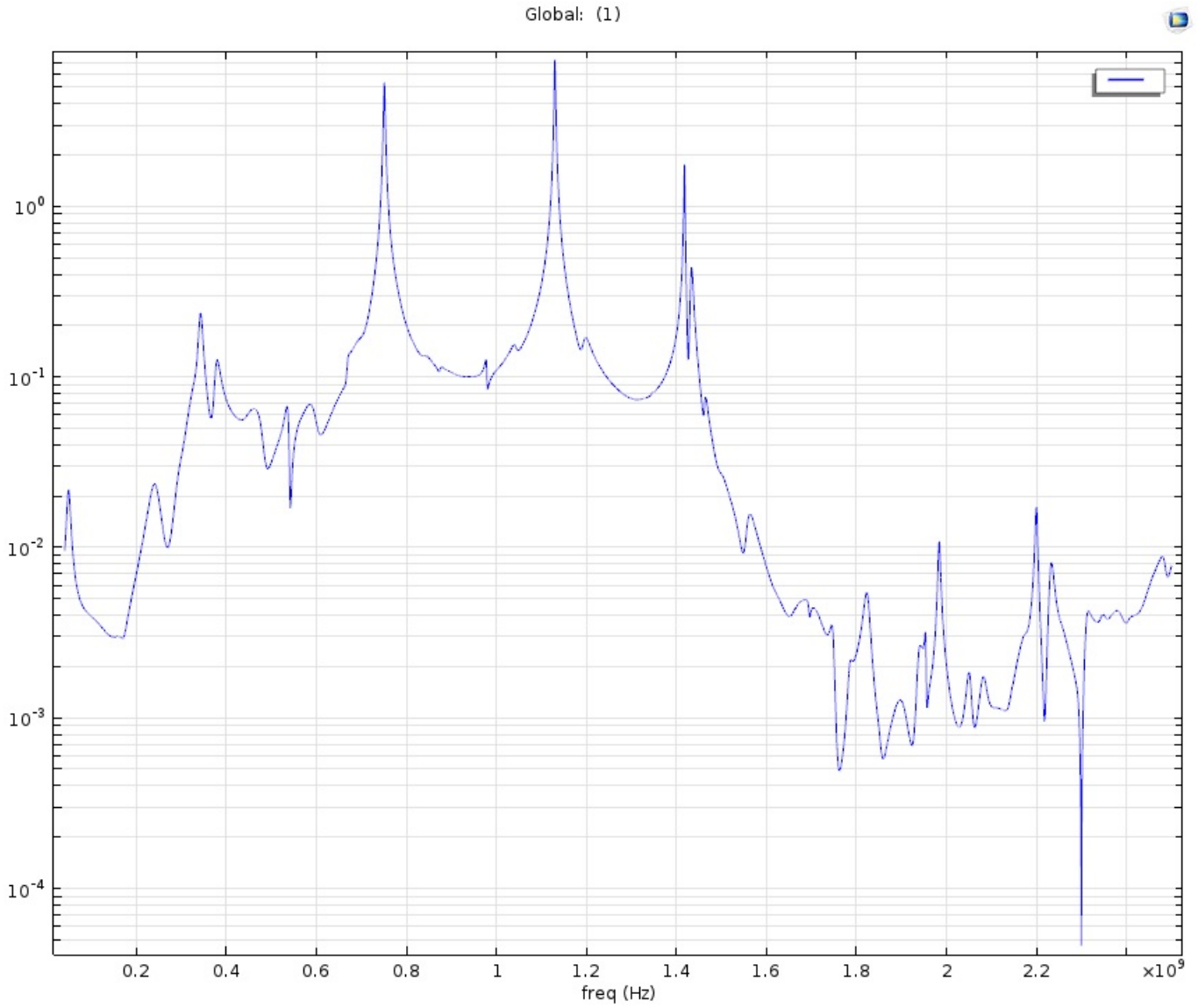

Figure 4-45: Acoustic coupling filter outcome

Chapter 5

Analysis and Discussion under progress

The last chapter of this work is dedicated to discussion and analyse all the results. This is a very important part of the thesis since all the functional requirements together with the contribution in this field are all overviewied in here. In addition to this, further challenges and suggestion for other researchers are listed here. Big attention is paid in physical phenomenas occurs in the proposed design and what encouragement are proposed for this active topic.

5.1 Discussion

FBAR are undoubtedly the most competitive approach in implementing bandpass filters for mobile telecommunication technology. Due to the already discussed extraordinary properties, FBAR technology has attracted a lot of research from leading Universities world wide. The operation of the filter depends significantly on the geometry of the 3D structure therefore enabling a lot of space for improvement. Regarding the material choice utilized in the medium depends significantly on the deposition technology.

The geometry of the FBAR is altered with the aim of increasing the tuneability. Instead of a homogeneous layer the medium is fabricated by two different mediums. Equation 3.25 is the constitutive equation for this model. The presence of two different materials will impose two different resonating conditioning. In other words the composite resonator will resonate at two distinct frequencies.

Electric impedance over a range of frequencies is that main property of the FBAR. This characteristic curve shift in frequency due to the superposition of a DC bias voltage. This is relevant in homogeneous and heterogeneous ferroelectric medium. Antiresonance frequency rate is inherently much higher compare to the resonance rate. Data from the proposed model claim an improvement of the resonance rate. Moreover it is important to highlight that antiresonance rate is strictly unchanged in the new design.

Many other previous study are using different fabrication technologies to deposit the ferroelectric

medium. The encouragement for a composite medium arise after the promising approach of the gradient stoichiometry [44]. The finding of this research proves that the overall tuneability of the resonator will be improved. However the data presented from **Tian** et al 2003 are acquired from direct C-V measurement without any analytical expression. The lack of an mathematical description makes this model extremely hard to further optimisation of desired parameters and not easy to adjust efficiently at a required frequency.

In another study **Liang** et al 2005 [27] doping of other MgO ions inside BST is aimed to be promising. The research is carried out with a highly accurate ion implantation technique. This is a vital necessity for this approach because the outcome is extremely sensitive on the out ion concentration. Even in this scenario there is no improvement of the resonance frequency rate in particular but an overall enhancement of tuneability.

Even though both these composite methods significantly improve the tuneability they require a very expensive fabrication method. On the other hand, the proposed method is only restricted on the thickness control of each layer. Ferroelectric material is another important parameter for FBAR specification where BST provides different properties consistently to the stoichiometry.

Temperature dependence is not modeled at neither of the simulation, however a research of **Astafiev** [8] proves that Curry temperature will decrease in composite structure. Since the tuneable filter is desired to work in the environment temperature this becomes even more stable when the resonator is a composite medium. This is not a very important aspect for the tuneability but a rather benefit for the stability.

5.1.1 Homogeneous structure

Benchmarking the homogeneous structure, the range of resonance frequency goes around 360 MHz. The accurate admittance plot resulted from comsol is in figure 4-4. Nearly the same characteristic is acquired from the analytical model the homogeneous structure but simulated in matlab. The admittance for this model plotted in figure 4-3 differ from its equivalent comsol model. Comsol model consider finite thin electrode consequently from the equation 2.49 the respective resonance and antiresonance frequency tend to be lower. In addition to this matlab and comsol are producing results upon two fundamentally different mathematical methods. Comsol is using finite element method (FEM) where the entire structure is broken down into finitely small elements. The main considerable assumption in this model is that the inner part of these small elements is considered absolutely homogeneous. This assumption will produce a systematic error which is inverse proportional to the size of mesh. The analytical model programmed in matlab on the other hand is a simple 1D model where the entire structure assumes the medium homogeneous. Differently from the 3D comsol model, meaning there are no generated phenomenas from different coupled models. Moreover the anisotropy

of the ferroelectric material is completely disregarding and there is no coupling happening among different modes. The quality factor can only be provided from the comsol model.

Regarding the tuneability which is the main purpose of this work, analytical model will still produce relatively consistent results. This models has been biased under range of DC voltages from 0V up to 20V. The resonance and antiresonance frequency will keep on sitting on higher frequency as the voltage increases. The total characteristic impedance will be unevenly shifted into higher frequencies as in figure 4-6. The extremely good quality factor provided by the FBAR is what makes this technology very special. The slope is translated into better selectivity of the filter. Tuning the FBAR will eventually increase this distance between the resonance and antiresonance frequency. Seen from the selectivity prospective tuneability will decrease this quantity significantly.

Employing this resonator into the main two topologies ladder and lattice filter yield an acceptable bandpass filter characteristic. The minimum configuration for the ladder requires two FBAR and tuning both of this will will cause the tune of the whole filter characteristics. In the figure 4-9 bias voltage will mainly increases the bandwidth rather than any other aim. This is a result only of the uneven rate of resonance and antiresonance rate. In addition to this as already stated selectivity worsen coherently with the tuneability.

Selectivity is reflected to the quality factor of the resonator. Q factor and selectivity are proportionally related together. In the figure 4-11 is plotted the decrease of the Q factors associate with DC voltage. It starts at 900 and decreases all the way down to 700. Even though high Q is not strongly the aim of this work it still remains at the attention. It is an extremely important parameter when designing a FBAR for any type of applications. A further investigation the Q factor will require the impact of the electrical field in many loss mechanism. This is translated into a precise variation of each non-zero tensor notation of the ferroelectric material.

Once again, resonance and antiresonance rate are significantly different in all the designs. This feature is inevitable as far as the medium is homogeneous and will be present at any further enhancement of the overall tuneability. In the figure 4-13 is the rate at which each resonance rise. In order to emphasize the differences in each quantity, the antiresonance case could be fit into a quadratic relation whereas the resonance case could be fit is a low gradient, linear relations. Most of the proposals so far improve materials properties. In all the cases this will be reflected similarly at both resonance and antiresonance. The only feature that won't be affected is the relative rate defined as in equation 5.1.

$$RT = \frac{(dF_a/dE)}{(dF_r/dE)} \tag{5.1}$$

Material properties are the very important parameters taken into consideration regarding tuneability in particular. The main three parameters running everything are dielectric constant, piezo-

electric coefficient and elastic constant. Electrical field will vary the parameter significantly and therefore the impedance will shift. The contribution to the overall tuneability will still be different from distinct parameters. In addition respective parameters are sensitive from the electrical field at different rate. Piezoelectric coefficient will be rather insensitive quantity with a maximum tuneability of

$$T_e = \frac{e_{E_{max}}}{e_{E=0}}(MinValue - MaxVal) * 100\% = 0.16\% \tag{5.2}$$

The dielectric permittivity is a far more sensitive quantity to the electrical field. It is the most influential quantity on the tuneability and it is a common quantity among all the ferroelectric materials. BST materials posses very promising microwave properties with a breakdown electric field of $540\frac{kV}{cm}$. This relation is plotted in the figure 4-15 Due to its symmetry the electrical field will actually impose only along the direction of propagation. This is concluded from the tensor notation of the pervoskite where the non zero quantity are only main diagonal. The microwave tunability within the breakdown voltage is significantly higher compare to the other two quantities

$$T_\epsilon = \frac{\epsilon_{E_{max}}}{\epsilon_{E=0}} = 20\% \tag{5.3}$$

Electric coefficient will also make the ferroelectric material stiffer. This quantity is linearly related to the piezoelectric coefficient and dielectric permittivity as in equation 2.54. In this expression c^E will remain unchanged at any electrical field [9]. Tuning dielectric permittivity and piezoelectric coefficient will give simultaneously stiffen the ferroelectric medium. Since the main contribution comes from the variation of the dielectric permittivity makes it sensitive only to the propagation of the electrical field. From the figure 4-12 the maximum tuneability of the stiffness coefficient is

$$T_{c^D} = \frac{c^D_{E_{max}}}{c^D_{E=0}} * 100\% = 6\% \tag{5.4}$$

In the homogeneous case these material parameters will have a uniform contribution to the total impedance since $Z \approx \frac{e}{c^D \epsilon}$. However this is a rather less important quantity since the the value of the impedance doesn't affect the filter efficiency.

Coupling coefficient is another the last important parameter of the homogeneous impedance which is a quantity directly related to the materials parameters $K = \frac{e^2}{c^D \epsilon}$. It describes the capability of the design to convert the electrical to mechanical energy. Electrode thickness will also be the vary the coupling proportionality as in equation 2.48. The input RF signal in the FBAR will be converted into acoustic vibration at constant rate over all the frequencies. Every present frequency component will be translated into the same quantity compared to the every other frequency. Coupling coefficient is responsible for filter bandwidth where from the equation 2.36 the increase of coupling will be

reflected into higher bandwidth. Under a DC electrical field will rise the piezoelectric coefficient, and significantly decrease dielectric permittivity whereby this will lead to increase of the coupling coefficient.

5.1.2 Compisite FBAR

The overall discussion so far are only for the homogeneous structure. The proposed structure has a double layer of two different types of ferroelectric materials. Fabrication of this topology is inexpensive using a sol-gel technique developed by Adikary et al 2011 [4]. The main requirements of this fabrication technique is continuity of stress and displacement at the junction of this two mediums.

The new structure possess two distinct resonating condition where the antiresonance frequency is strictly defined by the thickness and material of each layer equation 3.30 and 3.31. Antiresonance frequency is the only autonomous term which is defined directly from the either layer independently. The rest of quantities strictly depend on combination of both layers. Starting with the total impedance which consist on the independent terms 3.27 and 3.28 Regarding the term 3.29 represent the impedance coming from the interaction of both mediums. This quantity is proportional to how much different the materials are and goes to zero if the materials are the same. However the impedance is a rather not so important description for filter implementation. The other and the most important quantity is the resonance frequency. Resonance frequency is fulfill the condition where all the three impedance components 3.26 sum up to zero. This depends from the both materials and geometry dimensions into a very complex relation.

A numerical model has been programmed for tuneable composite FBAR and the impedance profile is in figure 4-19. This compared to the impedance of homogeneous structure in figure 4-18 at almost the same resonating frequency. In this two figures is easily seen that resonance frequency is shifted into higher frequencies much faster in the heterogeneous case. Whereas the rate of antiresonance frequency remains unchanged. The proposed model doesn't have a derived analytical expression regarding resonance frequency and this makes a bit hard to physically explain the resonance frequency. The resonance frequency depends from both mediums dimensions and properties. In the figure 4-20 are the rate of resonance and antiresonance frequency for both structures where the resonance rate of heterogeneous is significantly improved.

This is the first quantity which is differently defined from the homogeneous structure where the data shows a better tuneability. Another important parameter which is differently defined in the heterogeneous case is the electrical field. This interacts at each medium and therefore tunes the FBAR. Electrical field is derived into a recursive equation 3.43 and 3.44 and similarly to the resonance frequency depends on the dimensions of both mediums. The electrical field tends to increase as the voltage increases however the precise values at specific time is still hard to be optimise without a

non recursive equations. Ration of thicknesses among the two materials will vary the distribution of electrical field in both mediums as in figure 4-30 and 4-31. Despite the complicated relation of the electrical field, in the thinner mediums electrical field is higher. Electrical field increases faster at lower ration at smaller ration of thicknesses.

Material parameters of both structure will also vary proportionally to the acquired electrical field in both mediums. Similarly to the antiresonance rate, the properties of the materials in the heterogeneous case will vary strictly the same as in the homogeneous case. This comparison is when the same quantity of the electrical field interact at both instants. The differences in these models is that the electrical field they get from the shared voltage is unequal. The first medium acquires electrical field at lower quantities for the same voltage and figures 4-22 4-24 and 4-26 shows the x axis for the first medium ending up at lower values.

On the other hand, coupling coefficient is another property that is much different from the homogeneous case. In order to confirm the consistency of the comparison the equation 2.36 is utilized in both cases. Based on this formula the heterogeneous case possesses lower capability for electro-mechanical coupling. The coupling coefficient of the proposed model is significantly lower even though the electrode thicknesses are considered infinitely thin for both structure. Due to the tuneability the impedance characteristics coupling coefficient for the stimulated structure behaves differently. In the homogeneous case its increases throughout the range of voltages, whereas in the proposed structure coupling increases at a low rate up to its maximum value and decreases significantly after 14V bias voltage figure 4.2. This is an expectable behaviour since the difference $f_a - f_r$ increases at a lower rate comparing to how much f_a increases.

A simple ladder and lattice filter is implemented where the resonators are composite structure and this model is simulated in matlab. There are three main important properties of the bandpass filter including selectivity, bandwidth and the operating frequency. Applying the bias voltage will yield the shift the transfer function of the filter evenly figure 4-32 and 4-33. Another import feature of the coupling layer is that input impedance is insensitive to the operation frequency. This property doesn't increase the bandwidth of the filter with is prevalent in the homogeneous case. In addition to this selectivity doesn't decay due the same rate of the tuneability of resonance and antiresonance frequency. At the end the main goal is a tuneable filter which could be truly tuned via a DC bias voltage.

5.1.3 Acoustic coupling

Acoustic coupling is another competitive approach utilized for filter application. However coupling acoustically tuneable FBAR is very challenging. The model utilized in this section has a simple coupling layer sandwiched by two resonators. This design works perfectly in the absence of the DC

bias voltage. The bias voltage differs the material parameters significantly, and therefore the input impedance will drastically change. The coupling layer for the proposed design is CDO with static properties. When the input acoustic impedance of both FBAR vary the total transmission efficiency will also vary significantly. Via the transmission line method input impedance of the FBAR over the range of DC voltages behaves into a periodic structure in frequency range figure 4-38.

The bias voltage will however change the pattern amplitude of the impedance quite drastically. This is associated with an predictability over a specific range of voltages with a quasi periodic pattern pattern 4-37. Both resonator have a similar acoustic properties and they work under the same bias voltage. In figure 4-40 is the impact of bias voltage over the range of frequencies regarding the transmission efficiency. Similarly to the input impedance, transmission efficiency follow the input impedance pattern over the range of applied voltages. This makes extremely hard to meet the acoustic impedance condition in equation 3.51 for a perfect transmission coupler. The transmission efficiency sustains the same periodicity at any voltage however for particular values the phase inversion might occurs. In order to suppress these variation the coupling layer needs to have a variation of the acoustic impedance consistently to the variation of the input impedance of the FBARs. In this particular implementation bias voltage will require to acoustic impedance as in figure 4-42.

Selecting a coupling layer is a very hard task and in many cases a combination of multiple layer is needed to meet the required impedance. It is even more difficult to provide a coupling layer where the internal input acoustic impedance will vary as in figure 4-42. In the specified design the best transmission efficiency that could be reached doesn't have any variation at any DC bias voltage and still sustaining the same periodicity figure 4-44. Even though this transfer characteristics is very ideal to be reached, the proposal in figure 3-13 could be a very competitive approach. In this structure the coupling layer is doesn't have a static acoustic impedance but a the middle ferroelectric medium will be tuned by another bias voltage. This will provide a acoustic impedance which is presumable to meet the desired input impedance of figure 4-38. This structure has not been investigated due to the limited time but could be proposed for a possible future work on this topic.

5.2 Conclusion

In this thesis work the result is carried out a study on tuneable FBAR and partly acoustic coupling. Tuneable FBAR are feasible only through ferroelectric medium. Bias voltage vary the material properties where the most notable one is dielectric permittivity therefore the impedance profile of the composite structure will be shifted into higher frequencies. The majority of the topologies employ a homogeneous medium sandwiched by two thin electrodes. Tuneability of the resonance frequency for the homogeneous structure in particular is inherently lower for any material parameters compared to the antiresonance frequency. This configuration however doesn't provide satisfied properties for

tuneable filter. Instead of moving the bandwidth of the filter what happen is the increase of the bandwidth. This is mainly because the antiresonance rate goes faster into higher frequency than resonance frequency. Moreover a secondary effect is the decrease of the selectivity since the distance between resonance and antiresonance frequency become bigger.

In order to overcome this drawback a double layer medium has been proposed in this work. This structure exhibits extraordinary tuneability rate of the resonance frequency. Utilizing the proposed structure for a filter implementation outcomes a much better tuneable bandpass pattern. Applying a bias voltage in this scenario causes a shift of the total bandpass structure instead of increasing the bandwidth. The drawback arising from the composite structure is the law coupling coefficient. In addition this resonators has distinguishable distribution of the electrical field which is controlled by the material parameters rather than just the thickness of the layer. The new structure doesn't need to upgrade any fabrication technology since it contains a nested layer above the existing one.

The proposed structure is not fully described analytically. There is no derived expression regarding the full description of coupling coefficient and resonance frequency. One possible path for the coupling coefficient is via equations 2-20 due to the complexity of equations time was not enough for this task. In addition electrical field is not expressed into a fully transcendental equation but a rather recursive expression for a chosen value. Precise formulas of these quantities would be a tool to design better tuneable FBAR. Optimisation of quality factor for the composite structure is another important parameter for the design of resonators.

Last but not least, coupling acoustically tuneable FBAR for filter implementation is a rather hard task. The transmission efficiency of this structure varies significantly as the voltage increases. This is a result of acoustic impedance variation at each resonator. Material parameters that are being tuned are responsible for the variation of both acoustic impedance and resonance frequency. The transmission drift cannot be neglected since in some values there are even inverted values from maximum to minimum transmission. In order to keep the transmission efficiency not affect by the resonance tuneability a proposal different coupler configuration has been proposed. This structure is aimed to vary the internal input impedance of the coupling layer consistently the variation of the input impedance of each resonator. The proposed coupler has a ferroelectric layer sandwiched by two electrodes where DC voltage varies the properties of the ferroelectric layer. Due to the limited time this design has not been fully analysed but is a very competitive approach for acoustic coupling tuneable filter.

Bibliography

[1] Comsol official website. www.comsol.com. Accessed: July 24, 2015.

[2] Dissemination of IT for the Promotion of Materials Science cambridge university. http://www.doitpoms.ac.uk/tlplib/piezoelectrics/dipole.php. Accessed: July 24, 2015.

[3] Onda corporation. http://www.ondacorp.com/. Accessed: July 24, 2015.

[4] SU Adikary and HLW Chan. Compositionally graded ba x sr 1- x tio 3 thin films for tunable microwave applications. *Materials Chemistry and Physics*, 79(2):157–160, 2003.

[5] SU Adikary and HLW Chan. Ferroelectric and dielectric properties of sol–gel derived ba x sr 1- x tio 3 thin films. *Thin Solid Films*, 424(1):70–74, 2003.

[6] Aftab Ahmed, Irene A. Goldthorpe, and Amir K. Khandani. Electrically tunable materials for microwave applications. *Applied Physics Reviews*, 2(1):–, 2015.

[7] R. Aigner. Saw and baw technologies for rf filter applications: A review of the relative strengths and weaknesses. In *Ultrasonics Symposium, 2008. IUS 2008. IEEE*, pages 582–589, Nov 2008.

[8] K.F. Astafiev, V.O. Sherman, A.K. Tagantsev, and N. Setter. Can the addition of a dielectric improve the figure of merit of a tunable material? *Journal of the European Ceramic Society*, 23(14):2381 – 2386, 2003. Microwave Materials and Applications.

[9] B. A. Auld. *Acoustic fields and waves in solids*. Wiley, New York, 1973.

[10] B. A. Auld. *Acoustic fields and waves in solids*. R.E. Krieger, Malabar, Fla, 1990.

[11] I Aulika, J Pokorny, V Zauls, K Kundzins, M Rutkis, and J Petzelt. Structural and optical characterization of ba 0.8 sr 0.2 tio 3 pld deposited films. *Optical Materials*, 30(7):1017–1022, 2008.

[12] A.H. Cardona and R.A. York. Switchable tunable acoustic resonator using bst material, March 9 2010. US Patent 7,675,388.

[13] S-H Chang, NN Rogacheva, and CC Chou. Analysis of methods for determining electromechanical coupling coefficients of piezoelectric elements. *Ultrasonics, Ferroelectrics, and Frequency Control, IEEE Transactions on*, 42(4):630–640, 1995.

[14] Matthieu Chatras. *Modeling and Measurement Methods for Acoustic Waves and for Acoustic Microdevices*.

[15] Ding-Yuan Chen and JamieD. Phillips. Electric field dependence of piezoelectric coefficient in ferroelectric thin films. *Journal of Electroceramics*, 17(2-4):613–617, 2006.

[16] Richard S. C. Cobbold. *Foundations of Biomedical Ultrasound*. December 2007.

[17] M.A. Dubois. Thin film bulk acoustic wave resonators: A technology overview. *MEMSWAVE,*, July, 2003.

[18] G.G. Fattinger, S. Marksteiner, J. Kaitila, and R. Aigner. Optimization of acoustic dispersion for high performance thin film baw resonators. In *Ultrasonics Symposium, 2005 IEEE*, volume 2, pages 1175–1178, Sept 2005.

[19] Spartak Gevorgian. *Tuneable film bulk acoustic wave resonators*. Springer, London New York, 2013.

[20] Motoaki Hara and Hiroki Kuwano. Spurious suppression without energy dissipation in aluminum–nitride-based thin-film bulk acoustic resonator using thin ring on electrode edge. *Japanese Journal of Applied Physics*, 51(7S):07GC11, 2012.

[21] Ken-ya Hashimoto. *RF Bulk acoustic wave filters for communications*. Artech House, 2009.

[22] T. Jamneala, U. Koelle, A. Shirakawa, S.R. Gilbert, P. Nikkel, C. Feng, and R. Ruby. Ultra-miniature coupled resonator filter with single-layer acoustic coupler. *Ultrasonics, Ferroelectrics, and Frequency Control, IEEE Transactions on*, 56(11):2553–2558, November 2009.

[23] J. Kaitila, M. Ylilammi, J. Ella, and R. Aigner. Spurious resonance free bulk acoustic wave resonators. In *Ultrasonics, 2003 IEEE Symposium on*, volume 1, pages 84–87 Vol.1, Oct 2003.

[24] Kenneth M Lakin. Thin film resonator technology. *Ultrasonics, Ferroelectrics, and Frequency Control, IEEE Transactions on*, 52(5):707–716, 2005.

[25] K.M. Lakin, G.R. Kline, and K.T. McCarron. High q microwave acoustic resonators and filters. In *Microwave Symposium Digest, 1993., IEEE MTT-S International*, pages 1517–1520 vol.3, June 1993.

[26] Sidney B Lang. Pyroelectricity: from ancient curiosity to modern imaging tool. *Physics Today*, 58(8):31–36, 2005.

[27] Rui-Hong Liang, Xian-Lin Dong, Ying Chen, Fei Cao, and Yong-Ling Wang. Effect of la2o3 doping on the tunable and dielectric properties of bst/mgo composite for microwave tunable application. *Materials Chemistry and Physics*, 95(2–3):222 – 228, 2006.

[28] A. Link, E. Schmidhammer, H. Heinze, M. Mayer, B. Bader, and R. Weigel. Appropriate methods to suppress spurious fbar modes in volume production. In *Microwave Symposium Digest, 2006. IEEE MTT-S International*, pages 394–397, June 2006.

[29] A. Link, E. Schmidhammer, H. Heinze, M. Mayer, B. Bader, and R. Weigel. Appropriate methods to suppress spurious fbar modes in volume production. In *Microwave Symposium Digest, 2006. IEEE MTT-S International*, pages 394–397, June 2006.

[30] Hua Long, Guang Yang, Aiping Chen, Yuhua Li, and Peixiang Lu. Growth and characteristics of laser deposited anatase and rutile tio2 films on si substrates. *Thin Solid Films*, 517(2):745 – 749, 2008.

[31] Martin Maldovan. *Periodic materials and interference lithography for photonics, phononics and mechanics*. Wiley-VCH, Weinheim, 2009.

[32] R. Nath, S. Zhong, S. P. Alpay, B. D. Huey, and M. W. Cole. Enhanced piezoelectric response from barium strontium titanate multilayer films. *Applied Physics Letters*, 92(1):–, 2008.

[33] J. F. Nye. *Physical properties of crystals : their representation by tensors and matrices*. Clarendon Press Oxford University Press, Oxford Oxfordshire New York, 1985.

[34] Wanling Pan, Vikram A Thakar, Mina Rais-Zadeh, and Farrokh Ayazi. Acoustically coupled thickness-mode **AIN-on-Si** band-pass filters-part i: principle and devices. *Ultrasonics, Ferroelectrics, and Frequency Control, IEEE Transactions on*, 59(10):2262–2269, 2012.

[35] Lorena Pardo. *Multifunctional polycrystalline ferroelectric materials processing and properties.* Springer, Dordrecht New York, 2011.

[36] T. Pensala, J. Meltaus, K. Kokkonen, and M. Ylilammi. 2-d modeling of laterally acoustically coupled thin film bulk acoustic wave resonator filters. *Ultrasonics, Ferroelectrics, and Frequency Control, IEEE Transactions on*, 57(11):2537–2549, November 2010.

[37] Joel Rosenbaum. *Bulk acoustic wave theory and devices.* Artech House, Boston, 1988.

[38] R. Ruby. 11e-2 review and comparison of bulk acoustic wave fbar, smr technology. In *Ultrasonics Symposium, 2007. IEEE*, pages 1029–1040, Oct 2007.

[39] R. Ruby. Review and comparison of bulk acoustic wave fbar, smr technology. In *Ultrasonics Symposium, 2007. IEEE*, pages 1029–1040, Oct 2007.

[40] Seyit Ahmet Sis, Victor Lee, Jamie D Phillips, and Amir Mortazawi. Intrinsically switchable thin film ferroelectric resonators. In *Microwave Symposium Digest (MTT), 2012 IEEE MTT-S International*, pages 1–3. IEEE, 2012.

[41] Vikram A Thakar, Wanling Pan, Farrokh Ayazi, and Mina Rais-Zadeh. Acoustically coupled thickness-mode **AlN-on-Si** band-pass filters-part ii: simulation and analysis. *Ultrasonics, Ferroelectrics, and Frequency Control, IEEE Transactions on*, 59(10):2270–2277, 2012.

[42] R. Thalhammer, G. Fattinger, M. Handtmann, and S. Marksteiner. Ohmic effects in baw-resonators. In *Microwave Symposium Digest, 2006. IEEE MTT-S International*, pages 390–393, June 2006.

[43] Robert Thalhammer, Jyrki Kaitila, Sebastian Zieglmeier, and Lueder Elbrecht. 4e-3 spurious mode suppression in baw resonators. In *Ultrasonics Symposium, 2006. IEEE*, pages 456–459. IEEE, 2006.

[44] Hu Yong Tian, Helen Lai Wa Chan, Chung Loong Choy, and Kwangsoo No. The effects of composition gradients of ba x sr 1- x tio 3 thin films on their microstructures, dielectric and optical properties. *Materials Science and Engineering: B*, 103(3):246–252, 2003.

[45] Andrei Vorobiev, Spartak Gevorgian, Markus Löffler, and Eva Olsson. Correlations between microstructure and q-factor of tunable thin film bulk acoustic wave resonators. *Journal of Applied Physics*, 110(5):054102, 2011.

[46] Ryan S Westafer, Saeed Mohammadi, Ali Adibi, and William D Hunt. Computing surface acoustic wave dispersion and band gaps. In *Excerpt from the Proceedings of the COMSOL Conference*, 2009.

[47] Tao Zhang, Hui Zhang, Zuo-qing Wang, and Shu-yi Zhang. Effects of electrodes on performance figures of thin film bulk acoustic resonators. *The Journal of the Acoustical Society of America*, 122(3), 2007.

[48] Yafei Zhang. *Multilayer integrated film bulk acoustic resonators.* Springer Shanghai Jiao Tong University Press, Heidelberg New York Shanghai, 2013.

Appendix A

Simulation Code

A.1 Tune rate

```
%%
clear all
close all
clc
%%
%Applied Voltage
V=0;%Volt
%Thicekness
d=9*10^(-6);%meter
%Density
rho=2.5*10^6;%g/m^3
%Piezoelecetrice ceoefficeient
e=1:.01:10;
e=10^5*e;
%Elecetriceal permitivity
epsO=100:350;
% meshgriding Electrostriction and dielectric constant
[e1,eps1]=meshgrid(e,epsO);
%Freee space dielectric constant
epso=8.8*10^(-12);
%Elastice ceoefficeient
ce=1.214*10^11;
%Elecetriceal field
```

```
E=V/d;
%Beta ceoefficeient
b=10^(11);
%Mju ceoefficeient
mu=478*10^(-11);
%Resonancee frequency
% Fr=(sqrt(ce/rho)/(2*d))*sqrt(1+e^2/ce*epsO);
% %Antirezonance frequency
% Far=(sqrt(ce/rho)/(2*d))*sqrt((ce*epsO+e^2)/ce*epsO*((ce*epsO)^2-e^4))
    ;

V=0;
E=V/d;

eps=eps1./(1*(ones(size(eps1)))+b*(eps1*epso).^3*E^2);
eE=e1*(1+mu*abs(E));

% Antiresonance rate
t1=3*b*(eps1).^4*(epso).^3*E;
t2=ones(size(eps1))+3*b*(eps1).^3*(epso).^3*E^2;
t3=t1./(t2.^2);
t4=(eE./eps);
t5=(2.*e1.*mu)-(t3.*t4);
t6=(1/(2*d*sqrt(ce*rho)));
t7=((ones(size(e1))+(eE.^2)./(ce*eps)).^(-1/2));
RT=t6.*t7.*t4.*t5;
% Antiresonance frequency
FA=t6.*t7.*ce;
% Resonance rate
m1=(2*e1.*eps1.*ce)./(e1.^2+eps.*ce).^2;
m2=(-e1.^2.*ce)./(e1.^2+eps.*ce).^2;
K=(e1.^2)./(e1.^2+eps.*ce);
dK=(m1.*e1.*mu)+(m2.*t4.*3);
m3=sqrt(ones(size(K))-K);
RT1=RT.*m3-2*(FA.*sqrt(K).*dK)./m3;
```

```
% Resonance frequency
FR=FA.*m3;

figure
%     subplot(131)
mesh(e1,eps1,(RT));
%     surf(e1,eps1,(RT),'FaceColor','red','EdgeColor','none')
camlight left;
lighting phong;
colormap hsv
colorbar
alpha(.4)
title('');
ylabel('Dielectricity'),xlabel('Electrostriction'),zlabel('Antirezonance
    rate(Hz/(V/m))');
figure

%     subplot(133);
mesh(e1,eps1,(RT1));
camlight left;
lighting phong;
colormap hsv
colorbar
alpha(.4)
title('');
ylabel('Dielectricity'),xlabel('Electrostriction'),zlabel('Rezonance
   rate (Hz/(V/m))');
figure
% subplot(223)
mesh(e1,eps1,(FA));
camlight left;
lighting phong;
colormap hsv
colorbar
alpha(.4)
```

```
91 title('');
92 ylabel('Dielectricity \eps'),xlabel('Electrostriction'),zlabel('
     Antirezonance frequency Hz');
93 figure
94 % subplot(223)
95 mesh(e1,eps1,(FR));
96 camlight left;
97 lighting phong;
98 colormap hsv
99 colorbar
100 alpha(.4)
101 title('');
102 ylabel('Dielectricity'),xlabel('Electrostriction'),zlabel('Rezonance
     frequency Hz');
103 figure
104 % subplot(224)
105 mesh(e1,eps1,sqrt(K));
106 camlight left;
107 lighting phong;
108 colormap hsv
109 colorbar
110 alpha(.4)
111 title('');
112 ylabel('Dielectricity'),xlabel('Electrostriction'),zlabel('Coupling
     coefficient');
```

A.2 Impedance of composite medium

```
1 function CompositeStructure()
2 %%
3 clear all
4 close all
5 clc
6 %%
7 %First material properties
8 %Range of frequencies
```

```
w=1500:.001:3800;
w=10^6*w;
%First materials properties
%Thicekness
d=3*10^(-6);%meter
% Active area
A=1.7*10^(-9);%square meter
%Density
rho=5.5*10^3;%kg/m^3
%Piezoelecetrice ceoefficeient
e=10.9;
%Freee space dielectric constant
epsO=8.8*10^(-12);
epsr=1234;
epso=epsr*epsO ;
%Elastice ceoefficeient
cd=2.214*10^(11);%
%Stiffned elastic constant
% cd=ce+e/eps;
%Acoustic velocity
v=sqrt(cd/rho);%m/s
%%
%Second materials properties
%Thicekness
d1=3.4*10^(-6);%meter
% Active area
A=1.7*10^(-9);%square meter
%Density
rho1=5.5*10^3;%kg/m^3
%Piezoelecetrice ceoefficeient
e1=11.9;
%Freee space dielectric constant
epsO=8.8*10^(-12);
epsr=1034;
epso1=epsr*epsO ;
```

```
%Elastice ceoefficeient
cd1=1.214*10^(11);%
%Acoustic velocity
v1=sqrt(cd1/rho1);%m/s
%&%
[Z,Z1,Z2,K10]=ImpedanceComposite(d,d1,A,e,e1,cd,cd1,epso,epso1,w,v,v1);
%%
plot(w/(2*pi),log10(abs(Z)),'k')
hold on
%%
plot(w/(2*pi),log10(abs(K10)),'r')
hold on
%%
plot(w/(2*pi),log10(abs(Z2)),'m')
legend('FBAR1')
hold on
%%
plot(w/(2*pi),log10(abs(Z1)),'g'),xlabel('Frequency Hz'),ylabel('
    Impendance Ohm in log_{10} scale')
legend('Z Totals','Common term','FBAR1','FBAR2')
hold on
end
```

A.3 Homogeneous FBAR

```
function HomogeneousFBAR()
%
%
%%
clear all
close all
clc
%%
MaxVoltage=20;
%Range of frequencies
w=1600:3500;
```

```
% w=1000:1800;
w=10^6*w;
%Materials properties
%Thicekness
d=3*10^(-6);%meter
% d=d/2;
% Active area
A=1.7*10^(-9);%square meter
%Piezoelecetrice ceoefficeient
e=10.9;
%Freee space dielectric constant
epsO=8.8*10^(-12);
epsr=1134;
epso=epsr*epsO ;
%Elastice ceoefficeient
cd=1.014*10^(11);%
%Stiffned elastic constant
% cd=ce+e/eps;
%Density
rho=5.5*10^3;%kg/m^3
%Acoustic velocity
v=sqrt(cd/rho);%m/s
%Couling coefficient
[Z2]=ImpedanceCurve(A,d,e,cd,epso,w,v);
%%
%Finding the matching thickenss of the second resonator
[~,y]=min(Z2);
W=w(y);
[~,y1]=max(Z2);
W1=w(y1);
d1=double(pi*v/(2*W));
%%
[Z1]=ImpedanceCurve(A,d1,e,cd,epso,w,v);
%%
hold on
```

```
47 plot(w/(2*pi),log10(abs(Z2)),'b')
48 hold on
49 plot(w/(2*pi),log10(abs(Z1)),'r')
50 xlabel('Frequency Hz'),ylabel('Impendance Ohm in log_{10} scale')
51 title('FBAR Impendance')
52 legend('Z2','Z1')
53 %%
54
55 %%
56 % Tuning microwave parameters
57 beta=7*10^10; % Vm^5/C^3
58 %%
59 %Tuning electrostriction
60 mu=463*10^(-12); %
61 %%
62 % Elastic constant
63 ce=1.25*10^(11);
64 V=20;
65 [eps,e1,cd1,K,E]=TuneParametersHomogeneous(e,ce,epsO,epsr,beta,mu,d,V);
66 figure
67 plot(E,cd1,'o')
68 hold on
69 plot(E,cd1,'r')
70 xlabel('Electric field V/m')
71 ylabel('Elastic constant (Pa)'),title('Tuneability of elastic constant
      cd')
72 %%
73 figure
74 plot(E,eps,'o')
75 hold on
76 plot(E,eps,'r')
77 xlabel('Electric field V/m')
78 ylabel('Dielectric constant relative (unit)'),title('Tuneability of
      microwave parameter eps')
79 %%
```

```
figure
plot(E,log10(e1),'o')
hold on
plot(E,log10(e1),'r')
xlabel('Electric field V/m')
ylabel('Piezoelectric constant C/m^2'),title('Tuneability of
    electrostriction e')
%%
figure
plot(E,K,'o')
hold on
plot(E,K,'r')
xlabel('Electric field V/m')
ylabel('Coupling coeff K'),title('Tuneability of Coupling coeff')
%%
%%
d=3*10^(-6);%meter
[~,y]=min(Z1);
W=w(y);
d1=double(pi*v/(2*W));
%%
for j=1:MaxVoltage+1
    e=e1(j);
    %Freee space dielectric constant
    epsO=8.8*10^(-12);
    epsr=eps(j);
    epso=epsr*epsO ;
    %Elastice ceoefficeient
    cd=cd1(j);%
    %Acoustic velocity
    v=sqrt(cd/rho);%m/s
    %%
    Z2T(j,:)=ImpedanceCurve(A,d,e,cd,epso,w,v);
    Z1T(j,:)=ImpedanceCurve(A,d1,e,cd,epso,w,v);
    %%
```

```
114         TFT(j,:)=Z1T(j,:)./(Z2T(j,:)+Z1T(j,:));
115         TFT1(j,:)=Z1T(j,:)./(Z2T(j,:)+Z1T(j,:))-Z2T(j,:)./(Z2T(j,:)+Z1T(j,:)
                );
116         %%
117         [~,y]=min(Z1T(j,:));
118         WR1(j)=w(y);
119         [~,y]=max(Z1T(j,:));
120         WAR1(j)=w(y);
121
122 end
123 %%
124 figure
125 plot(w./(2*pi),log10(abs(1./Z1T(1,:)))),xlabel('Frequency Hz')
126 ylabel('Admittance Siemens in log_{10} scales'),title('Admittance of the
        FBAR')
127 %%
128 PLT(Z2T,w,MaxVoltage)
129 title('Tuneable FBAR Z2')
130 %
131 PLT(Z1T,w,MaxVoltage)
132 title('Tuneable FBAR Z1')
133 %
134 PLT1(TFT1,w,MaxVoltage)
135 title('Lattice bandpass filter')
136 %
137 PLT1(TFT,w,MaxVoltage)
138 title('Ladder bandpass filter')
139 %
140 figure
141 V=0:20;
142 E=V./d;
143 plot(E,WR1/(2*pi),'<')
144 hold on
145 plot(E,WAR1/(2*pi),'o')
146 legend('Rezonance rate','Antirezonance rate')
```

```
147 hold on
148 plot(E,WR1/(2*pi),'r')
149 hold on
150 plot(E,WAR1/(2*pi),'b')
151 xlabel('Electric field V/m')
152 ylabel('Frequency Hz'),title('Tuneability rate of resonance frequency')
153 %%
154 figure
155 t=WR1./WR1(1);
156 plot(E,t,'<')
157 hold on
158 plot(E,t,'r')
159 xlabel('Electric field V/m ')
160 ylabel('V-acoustic_{E}/V-acoustic_{E=0}'),title('Ratio of acoustic
      velocity')
161 %%
162 end
```

A.4 Quality factor

```
1 %%
2 close all
3 clear all
4 clc
5 %%
6 A=load('0VQ.dat');
7 B=load('5VQ.dat');
8 C=load('10VQ.dat');
9 D=load('15VQ.dat');
10 % E=load('20VQ.dat');
11 %%
12 plot((abs(A(:,1)))/(2*pi),(abs(A(:,2))),'b')
13 hold on
14 plot((abs(B(:,1)))/(2*pi),(abs(B(:,2))),'r')
15 hold on
16 plot((abs(C(:,1)))/(2*pi),(abs(C(:,2))),'g')
```

```
hold on
plot((abs(D(:,1)))/(2*pi),(abs(D(:,2))),'k')
hold on
plot((abs(E(:,1)))/(2*pi),(abs(E(:,2))),'m')
%%
xlabel('Frequency Hz'),ylabel('Q [unit]')
title('Variation of quality factor')
legend('0V','5V','10V','15V','20V')
%%
```

A.5 Tuneable filter, composite structure

```
function TuneableFilter()
%%
close all
clear all
clc
%Thicknesses of first FBAR
d=4.5*10^(-6);
d1=3*10^(-6);%meter
%Maximum voltage used to tune
MaxVoltage=20;
%Range of frequencies
w=2300:2900;
w=10^6*w;
%%
A=1.7*10^(-9);%square meter
%Density
rho=5.5*10^3;%kg/m^3
rho1=5*10^3;%kg/m^3
%Piezoelecetrice ceoefficeient
e=10.9;
e1=11.9;
%Freee space dielectric constant
epsr=1134;
epsr1=1034;
```

```
25 epsO=8.8*10^(-12);
26 % Elastice ceoefficeient
27 cd=2.214*10^(11);%
28 cd1=1.014*10^(11);%
29 % Tuning microwave parameters
30 beta=7*10^10; % Vm^5/C^3
31 beta1=7*10^10; % Vm^5/C^3
32 %%
33 %Tuning electrostriction
34 mu=463*10^(-12); % Vm^5/C^3
35 mu1=463*10^(-12); % Vm^5/C^3
36 %%
37 % Elastic constant
38 ce=1.25*10^(11);
39 ce1=1.25*10^(11);
40 %%
41 [Ele,Ele1,eps,eps1,cd1,cd1_1,e_1,e1_1,ZT2,Z2T1,v]=TuneComposite(d,d1,
       MaxVoltage,w,e,e1,epsr,epsr1,epsO,cd,cd1,rho,rho1,A,ce,ce1,mu,mu1,
       beta,beta1);
42 %%
43 %Thiceknesses of second FBAR
44 [~,y]=min(ZT2(1,:));
45 W=w(y);
46 d1=double(pi*v/(2*W));
47 d=d1*1.18;
48 %%
49 [~,~,~,~,~,~,~,~,ZT1,Z1T1,v]=TuneComposite(d,d1,MaxVoltage,w,e,e1,epsr,
       epsr1,epsO,cd,cd1,rho,rho1,A,ce,ce1,mu,mu1,beta,beta1);
50 %%
51 for j=1:MaxVoltage+1
52 %    Ladder topology
53     TF(j,:)=ZT1(j,:)./(ZT2(j,:)+ZT1(j,:));
54 %    Lattice topology
55     TFT1(j,:)=ZT2(j,:)./(ZT2(j,:)+ZT1(j,:))-ZT1(j,:)./(ZT2(j,:)+ZT1(j,:)
           );
```

```
56      %%
57  %   Rezonance and antirezonance of composite structure
58      [~,y]=min(ZT1(j,:));
59      WR(j)=w(y);
60      [~,y]=max(ZT1(j,:));
61      WAR(j)=w(y);
62      %%
63  %   Rezonance and antirezonance of homogeneous structure
64      [~,y]=min(Z1T1(j,:));
65      WR1(j)=w(y);
66      [~,y]=max(Z1T1(j,:));
67      WAR1(j)=w(y);
68      %%
69  end
70  %%
71  PLT(Z1T1,w,MaxVoltage)
72  title('Z1')
73  %%
74  PLT(ZT1,w,MaxVoltage)
75  title('ZT')
76  %%
77  figure
78  plot(Ele,WR1/(2*pi),'<')
79  hold on
80  plot(Ele,WR/(2*pi),'>')
81  hold on
82  plot(Ele,WAR1/(2*pi),'x')
83  hold on
84  plot(Ele,WAR/(2*pi),'o')
85  legend('Rezonance, homogeneous','Rezonanc hetereoneous','Antirezonance
        homogeneous','Antirezonance hetereoneous')
86  plot(Ele,WAR/(2*pi),'g')
87  hold on
88  plot(Ele,WR1/(2*pi),'r')
89  hold on
```

```
90 plot(Ele,WR/(2*pi),'k')
91 xlabel('Electric field V/m'),ylabel('Frequency Hz')
92 %%
93 [Coupl1]=CouplingCoeff(WAR1,WR1);
94 [Coupl]=CouplingCoeff(WAR,WR);
95 %%
96 V=0:MaxVoltage;
97 PLT2(V,V,Coupl,Coupl1)
98 xlabel('Applied voltage V')
99 ylabel('Coupling coeff K')
100 title('Tuneability rate of Coupling coeff')
101 legend('Hetereogeneous','Homogeneous')
102 %%
103 figure
104 plot(V,Coupl,'b')
105 hold on
106 plot(V,Coupl,'<')
107 xlabel('Applied voltage V')
108 ylabel('Coupling coeff K')
109 title('Tuneability of hetereogeneous Coupling coeff')
110 %%
111 PLT1(TF,w,MaxVoltage)
112 title('Ladder bandpass')
113 PLT1(TFT1,w,MaxVoltage)
114 title('Lattice bandpass')
115 %%
116 % Electric field
117 V=0:MaxVoltage;
118 PLT2(V,V,Ele,Ele1)
119 title('Electric field ')
120 ylabel('Electric field V/m')
121 xlabel('Applied voltage V')
122 %%
123 PLT2(Ele,Ele1,eps,eps1)
124 title('Dielectric permitivity tuneability')
```

```
125 xlabel('Electric field V/m'),ylabel('Relative permitivity (unit)')
126 %%
127 PLT2(V,V,eps,eps1)
128 title('Dielectric permitivity tuneability')
129 legend('Second medium','First medium')
130 xlabel('Applied voltage V'),ylabel('Relative permitivity (unit)')
131 %%
132 PLT2(Ele,Ele1,cd1,cd1_1)
133 title('Elastic constant  tuneability')
134 xlabel('Electric field V/m'),ylabel('Elastic constant (Pa)')
135 %%
136 PLT2(V,V,cd1,cd1_1)
137 title('Elastic constant tuneability')
138 xlabel('Applied voltage V'),ylabel('Elastic constant (Pa)')
139 %%
140 PLT2(Ele,Ele1,e_1,e1_1)
141 title('Piezoelectric coeff tuneability')
142 xlabel('Electric field V/m'),ylabel('Piezoelectric coeff C/m^2')
143 %%
144 PLT2(V,V,e_1,e1_1)
145 title('Piezoelectric coeff tuneability')
146 xlabel('Applied voltage V'),ylabel('Piezoelectric coeff C/m^2')
147 %%
148 %First medium thickness
149 d1_1=3;
150 d1=d1_1*10^(-6);%meter
151 %Second medium thickness
152 d2_1=0:.1:2*d1_1;%meter
153 d2=d2_1*10^(-6);%meter
154 for i=1:max(size(d2))
155     d=d2(i);
156     [Ele(i,:),Ele1(i,:),~,~,~,~,~]=TuneParametersHetereogeneous(d1,d,
          epsr1,epsr,ce1,ce,e1,e,beta1,beta,mu1,mu,epsO,MaxVoltage);
157 end
158 %%
```

```
159 V=0:MaxVoltage;
160 [x,y]=meshgrid(V,d2_1./d1_1);
161 %%
162 PLT3(x,y,Ele')
163 title('Second electric field d1=3um')
164 xlabel('Applied voltage V'),ylabel('Thicknesses ration d2/d1')
165 zlabel('Electrical field V/m'),colorbar;
166 %%
167 PLT3(x,y,Ele1')
168 title('First electric field d1=3um')
169 xlabel('Applied voltage V'),zlabel('Electrical field V/m'),ylabel('
      Thicknesses ration d2/d1')
170 colorbar;
171 %
172 MaxVoltage=20;
173 V=0:MaxVoltage;
174 [Ele,Ele1,~,~,~,~,~]=TuneParametersHetereogeneous(d1,d,epsr1,epsr,ce1,
      ce,e1,e,beta1,beta,mu1,mu,epsO,MaxVoltage);
175 [B1,B2,El,El1]=TuneParameterApproximately(d1,d,epsr1,epsr,ce1,ce,e1,e,
      beta1,beta,mu1,mu,epsO,MaxVoltage);
176 PLT2(V,V,B1,B2)
177 xlabel('Voltage V'),ylabel('Ration (unit)')
178 title('Common Ration'),legend('B1','B2')
179
180 %%
181 %Electric field
182 figure
183 plot(V,Ele1,'o')
184 hold on
185 plot(V,El1,'x')
186 hold on
187 plot(V,Ele,'<')
188 hold on
189 plot(V,El,'>')
190 legend('First Electric field','First Electric field approximated','
```

```
    Second Electric field','Second Electric field approximated')
hold on
plot(V,Ele,'k')
hold on
plot(V,El,'b')
hold on
plot(V,Ele1,'g')
hold on
plot(V,El1,'r')
xlabel('Voltage V'),ylabel('Electrical field V/m'),title('Electric field
    vs Voltage')
%%
%%
end
```

A.6 Acoustic coupled

```
function TransmissionLineTune()
%%
close all
clear all
clc
%Thicknesses of FBAR
d=4.5*10^(-6);
d1=3*10^(-6);%meter
%Maximum voltage used to tune
MaxVoltage=40;
%Range of frequencies
w=2300:1:2400;
w=10^6*w;
%Active area
A=1.7*10^(-9);%square meter
%Density
rho=5.5*10^3;%kg/m^3
rho1=5*10^3;%kg/m^3
%Piezoelecetrice ceoefficeient
```

```
e=10.9;
e1=11.9;
%Freee space dielectric constant
epsr=1134;
epsr1=1034;
epsO=8.8*10^(-12);
epso=epsO*epsr;
epso1=epsO*epsr1;
% Elastice ceoefficeient
cd=2.214*10^(11);%
cd1=1.014*10^(11);%
% Elastic constant
ce=1.25*10^(11);
ce1=1.15*10^(11);
% Tuning microwave parameters
beta=7*10^10; %
beta1=7*10^10; %
%%
%Tuning electrostriction
mu=463*10^(-12); %
mu1=463*10^(-12); %
%
%Acoustic velocity
v=sqrt(cd/rho);%m/s
%Acoustic velocity
v1=sqrt(cd1/rho1);%m/s
%%
[Z,~,~,~]=ImpedanceComposite(d,d1,A,e,e1,cd,cd1,epso,epso1,w,v,v1);
%%
[~,y]=max(Z);
AntiRezonance=w(y);
%%
[~,~,~,~,cd1,cd1_1,~,~,~,~,v]=TuneComposite(d,d1,MaxVoltage,w,e,e1,epsr,
    epsr1,epsO,cd,cd1,rho,rho1,A,ce,ce1,mu,mu1,beta,beta1);
[~,~,cd1,~,~]=TuneParametersHomogeneous(e,ce,epsO,epsr,beta,mu,d,
```

```
    MaxVoltage);
%Input impedance
%%
Z_acoustic=sqrt(cd1.*rho);
Z_acoustic1=sqrt(cd1_1.*rho1);
%%
v_acoustic=sqrt(cd1./rho);
v_acoustic1=sqrt(cd1_1./rho1);
%%
[X,Y]=meshgrid(1:MaxVoltage+1,w);
[v_acousticX,wX]=meshgrid(v_acoustic,w);
[v_acousticX1,wX1]=meshgrid(v_acoustic1,w);
%%
Gama=(2*pi./v_acousticX).*wX;
Gama1=(2*pi./v_acousticX1).*wX1;
%%
Z_electrode=40.6*10^6*ones(size(Z_acoustic));
t=.2;
V_acoustic_electrode=10.5*10^(3)*ones(size(v_acoustic));
[V_acoustic_electrode1,wX]=meshgrid(V_acoustic_electrode,w);
GamaElectrode=(2*pi./V_acoustic_electrode1).*wX;
%%
Zair=10^(-4+6)*ones(size(Z_acoustic));
%%
% %Electrode
% Z=20*10^(6);
% t=.2;
% V_acoustic_electrode=10.5*10^(3)*ones(size(v_acoustic));
%%
V_coupler=5*10^(3);%m/s
lambda=V_coupler/AntiRezonance;
l=lambda/4;
%%
%FBAR1
[Z1]=Z_Input(Z_electrode,Zair,t,GamaElectrode);
```

```
88  [Z2]=Z_Input(Z_acoustic,Z1,d,Gama);
89  % [Z3]=Z_Input(Z_acoustic1,Z2,d1,Gama1);
90  Zin=Z_Input(Z_electrode,Z2,t,GamaElectrode);
91  %%
92  %FBAR2
93  [Z1]=Z_Input(Z_electrode,Zair,t,GamaElectrode);
94  % [Z2]=Z_Input(Z_acoustic1,Z1,d1,Gama1);
95  [Z3]=Z_Input(Z_acoustic,Z1,d,Gama);
96  Zin1=Z_Input(Z_electrode,Z3,t,GamaElectrode);
97  %%
98  %Coupling layer
99  Z_Coupling_tuned=abs(sqrt(Zin(:,1).*Zin1(:,1)));
100 Z_Coupling_static=abs(sqrt(Zin(1,1).*Zin1(1,1)));
101 Z_Coupling_tuned=repmat(Z_Coupling_tuned,1,max(size(w)));
102 Z_Coupling_static=Z_Coupling_static*ones(size(Zin));
103
104 %%
105 [T]=TransferFunction(Zin,Zin1,Z_Coupling_tuned,w,l,V_coupler);
106 [T1]=TransferFunction(Zin,Zin1,Z_Coupling_static,w,l,V_coupler);
107 %%
108 PLT3(X,Y./(2*pi),Z_Coupling_tuned)
109 title('Coupling layer tuned');
110 zlabel('Coupling layer acoustic impedance (rayl)');
111 %%
112 % figure
113 % fill3(X,Y,Z_Coupling_static,'r')
114 % title('Coupling layer static'),ylabel('Operational frequency');
115 % zlabel('Coupling layer'),xlabel('Applied voltage');
116 %%
117 PLT3(X,Y./(2*pi),T)
118 title('Tuneability of the transfer function');
119 zlabel('Transfer function in log_{10} scale');
120 ylabel('Transfer function');
121 %%
122 PLT(T,w,MaxVoltage)
```

```
123 title('Tuneability of the transfer function');
124 %%
125 PLT3(X,Y./(2*pi),T1)
126 title('Static transfer function ');
127 zlabel('Transfer function in log_{10} scale');
128 ylabel('Transfer function');
129 %%
130 PLT(T1,w,MaxVoltage)
131 title('Static transfer function ');
132 ylabel('Transfer function in log_{10} scale');
133 %%
134 PLT3(X,Y./(2*pi),Zin)
135 title('Tuneability of the input impedance FBAR1');
136 zlabel('Acoustic impedance (rayl)');
137 %%
138 PLT(Zin,w,MaxVoltage)
139 ylabel('Acoustic Impedance (rayl)')
140 title('Tuneability of the input impedance FBAR1');
141
142 figure;
143 plot(1:MaxVoltage+1,Zin(:,1))
144 xlabel('DC voltage V'),ylabel('Initial Acoustic Impedance (rayl)')
145 title('Behaviour of the input acoustic impedance')
146 %%
147 % PLT3(X,Y./(2*pi),Zin1)
148 % title('Tuneability of the input impedance FBAR2');
149 % zlabel('Acoustic impedance');
150 % %%
151 % PLT(Zin1,w,MaxVoltage)
152 % title('Tuneability of the input impedance FBAR2');
153 end
```

A.7 Aid functions

```
1 function PLT(A,w,MaxVoltage)
2 %%
```

```
figure
B=zeros(size(A(1,:)));
for j=1:MaxVoltage+1
    B(:)=A(j,:);
    if j==1
        plot(w/(2*pi),(log10(abs(B))),'b')
    end
    if j==6
        plot(w/(2*pi),(log10(abs(B))),'g')
    end
    if j==11
        plot(w/(2*pi),(log10(abs(B))),'r')
    end
    if j==16
        plot(w/(2*pi),(log10(abs(B))),'c')
    end
    if j==21
        plot(w/(2*pi),(log10(abs(B))),'m')
    end
    if j==26
        plot(w/(2*pi),(log10(abs(B))),'k')
    end
    if j==31
        plot(w/(2*pi),(log10(abs(B))),'-')
    end
    if j==36
        plot(w/(2*pi),(log10(abs(B))),'--')
    end
    hold on
    pause(.1)
end
xlabel('Frequency Hz'),ylabel('Imendapnce Ohm in log_{10} scale')
legend('0V','5V','10V','15V','20V','25V','30V','35V')
%%
end
```

```
function PLT1(A,w,MaxVoltage)
%%
figure
B=zeros(size(A(1,:)));
for j=1:MaxVoltage+1
    B(:)=A(j,:);
    if j==1
        plot(w/(2*pi),(log10(abs(10^(j)*B))),'b')
    end
    if j==6
        plot(w/(2*pi),(log10(abs(10^(j)*B))),'g')
    end
    if j==11
        plot(w/(2*pi),(log10(abs(10^(j)*B))),'r')
    end
    if j==16
        plot(w/(2*pi),(log10(abs(10^(j)*B))),'c')
    end
    if j==21
        plot(w/(2*pi),(log10(abs(10^(j)*B))),'m')
    end
    if j==26
        plot(w/(2*pi),(log10(abs(10^(j)*B))),'k')
    end
    if j==31
        plot(w/(2*pi),(log10(abs(10^(j)*B))),'-')
    end
        if j==36
        plot(w/(2*pi),(log10(abs(10^(j)*B))),'--')
    end
    hold on
    pause(.1)
end
xlabel('Frequency Hz'),ylabel('Imendapnce Ohm in log_{10} scale')
legend('0V','5V','10V','15V','20V','25V','30V','35V')
```

```
%%
end
```

```
function PLT2(Values,Values1,Outcome,Outcome1)
%%
figure
plot(Values,Outcome,'<')
hold on
plot(Values1,Outcome1,'o')
legend('Second medium','First medium')
hold on
plot(Values,Outcome,'b')
hold on
plot(Values1,Outcome1,'r')
%%
end
```

```
function PLT3(X,Y,Z)
%%
figure
surf(abs(X),abs(Y),abs(Z)');
camlight left;
lighting flat;
shading interp
lightangle(-45,45)
h.FaceLighting = 'gouraud';
h.AmbientStrength = 10;
h.DiffuseStrength = 10;
h.SpecularStrength = 10;
h.SpecularExponent = 250;
h.BackFaceLighting = 'unlit';
colormap hsv ;
colorbar
alpha(.4)
xlabel('Applied voltage V'),ylabel('Operational frequency Hz');
%%
```

```
20 end

1  function [Ele,Ele1,eps,eps1,cd1,cd1_1,e_1,e1_1,ZT1,Z1T1,v]=TuneComposite
       (d,d1,MaxVoltage,w,e,e1,epsr,epsr1,epsO,cd,cd1,rho,rho1,A,ce,ce1,mu,
       mu1,beta,beta1)
2  %%
3  %Acoustic velocity
4  v=sqrt(cd/rho);%m/s
5  v1=sqrt(cd1/rho1);%m/s
6  % Tune composite materials
7  [Ele,Ele1,eps,eps1,cd1,cd1_1,e_1,e1_1]=TuneParametersHetereogeneous(d1,d
       ,epsr1,epsr,ce1,ce,e1,e,beta1,beta,mu1,mu,epsO,MaxVoltage);
8  %%
9  for j=1:MaxVoltage+1
10     %Piezoelecetrice ceoefficeient
11     e=e_1(j);
12     %Freee space dielectric constant
13     epsO=8.8*10^(-12);
14     epsr=eps(j);
15     epso=epsr*epsO ;
16     %Elastice ceoefficeient
17     cd=cd1(j);%
18     %Acoustic velocity
19     v=sqrt(cd/rho);%m/s
20     %%
21     %Piezoelecetrice ceoefficeient
22     e1=e1_1(j);
23     %Freee space dielectric constant
24     epsO=8.8*10^(-12);
25     epsr=eps1(j);
26     epso1=epsr*epsO ;
27     %Elastice ceoefficeient
28     cd12=cd1_1(j);%
29     %Acoustic velocity
30     v1=sqrt(cd12/rho);%m/s
31     %%
```

```
32        [Z,Z1,Z2,K10]=ImpedanceComposite(d,d1,A,e,e1,cd,cd12,epso,epso1,w,v,
              v1);
33        ZT1(j,:)=Z(:);
34        Z1T1(j,:)=Z1(:);
35        Z2T1(j,:)=Z2(:);
36    end
37    %%
38    end
```

```
1   function [Ele,Ele1,eps,eps1,cd1,cd1_1,e_1,e1_1]=
        TuneParametersHetereogeneous(d1,d,epsr1,epsr,ce1,ce,e1,e,beta1,beta,
        mu1,mu,epsO,MaxVoltage)
2   %%
3   E1=0;
4   E=0;
5   %%
6   j=1;
7   for V=0:MaxVoltage
8       %%
9       %%
10      eps(j)=epsr/(1+3*beta*(epsr*epsO)^3*E^2);
11      eps1(j)=epsr1/(1+3*beta1*(epsr1*epsO)^3*E1^2);
12      %%
13      e_1(j)=e*(1+mu*E);
14      e1_1(j)=e1*(1+mu1*E1);
15      %%
16      cd1(j)=ce+e_1(j).^2./(eps(j)*epsO);
17      cd1_1(j)=ce1+e1_1(j).^2./(eps1(j)*epsO);
18      %%
19      K(j)=(e_1(j).^2)./(epsO*eps(j).*cd1(j));
20      K_1(j)=(e1_1(j).^2)./(epsO*eps1(j).*cd1_1(j));
21      %%
22      B1=(1-K(j))./(1-K_1(j));
23      B2=1/B1;
24      %%
25      E1=V/(d1*(1+B1*(d/d1)*(eps1(j)/eps(j))));
```

```
26        E=V/(d*(1+B2*(d1/d)*(eps(j)/eps1(j))));
27        Ele(j)=E;
28        Ele1(j)=E1;
29        %%
30        j=j+1;
31    end
32    %%
33    end
```

```
1   function [Coupl1]=CouplingCoeff(WAR1,WR1)
2   %%
3   %Definition fo coupling coefficient from analytical approximation
4   for i=1:max(size(WAR1))
5         Coupl1(i)=(pi/2)*sqrt(double(WAR1(i)^2-WR1(i)^2)/WAR1(i)^2);
6   end
7   %%
8   end
```

```
1   function [B1,B2,El,El1]=TuneParameterApproximately(d1,d,epsr1,epsr,ce1,
        ce,e1,e,beta1,beta,mu1,mu,epsO,MaxVoltage)
2
3   V=0;
4   E1=V/(d1*(1+(d/d1)*(epsr1/epsr)));
5   E=V/(d*(1+(d1/d)*(epsr/epsr1)));
6   %%
7   j=1;
8   for V=0:MaxVoltage
9         %%
10        eps(j)=epsr/(1+3*beta*(epsr*epsO)^3*E^2);
11        eps1(j)=epsr1/(1+3*beta1*(epsr1*epsO)^3*E1^2);
12        %%
13        e_1(j)=e*(1+mu*E);
14        e1_1(j)=e1*(1+mu1*E1);
15        %%
16        cd1(j)=ce+e_1(j).^2./(eps(j)*epsO);
17        cd1_1(j)=ce1+e1_1(j).^2./(eps1(j)*epsO);
```

```
18        %%
19        K(j)=(e_1(j).^2)./(epsO*eps(j).*cd1(j));
20        K_1(j)=(e1_1(j).^2)./(epsO*eps1(j).*cd1_1(j));
21        %%
22        E1=V/(d1*(1+(d/d1)*(eps1(j)/eps(j))));
23        E=V/(d*(1+(d1/d)*(eps(j)/eps1(j))));
24        El(j)=E;
25        El1(j)=E1;
26        %%
27        j=j+1;
28    end
29    %%
30    V=0:20;
31    B1=(ones(size(K))-K)./(ones(size(K))-K_1);
32    B2=(ones(size(K_1))-K_1)./(ones(size(K))-K);
33
34    end
```

```
1   function [Z,Z1,Z2,K10]=ImpedanceComposite(d,d1,A,e,e1,cd,cd1,epso,epso1,
        w,v,v1)
2   %%
3    [Z2]=ImpedanceCurve(A,d,e,cd,epso,w,v);
4    [Z1]=ImpedanceCurve(A,d1,e1,cd1,epso1,w,v1);
5   %%
6   %Second component
7   K2=(e1/epso1);
8   K3=ones(size(w));
9   K4=(double(K3))-double(cos(w*d1/v1));
10  K5=cos(w*d1/v1);
11  K6=K4./K5;
12  K7=K2.*K6.^2;
13  %%
14  %First component
15  K2=(e/epso);
16  K3=ones(size(w));
17  K4=(double(K3))-double(cos(w*d/v));
```

```
K5=cos(w*d/v);
K6=K4./K5;
K8=K2.*K6.^2;
%%
%Common parameter
K1=1./(w.*((cd1/v1).*double(tan(w*(d1/v1)))+(cd/v).*double(tan(w*(d/v)))
    ));
K9=K8-K7;
K10=K9.*K1;
%%
%Total impendance
Z=Z1+Z2+K10;
%%
end
```

```
function [Zi1n]=Z_Input(Z,Z1,t,gama)
%%
t=t*ones(size(gama));
for i=1:max(size(Z))
    K11(i,:)=tan(gama(:,i).*t(:,i));
    K21(i,:)=Z1(i).*K11(i,:);
    K31(i,:)=K21(i,:)+1i*Z(i)*ones(size(K21(i,:)));
    K41(i,:)=Z(i).*K11(i,:);
    K51(i,:)=Z1(i)*ones(size(K21(i,:)))+1i*K41(i,:);
    K61(i,:)=K51(i,:)./K31(i,:);
    Zi1n(i,:)=Z(i).*K61(i,:);
end
%%
end
```

```
function [T]=TransferFunction(Z1,Z3,Z2,w,l,V_coupler)
%%
lambda=V_coupler./w;
lambda=repmat(lambda,min(size(abs(Z1))),1);
%%
K1=abs(4.*abs(Z1).*abs(Z3));
```

```
7  K2=abs((abs(Z1)+abs(Z3)).^2);
8  K3=abs((abs(Z1).*abs(Z3))./abs(Z2));
9  K4=abs((K3+abs(Z2)).^2);
10 theta=(2*pi*l)./lambda;
11 COS=abs(cos(theta));
12 SIN=abs(sin(theta));
13 T=K1./(K2.*COS+K4.*SIN);
14 %%
15 end
```

Appendix B

Tensor notation of the materials

This tensors are utilized for the FBAR models simulated in comsol

The elastic constant tensor is below where c has different values for different material. For the BST1 $c = 2.214$ whereas for the BST2 $c = 1.214$

$$\begin{pmatrix} c*10^{11} & 1.21*10^{11} & 1.011*10^{11} & 0 & 0 & 0 \\ 0 & c*10^{11} & 1.053*10^{11} & 0 & 0 & 0 \\ 0 & 0 & c*10^{11} & 0 & 0 & 0 \\ 0 & 0 & 0 & 1.011*10^{11} & 0 & 0 \\ 0 & 0 & 0 & 0 & 1.011*10^{11}, & 0 \\ 0 & 0 & 0 & 0 & 0 & 1.011*10^{11} \end{pmatrix}$$

Figure B-1: Elastic constant tensor where unit is **Pa**

The tensor below represent the notation for the piezoelectric coefficient where again the **e** is different for different material. In the BST1 case **e=10.9** whereas for the BST2 case **e=11.9**.

$$\begin{pmatrix} 0 & 0 & 0 & 0 & -0.480508 & 0 \\ 0 & 0 & 0 & -0.480508 & 0 & 0 \\ e & e & e & 0 & 0 & 0 \end{pmatrix}$$

Figure B-2: Piezoelectric coefficient tensor where the unit is $\frac{C}{m^2}$

In this tensor ϵ has different values at different similarly to the other two tensors above $\epsilon = 1134$ for the BST1 and $\epsilon = 1034$ for the BST2 medium. Regarding the other quantity ,$\epsilon_1 = 934$ for the first material and $\epsilon_1 = 834$ for the second material.

$$\begin{pmatrix} \epsilon_1 & 0 & 0 \\ 0 & \epsilon_1 & 0 \\ 0 & 0 & \epsilon \end{pmatrix}$$

Figure B-3: Dielectric permittivity tensor

The comsol models for these simulations can be found here.

Glossary

BAW Bulk Acoustic Wave. 9, 17, 18, 22, 23

BST $Ba_xSr_{1-x}TiO$. 10, 13, 15, 33, 37, 42, 43, 51–53, 57, 59, 68, 70, 111

BTO Barium titanate. 42

BVD Butterworth-Van-Dyke. 9, 29, 30

CDO carbon-doped oxide. 49, 62, 63, 73

CRF Coupled Resonator Filter. 35

FBAR Film bulk acoustic resonator. 7–11, 13, 15, 17–19, 21, 22, 26, 29–31, 33, 35, 37, 38, 41–43, 45–49, 51–53, 61–63, 67–74, 111

FEM Finite element method. 68

RF Radio Frequency. 5, 17, 33, 70

SAW Sulk Acoustic Wave. 9, 17, 22, 23

SiLK Silicon Low k dielectric resin. 49

SMR Surface Mounted Solid. 9, 17, 18

SRF Stacked Resonator Filter. 35